Permeable reaction barrier system for the treatment of textile wastewater using cobalt oxide

By

Gunnar Lieb Visser

Thesis Submitted in Fulfilment of the Requirements for the Degree

Master of Engineering: Chemical Engineering

in the Faculty of Engineering

at the Cape Peninsula University of Technology

Supervisor: Prof V.G Fester

Cape Town Campus
December 2017

Declaration

I, Gunnar Lieb Visser, declare that the contents of this dissertation/thesis represent my own unaided work, and that the dissertation/thesis has not previously been submitted for academic examination towards any qualification. Furthermore, it represents my own opinions and not necessarily those of the Cape Peninsula University of Technology.

Signed

14/12/2017

Date

Abstract

Advanced oxidation processes (AOPs) have gained considerable interest in the wastewater treatment industry. Low selectivity to organic pollutants and the high oxidation potentials provided by the free radicals produced from these processes are the root of this interest. Hydroxyl radical based AOPs seemed to dominate the field but recently sulphate radical based AOPs started to become more popular due to their even higher oxidation potential.

The textile industry is known to be a considerable contributor to wastewater production. Many pollutants in this wastewater are organic pollutants which are very persistent to the more traditional treatment processes such as biological treatment and membrane filtration. Numerous studies have shown the potential and success of catalytic AOPs for the degradation of organic pollutants in wastewater. One such process is the use of a cobalt oxide nano-catalyst in conjunction with a peroxymonosulfate (PMS) oxidizer (Co_3O_4/PMS). The shortcoming with nano-catalysts however are the difficulty of recovering the catalyst in a slurry system or the effective immobilization of the catalyst in a continuous system.

To address the issue of nano-catalyst immobilization, two different methods were used in the study to effectively immobilize the catalyst in a substrate. The methods were compared by utilizing the permeable reaction barriers in a continuous flow reactor. A bench scale reactor of 2.4 L/hr was designed and used to study the effect of PMS, catalyst mass and flow rate on the degradation efficiency and to determine the residence time and catalyst per PRB cross-sectional area ratio. A scale up rationale was formulated based on a constant residence time and the catalyst mass per PRB cross-sectional area ratio. Two design correlations were developed to predict the size of the permeable barrier and the catalyst mass required for the scale up PRB system. These parameters were used to design a reactor 30 times that of the bench scale reactor. In both reactors the optimum degradation occurred within 2 minutes indicating the success for catalyst immobilization and the development of a continuous reactor utilizing the Co_3O_4/PMS advanced oxidation technology.

Acknowledgments

I wish to thank:

- Professor Veruscha Fester, for her encouragement, advice and faith in me. I am forever grateful for the opportunity she has provided me with.
- Dr. Mahabubur Rahman Chowdhury for his advice and mentorship.
- Mr. Richard du Toit and Mr. Alwyn Bester for their advice and aid in the construction of the reactors.
- All students that have assisted me with running experiments and completing tasks during the course of my research.
- The Flow Process and Rheology Centre for providing me with an encouraging and professional research environment.
- The Technology and Innovation Agency for financially supporting me during the course of the research.

Dedication

To my dearest and loving parents

Theuns and Jutta Visser.

For their loving support, their guidance and advice and for providing me with the privilege to obtain a tertiary qualification.

Table of Contents

List of Figures

List of Tables

Glossary - Terms and Concepts

Nanoparticles: Any ultrafine particles between the size of 1 to 100 nm.

Hydrothermal Synthesis: A synthesis method for growing crystals from an aqueous solution at high temperature and pressure.

Slurry System: A system whereby solid particles are suspended throughout the liquid.

Permeable Barrier: A porous substrate utilized for the immobilization of the catalyst.

Permeable Reaction Barrier (PRB): A porous substrate, filled with reactive material, placed in a stream of contaminated water to create contact between a catalyst and contaminated water for the purpose of creating a chemical reaction to degrade organic pollutants in the water.

Packed Bed Reactor (PBR): a tubular reactor packed with solid catalysts used to catalyse gas and liquid reactions

Heterogeneous: A process whereby the substances involved in the process are of different phases.

Homogeneous: A process whereby the substances involved in the process are of the same phase.

Immobilization: Restricting free movement of particles by fixing the particles to a surface to prevent it from being lost in a water stream.

SEM: Scanning electron microscopy; a type of electron microscope that produces images of a sample by scanning it with a focused beam of electrons.

AOP: Advanced oxidation process; chemical water treatment processes whereby organic pollutants are removed by oxidation reactions using radicals.

Process Flow Diagram (PFD): A diagram used in process engineering to indicate the general flow of the process and equipment.

List of Symbols

Symbol	Description of Symbol	Unit
A_{PRB}^{A}	Cross-sectional area of PRB A	cm^2
A_{PRB}^{B}	Cross-sectional area of PRB B	cm^2
B_1, B_2	Mass of beaker 1 and 2	g
C_t, C_0	Concentration at time t and time 0	mg/L
d_A, d_B	Diameter of PRB A and PRB B	cm
E_a	Activation energy	kJ/mol
E_{cat}	Energy of the catalyst	kJ/mol
F_{A_0}	Molar flow rate of A	mol/s
h_1, h_2	Pressure head at point 1 and point 2	m
k	Reaction rate constant	min^{-1}
k_0	Reaction rate constant at Temperature at time = 0	min^{-1}
K	Hydraulic conductivity	m/s
Δl	Length of the medium	m
m_{cat}^{A}, m_{cat}^{B}	Mass of catalyst in PRB A and PRB B	g
M_{cat}^{A}, M_{cat}^{B}	catalyst mass per cross-sectional area ratio of PRB A and PRB B	g/cm^2
$\dot{Q}$	Volumetric flow rate	m^3/s
R	Universal gas constant	$kJ/mol.K$
r_A	Reaction rate	$\frac{mol}{L}.s$
T	Temperature	K
t	Thickness of the PRB	m

Symbol	Description of Symbol	Unit
V	Volume	m^3
V_{PRB}^{A}, V_{PRB}^{B}	Total volume of PRB A and PRB B	m^3
$V_{Pore}^{A}, V_{Pore}^{B}$	Pore volume of PRB A and PRB B	m^3
W	Catalyst mass	kg
X	Conversion of reactant A to product	dimensionless
τ	Residence time in the permeable barrier	s
$\emptyset$	Porosity of the PRB	%
$\rho_{catalyst}$	Density of the catalyst	kg/m^3
$\emptyset$	Viscosity	$Pa.s$

CHAPTER ONE: Introduction

1.1 Background

Yearly about 80 000 tonnes of textile dyes are being produced which contribute to about 177 000 megalitre of textile wastewater (Allègre et al., 2006). This wastewater is being treated by traditional methods such as biological treatment, chemical treatment (flocculation and adsorption), membrane filtration and advanced oxidation processes (AOPs). These methods have a low efficiency with exception to advanced oxidation processes. AOPs have in recent years been one of the most researched fields in wastewater treatment as they show high efficiency in treating wastewater by oxidizing organic substances into CO_2 and H_2O (Sun and Wang, 2015). Cobalt catalysts have shown the best activation of peroxymonosulfate (PMS) compared to a number of other metals which produces sulfate radical species, prioritized over hydroxyl radicals, used to oxidize organic pollutants in the treatment of wastewater (Anipsitakis and Dionysiou, 2004; Yang et al., 2009). A great deal of research done by Chen et al., (2008), Chen et al., (2014), Chowdhury et al., (2015), Ding et al., (2012), Anipsitakis et al., (2005), Deng and Zhao, (2015), Liang et al., (2012a), Saputra et al., (2013), Saputra et al., (2017), Shi et al., (2012), Shi et al., (2014), Shi et al., (2015) and Yao et al., (2012) in the treatment of textile wastewater using heterogeneous cobalt oxide as a PMS activator in a slurry system. However, the slurry system proves to be very difficult to apply in an industrial setup as it shows a number of disadvantages such as solid waste production, high catalyst cost, difficulty in catalyst recovery and regeneration (Zhao et al., 2006).

To solve the problem of a slurry system, this study focuses on immobilization of the cobalt oxide catalyst in a permeable barrier and the design of a permeable reaction barrier system for the continuous treatment of textile effluent. A scale up of the permeable reaction barrier system was executed and used to continuously treat real textile effluent.

1.2 Research problem

There is currently no continuous treatment reactor available that utilises immobilised nano-Co_3O_4 for the degradation of textile effluent.

1.3 Aims and objectives

The aim of the study was to design and develop a permeable reaction barrier system which utilises an immobilised cobalt oxide nano-catalyst to continuously treat textile wastewater on an industrial scale.

To achieve the aim, the objectives of the study were:

- To identify a permeable barrier and immobilise a cobalt oxide catalyst in it.
- To design a continuous reactor utilizing a permeable reactive barrier.
- To determine the optimum operating conditions (PMS dosage, catalyst loading and flow rate) for the removal of colour.
- To design and build a scale-up model of at least an order of magnitude.

1.4 Significance of research

The study contributes to the treatment of wastewater using nano-based catalysts and to extend laboratory scale work to prototyping and industrial implementation.

1.5 Delineation

Only one permeable barrier was used, but different methods to immobilise the particles in the substrate were evaluated. The time-based intermediates that form during PMS and Co_3O_4/PMS degradation was not characterised as this formed part of another study.

1.6 Structure of thesis

- Chapter 1: The first chapter serves as an introduction to the research problem and research questions that are answered by the study.
- Chapter 2: A detailed and relevant literature review is provided in Chapter 2.
- Chapter 3: The third chapter provides the steps taken in the preliminary experiments and design of the bench scale permeable reaction barrier system that led to the final bench scale reactor.
- Chapter 4: In this chapter, the performance of the bench scale reactor is optimized using methylene blue as synthesised wastewater as well as real textile wastewater.
- Chapter 5: This chapter provides the design and operation of the scale up model as well as a hazard and operability study on the reactor.
- Chapter 6: Conclusions of the research and recommendations for future work is presented in this chapter.

CHAPTER TWO: Literature review

2.1 Introduction

This chapter provides a review of literature on the nature and kinetics of chemical reactions and the effects of temperature, catalyst and reactant concentration on reaction rates. A brief discussion of the design of chemical reactors is given focussing on tubular reactors and specifically packed bed reactors is provided. Previous studies done in the field of textile wastewater treatment are presented. Advanced oxidation technologies are discussed and the mechanisms for the formation of free radicals in the advanced oxidation technology specifically the sulphate radical based advanced oxidation process are described.

2.2 Kinetics of chemical reactions

Reaction kinetics enables the description of the rate at which reactants are transformed to the products in a chemical reaction. It also permits relating the rate of the reaction to a mechanism followed by the reactants to give the final product. Reaction kinetics also provides us with the tools to relate the reaction rate to the macroscopic parameters such as concentration, temperature and pressure. Kinetics of a reaction on a molecular level are considered as reaction dynamics (Chorkendorff and Niemantsverdriet, 2003).

2.3 The reaction rate

All chemical species have an identity which is identified by the kind, number and configuration of the atoms of that species. Chemical species with the same number and kind of atoms can be different if their atom arrangement is different. The reaction rate of a chemical reaction is an indicator of how fast a certain mass/moles of one chemical species loses its identity by forming a new product species (Fogler, 1999).

There are three different methods by which a species can lose its identity; decomposition, combination and isomerisation. During the process of decomposition, the original species is broken down by breaking the bonds to form smaller molecules or atoms. Combination involves the merging of two chemical species to form a third new species. Isomerisation involves the configuration of the arrangement of the atoms to change without changing the kind or number of atoms (Fogler, 1999). The rate of a reaction is dependent on the following factors (Masterton et al., 2012):

- Concentration of reactants
- Reaction process
- Temperature
- Presence of a catalyst

- Reaction mechanism

The effect of reactant concentration, temperature and catalyst presence on the rate of the reaction is elaborated on in the sections that follow.

2.3.1 Concentration of reactants and reaction rate

The concentration of reactants is directly related to the reaction rate. A reaction occurs due to the collisions of reactant molecules. Because of higher concentration, a higher frequency of collisions occurs resulting in a higher reaction rate. This however results in the consumption of molecules leading to a decrease in concentration and a decrease in collision frequency thereby decreasing the rate of the reaction. The reactant species with the lowest molecular concentration is the first species to completely react and is known as the rate limiting reactant (Masterton et al., 2012).

2.3.2 Temperature and reaction rate

Activation energy is the energy barrier in the reaction pathway that must be overcome by the reactant molecules in order for the reactant molecules to react and form product molecules. The Arrhenius equation is a relationship between the reaction rate constant (k) and the absolute temperature (T) by making use of the activation energy (E) of the reaction. Equation 2.1 shows the Arrhenius equation (Perry and Green, 1999):

$$\boldsymbol{k = k_0 exp\left(-\frac{E}{RT}\right)} \qquad \textbf{(2.1)}$$

Activation energy is required for the reaction to take place due to two reasons; 1) in order to distort or break bonds so that new bonds can be formed and 2) to overcome the repulsion forces between reacting molecules so that they can collide and react (Fogler, 1999).

With reference to Equation 2.1, the reaction temperature can strongly increase the rate of the reaction depending on the magnitude of the activation energy. The rate can increase exponentially depending on the activation energy (Perry and Green, 1999). The rates of most reactions are enhanced by the addition of energy or the elevation of temperature. In general, it is assumed that the reaction rate is doubled for every 10˚C temperature increase. When temperature is increased, the reactant molecules gain kinetic energy and therefore a larger portion of the reactant molecules have energy exceeding the activation energy leading to a more rapid reaction rate. The higher kinetic energy also leads to the molecules moving at higher speeds which also leads to more frequent collisions and hence a higher reaction rate. Figure 2.1 shows the fraction of molecules with energy above or equal to the activation energy at two different temperatures (Masterton et al., 2012).

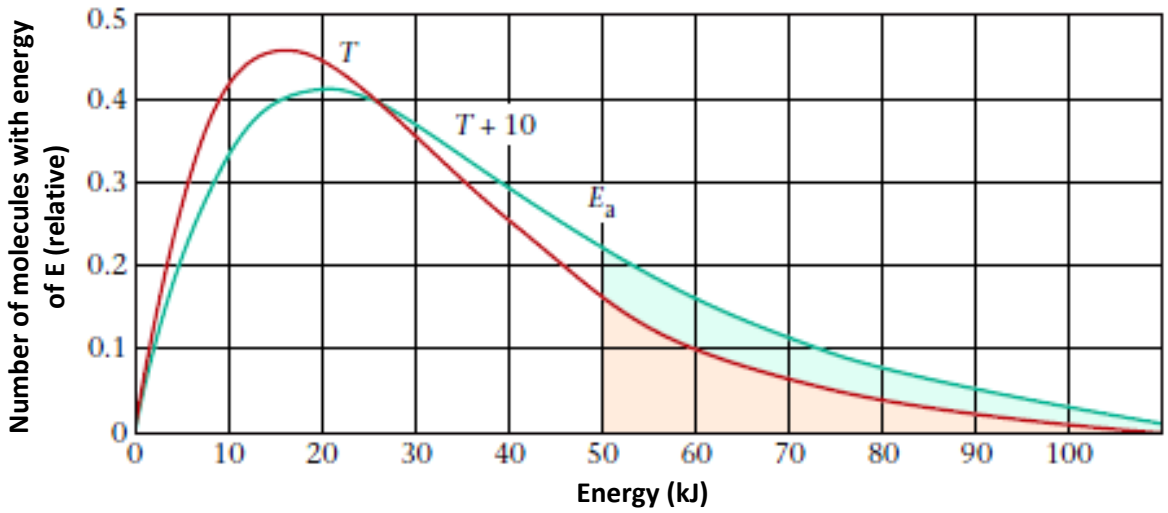

Figure 2.1: Distribution of kinetic energies of molecules at two different temperatures (Masterton et al., 2012)

2.3.3 Catalyst and reaction rate

A catalyst is a substance that is involved in the chemical reaction but is not consumed during the chemical reaction. The role of the catalyst is to lower the activation energy of the reaction by changing the reaction path (Masterton et al., 2012). Catalysis can be either heterogeneous or homogeneous. When a solid catalyst activates gaseous or liquid reactants it is considered as heterogeneous catalysis. Homogeneous catalysis in considered as the catalytic reaction where the catalysts as well as the reactants are in the same phase i.e. usually in the gas or more commonly liquid phase (Chorkendorff and Niemantsverdriet, 2003). Figure 2.2 compares the activation energy of a catalysed and non-catalysed reaction (Masterton et al., 2012).

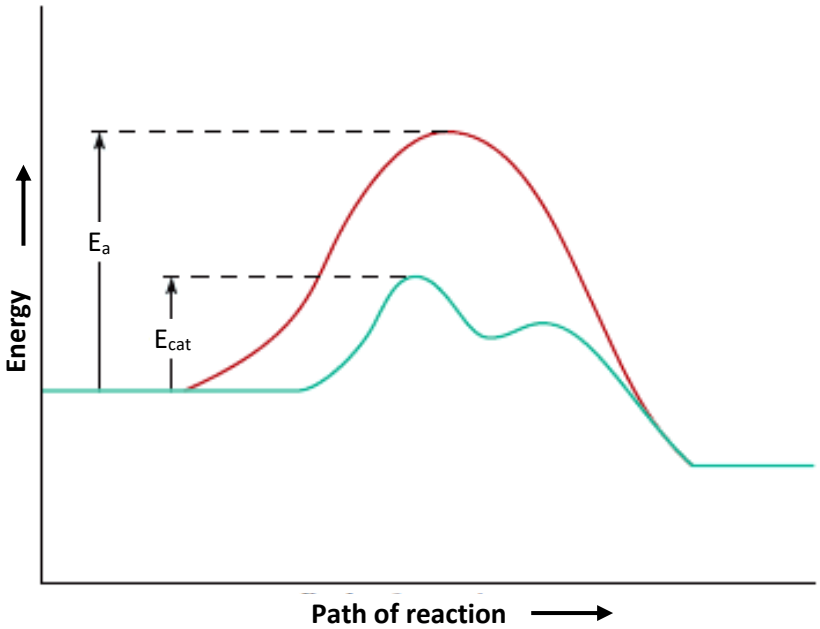

Figure 2.2: Activation energies of a catalysed and non-catalysed reaction (Masterton et al., 2012)

Catalytic processes have the drawback of catalyst deactivation. Catalyst deactivation occurs over time and causes the loss of catalytic activity and thereby a lower reaction rate (Argyle and Bartholomew, 2015).

2.3.3.1 Catalyst deactivation

Catalyst deactivation as stated in section 2.3.3 is the loss of catalytic activity over time caused by the degradation of the active surface of the catalyst by either thermal, chemical or mechanical factors. Chemical deactivation occurs due to poisoning or masking by the feed or product components (Perry and Green, 1999). The different forms of chemical deactivation are:

- Poisoning is caused by compounds that have free electron pairs that irreversibly bond to the catalyst causing a loss in active sites (Perry and Green, 1999).
- Masking is caused by the chemisorption of feed or product species onto the catalyst resulting in lower catalytic efficiency due to the loss of active sites (Perry and Green, 1999; Argyle and Bartholomew, 2015).
- Vapour formation: Dispersed metals, metal oxides, -sulphides and -carbides have similar bulk and surface compositions which lead to catalytic phases. For given reactions however one of these phases are substantially more catalytic. The loss of catalytic activity is observed when these metals are oxidized, carbided or sulphided (Argyle and Bartholomew, 2015).

Mechanical deactivation can be caused by two methods:

- Attrition is caused by the loss of catalyst by fines due to abrasion resulting in the loss of surface area (Argyle and Bartholomew, 2015; Perry and Green, 1999).
- Fouling occurs as species in the fluid are deposited on the catalyst surface or into catalyst pores also resulting in the loss of surface area (Argyle and Bartholomew, 2015).

Thermal deactivation occurs by the rearrangement of active sites at elevated temperatures due to sintering. This causes the loss of surface area by the agglomeration of active ingredients in the catalyst (Perry and Green, 1999; Argyle and Bartholomew, 2015).

Catalyst deactivation can be costly to the process and is more easily prevented rather than cured. Care should be taken to feed the catalyst with a pure reactant solution, if possible, to minimize deactivation and prolong the lifespan of the catalyst (Argyle and Bartholomew, 2015).

2.3.4 Reaction mechanism and reaction rate

The reaction mechanism is a sequence of steps that is followed by the reactants at a molecular level to describe how the reaction is taking place. The mechanism can be very simple where only a single step is followed or it can be very complex where multiple steps occur before the reaction is completed. The complexity of the reaction mechanism determines the rate of the reaction. Elementary steps are the individual steps that constitute the reaction mechanism. Temperature and in some cases, pressure can affect the mechanism of a reaction and thereby affect the rate of a reaction. the most complex elementary step is known as the rate limiting or rate determining step. A graphical representation of how one elementary step can affect the rate of a reaction by acting as a rate limiting step is presented in Figure 2.3 (Masterton et al., 2012).

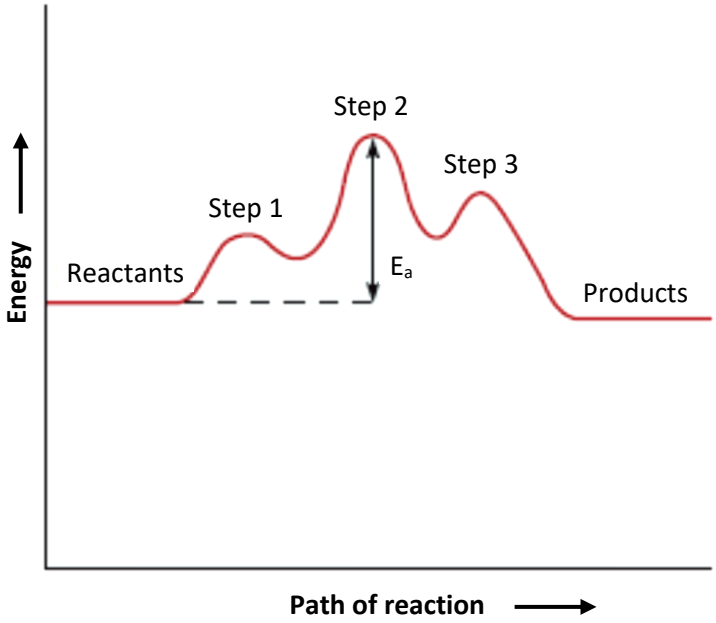

Figure 2.3: Reaction plot for a three-step reaction mechanism, adapted from (Masterton et al., 2012)

2.4 Porous media

A porous medium consists of a solid structure with regular or irregular void spaces that are distributed throughout the structure. These void spaces can be interconnected or not and the pores serve as elements for the void spaces. Irregularly shaped porous media are described by volume averaging (Bejan et al., 2004). The porous medium is characterised by the way the holes are imbedded, their interconnection, their location, size and shape. Porosity is the quantitative property that describes the fraction of the medium that is void and the effective porosity is the portion of the medium (pores) that contributes to flow (Greenkorn, 1981).

Modern technologies rely on the flow through small-scale complex passages and therefore designed porous media have been engineered. These media have purposefully designed

structures with specific size, shape and connections for specific applications (Bejan et al., 2004).

2.4.1 Flow through porous media

The matrix of a porous medium is the material in which the pores are imbedded and the properties of the matrix that affect the flow are used to characterize the porous media. Pseudotransport properties are used to describe the flow properties of the matrix and are (Greenkorn, 1981):

- Permeability – the conductance of the medium
- Dispersion – mixing caused by the meandering paths in the medium
- Capillary pressure – interfacial force due to the surface

Darcy's law is an empirical relationship that is used to relate the volumetric flow rate ($\dot{Q}$) of a fluid flowing linearly through a porous medium to the energy loss ($h_1 - h_2$), the length of the medium (Δl) and the hydraulic conductivity (K). Darcy's law is however only applicable to creeping flow where the Reynolds number is less than one and it is expressed as in Equation 2.2 (Darcy, 1856):

$$\dot{Q} = \frac{K * A * (h_1 - h_2)}{\mu * \Delta l} \quad (2.2)$$

Fluid flow through a bed is determined by the continuity equation utilizing superficial velocity (empty tube velocity). The superficial velocity (U_0) is the volumetric flow rate (Q) through the bed divided by the bed cross-sectional area (A). The presence of particles and reduction in area forces the velocity within the bed (interstitial velocity U) to be greater than the superficial velocity to preserve the fluid continuity. The superficial velocity is dependent on the porosity of the bed and can be determined by Equation 2.3. The interstitial velocity is equivalent to the velocity term in the Reynolds number relation, $U = u$ (Holdich and Todd, 2002).

$$U_0 = \frac{U}{\emptyset} \quad (2.3)$$

The consideration of energy losses from the fluid due to drag and viscous forces is critical in fluid flow. The Reynolds number (Equation 2.4) is adapted to a porous medium by determining the superficial velocity (U_0) and an adapted linear dimension term (d) (Equation 2.5) to give rise to the modified Reynolds number (Re_1), Equation 2.6, which accounts for the additional drag forces caused by turbulent flow (Holdich and Todd, 2002).

$$Re = \frac{\rho * u * d}{\mu} \quad (2.4)$$

$$d = \frac{\emptyset}{(1 - \emptyset) * S_V} \quad (2.5)$$

$$\boldsymbol{Re_1 = \frac{\rho * U_0}{(1-\emptyset) * S_V * \mu}} \quad \textbf{(2.6)}$$

The specific surface area can be specific either to the mass or the bulk volume of the bed. The specific surface area (S_V) as expressed in Equation 2.6 is specific to the bulk volume of the bed and is in units of (m^2/m^3).

2.4.2 Synthetic filters

Modern synthetic fabrics are typical examples of porous media developed to solve industrial filtration problems. These fabrics could be woven or non-woven. Chemical and mechanical properties of interwoven fibres are the sole contributor to the tensile strength and the tear resistance of the membranes. The fibre's structure also plays a crucial role in easing the flow through the membrane but yet preventing solid particles from passing (Rollin et al., 1982).

2.4.3 Determination of porosity

Porosity is dependent on the volume of the solid porous material and the volume of the pores imbedded in the medium. The amount of water present in rocks is important to many geotechnical practices. The water content is determined on a volume or mass basis (Huang et al., 2011; Harriott, 2002).

The water content on a mass basis is related to the oven dried soil sample. The following relationship is used to determine the water content (Huang et al., 2011; Harriott, 2002):

$$\boldsymbol{\theta_m = \frac{wet\ mass}{dry\ soil\ mass} = \frac{(wet\ soil\ mass) - (dry\ soil\ mass)}{dry\ soil\ mass}} \quad \textbf{(2.7)}$$

On a volume basis the volume water content is expressed per bulk volume of soil according to the expression (Huang et al., 2011):

$$\boldsymbol{\theta_v = \frac{volume\ of\ water}{bulk\ volume\ of\ soil} = \frac{mass\ of\ water / density\ of\ water}{sample\ volume}} \quad \textbf{(2.8)}$$

The surface area of a solid material can also be determined by the Brunauer-Emmett-Teller (BET) method by the nitrogen adsorption isotherm. A continuation of the adsorption leads to the pores filling by capillary condensation giving a pore volume per unit mass of solid material (Harriott, 2002)

2.5 Types of reactors

Chemical reactors may be classified by their mode of operation, by end use or by phase of operation. Batch reactors, continuous flow reactors and semi-batch reactors are classified by the mode of operation. Batch reactors are fed with a once off amount of reactants and operated at desired conditions until the desired conversion is achieved. Batch systems consist of tanks where stirring is achieved by some mechanical process and temperature is regulated by internal cooling. The composition inside the reactor is uniform but continuously

changes over time as the reaction continuous. These reactors are suited for long reaction times and small production rates (Perry and Green, 1999; Levenspiel, 1999).

In continuous reactors, reactants are added continuously and products are removed continuously from the reaction area at a constant mass flow rate. Different types of continuous reactors are being used depending on the desired product and flow patterns. Reactions in continuous reactors occur at steady-state. Continuously-stirred tank reactors (CSTR) or mixed flow reactors are batch reactors that have a continuous feed and product stream (Levenspiel, 1999; Perry and Green, 1999).

Tubular reactors have a continuous flow of reactants which are continuously being converted to products in a cylindrical pipe. In a tubular reactor, a concentration gradient exists in the direction of flow. The flow in this reactor may be horizontally or vertically and the diameter of the tube may also vary. If heat transfer is required the setup may be such that the tubes are situated inside a shell where heating or cooling takes place. A heterogeneous catalyst may be added in the tubular reactor for catalytic reactions resulting in a catalytic reactor (Perry and Green, 1999).

2.5.1 Tubular reactors

Tubular reactors consist of two forms, the plug flow reactor (PFR) and the packed bed reactor (PBR) and are mostly used, but not limited to gas-phase reactions. The main difference between the plug flow reactor and the packed bed reactor is that the PFR houses a homogeneous reaction between reactants and the PBR contains a fixed bed of a heterogeneous catalyst resulting in a catalytic reaction that occurs on the surface of the catalyst (Fogler, 1999).

When modelling tubular reactors these assumptions are made; 1) the concentration varies continuously along the length of the reactor, 2) there is no radial concentration gradient, 3) there is no variation in the reaction rate along the length of the reactor and 4) uniform velocity. The reaction rate for the PBR is based on the mass of catalyst used in the reactor. Equation 2.2 represents the design equation for a PBR under isobaric conditions, where (F_{A0}) is the molar flow rate of species A entering the reactor, (X) is the conversion of A to products, (W) is the mass of catalyst used and ($-r_A$) is the reaction rate in (mole of A reacted/s·g catalyst) (Fogler, 1999).

$$\boldsymbol{W = \rho_{catalyst} * V = F_{A0} \int_{X_{in}}^{X_{out}} \frac{dX}{-r_A}} \qquad \textbf{(2.9)}$$

The PBR can be modelled assuming pseudo-homogeneous conditions i.e. modelling the reactor to determine the volume required and ignoring the presence of a catalyst. Thereafter, using the volume determined and the catalyst density to determine the mass of catalyst required. For a liquid flow system, the volumetric flow rate entering and leaving the reactor is

equal and therefore $\boldsymbol{v = v_0}$. Equation 2.3 describes the design equation available to model a PBR, where ($\rho_{catalyst}$) is the density of the catalyst, (V) is the volume of the reactor required, ($\boldsymbol{k}$) is the reaction rate constant and ($\boldsymbol{v_0}$) is the volumetric flow rate of the reactants (Fogler, 1999).

$$\boldsymbol{W = \rho_{catalyst} * V = \frac{v_0}{k} * \ln(1 - X)} \quad \textbf{(2.10)}$$

2.6 Reactor design

A chemical reactor is a piece of equipment of a controlled volume in which a chemical reaction can occur between one or more reactants in a safe and controlled environment (Perry and Green, 1999). Reactor design requires knowledge and experience from a variety of areas of mass and heat transfer, chemical kinetics, thermodynamics, fluid mechanics and economics (Levenspiel, 1999). In a chemical reactor, there are essential aspects that need consideration. These aspects may be, flow distribution and residence time, appropriate mixing, reactant-reactant contact or reactant-catalyst contact, control of heat (addition or removal) and integration of the reactor with the downstream process. Various types of reactors are used in multiple industries depending on the raw material or desired product (Perry and Green, 1999).

2.6.1 Space time

According to Fogler (1999), the space time is the time required for one reactor volume to be processed based on the entrance conditions. It is also known as the holding time. It is determined by using the volume (V) of the reactor and the volumetric flow rate ($\dot{Q}$) entering the reactor. The space time (τ) is calculated using Equation 2.11 (Fogler, 1999):

$$\boldsymbol{\tau = \frac{V}{\dot{Q}}} \quad \textbf{(2.11)}$$

In the absence of dispersion, it is said that the space time is equal to the mean residence time (t_m). The mean residence time is the average time the molecules spend in the reactor and therefore Equation 2.11 becomes:

$$\boldsymbol{\tau = t_m = \frac{V}{\dot{Q}}} \quad \textbf{(2.12)}$$

2.6.2 Scale-up considerations

From the bench scale process, specific steps should be considered to ensure a successful scale up. Three key issues need to be addressed to ensure a successful scale up (Wood-Black, 2014):

1. Outlining the general process
2. Inclusion of safety and environmental controls
3. Development of the processing guidelines and operating system

Parameters such as temperature, pressure, mixing and timing of the reaction should be evaluated and met in the pilot plant scale. Other considerations are the material of construction. When a different material is used in the pilot plant, it could affect the nature of the reaction. From an economic perspective, a different construction material could determine the feasibility of the process on an industrial scale. The engineering of the human side of the process is as crucial as the physical side of the process. In a scaled up system, integrated control systems may have to be added and ultimately operators and technicians with the relevant skills are required to look over the process to ensure successful operation of the process (Wood-Black, 2014).

2.7 Textile wastewater industry

Industrial dyeing houses use extreme amounts of water and energy during the treatment processes of pre-treatment, dyeing, printing and finishing. Water is used in the form of steam to heat the pre-treatment baths, contributing to the high energy consumption and then water is used to transfer the dye to the material. Not only does this industry have a significant impact on the use of fresh water resources, but it also contributes to a considerable amount of chemical pollution (Allègre et al., 2006; Lin and Chen, 1997; Dos Santos et al., 2007). The dyed effluent prevents the penetration of sunlight and thereby increases biological oxygen demand (BOD) in water impacting aquatic life negatively (Dos Santos et al., 2007). It is estimated that worldwide about 10^6 tonnes of dyes are produced annually with 70% being azo dyes and more than 8000 chemical products are coupled in the dyeing process (Banat et al., 1996; Zollinger, 1987). The different chemicals include acid, reactive, basic, disperse, azo, diazo, anthraquinone-based and metal complex dyes which have different chemical structures (Banat et al., 1996). Cotton is the most dyed textile and is dyed using reactive dyes which are also the type of dyes that cause high colour concentrated wastewater including high levels of salts and COD (Allègre et al., 2006). Several types of dyes are used to dye different types of textile materials. Table 2.1 gives a summary of the volumes of water utilized for the dyeing of different textile materials (Moustafa, 2008):

Table 2.1: Average water consumption for dyeing of various textile materials (Moustafa, 2008)

Processing subcategory	Water consumption (m^3/ton fibre material)		
	Minimum	Median	Maximum
Wool	111	285	659
Woven	5	114	508
Knit	2	84	377
Carpet	8.3	47	163
Stock/yarn	3.3	100	558
Nonwoven	2.5	40	83
Felted fabric finishing	33	213	933

Dyes are classified according to their chemical structure and the implementation. The group of atoms responsible for the dye colour is called the chromophores. Some of the major chromophores are (Christie, 2001; Welham, 2000):

- Azo (-N=N-)
- Carbonyl (-C=O)
- Methine (-CH=)
- Nitro ($-NO_2$)
- Quinoid groups

Along with the chromophores are atomic groups that are electron donating or electron withdrawing substituents, responsible for the intensity of the colour of the chromophores and these groups are called the auxo chromes. Some of the most important auxo chromes are:

- Amine ($-NH_3$)
- Carboxyl (-COOH)
- Sulfonate ($-SO_3H$)
- Hydroxyl (-OH)

Figure 2.4 is an illustration of the structures of different dye molecules as presented by (Dos Santos et al., 2007):

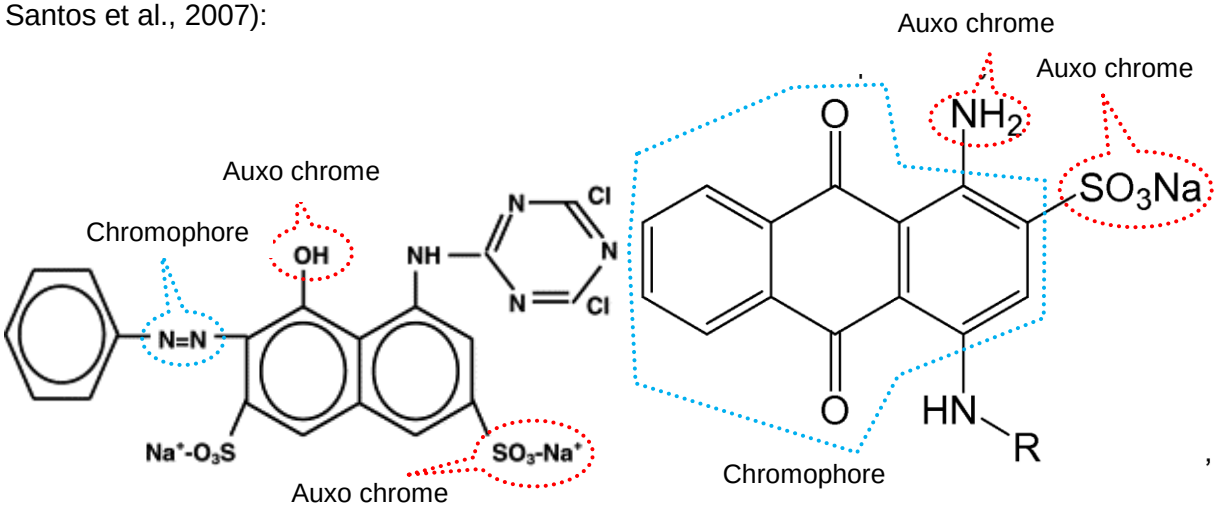

Figure 2.4: Chemical structures of two dye molecules illustrating the dye chromophores and auxo chromes of an azo dye (left) and an anthraquinone dye (right) (Dos Santos et al., 2007)

2.7.1 Treatment of dye containing wastewater

Dyes are difficult to treat due to their complex aromatic structures and their synthetic origin. The structures are designed to withstand fading when exposed to sweat, soap, light, water and oxidizing agents (Banat et al., 1996). The decolouration of textile wastewater polluted with organic colorants occurs on the reduction of –C=C- bonds, -N=N- bonds and heterocyclic and aromatic rings that make up the dye structures (Slokar and Majcen Le

Marechal, 1998). Different treatment methods, such as chemical and physical methods, have been employed for the treatment of textile wastewaters. These methods however involve inflated cost and are not favoured due to safety concerns (Buthelezi et al., 2012; Allègre et al., 2006).The textile effluent discharged from dye houses undergoes a three step treatment process (Ghaly et al., 2014):

1. Primary treatment: this step involves the removal of suspended solids such as some oil and grease, gritty materials and textile fibres such as yarn, lint and pieces of fabric. These suspended solids are removed by coarse screening (≥ 6 mm) followed by fine screening (1.5 – 6 mm) and very fine screening (0.2 – 1.5 mm). Settling by coagulation follows the screening process to remove colloidal particles after their surface properties have been changed. The addition of chemicals causes the particles to agglomerate and become heavier thereby settling to the bottom. Mechanical flocculation follows the settling step causing more small particles to clump and form larger particles to settle and be removed as sludge (Ghaly et al., 2014).
2. Secondary treatment: removal of the remaining oil, reduction of BOD and control of colour using biological treatment processes. The biological treatment process is done under aerobic and anaerobic conditions. Aerobic treatment occurs under oxygenated conditions where aerobic bacteria convert sludge into CO_2 biomass and water. Anaerobic treatment occurs in the absence of oxygen with anaerobic bacteria that breakdown sludge into biomass, CH_4 and CO_2 (Mittal, 2011). The secondary treatment can also be done by the utilization of membrane processes (microfiltration, nanofiltration and ultrafiltration).
3. Tertiary treatment: removal of the final contaminants by electrodialysis, reverse osmosis and ion exchange (Ghaly et al., 2014). AOPs such as photocatalysis and catalytic oxidation via the Co_3O_4/PMS system are also a tertiary treatment method (Saputra et al., 2017).

Physical treatment methods include different precipitation methods such as flocculation, coagulation and sedimentation; adsorption by activated carbon; filtration and membrane processes such as reverse osmosis (Allègre et al., 2006; Chollom et al., 2015). Chemical treatment methods involve the use of oxidizers such as hydrogen peroxide and ozone but provide for the financial benefit of their unselective behaviour of the oxidizing species. Biological treatment methods make use of aerobic and anaerobic biological oxidation (Scott and Ollis, 1995). The biological methods have the disadvantage of stunted microorganism growth due to the presence of toxic metals in effluent water and the long retention time for efficient treatment (Ghaly et al., 2014).

2.7.2 Physical treatment

Flocculation separation is a physical treatment method widely used in Germany. It involves the use of a flocculent for the removal of organic substances and to remove insoluble dyes from wastewater (Allègre et al., 2006). The disadvantage with flocculation is that the pollutant is simply separated from the aqueous phase into a secondary pollutant requiring further treatment (Scott and Ollis, 1995). The secondary pollutant generation causes economic concern and the limitations on the disposal of such sludge make it an unappealing method (Allègre et al., 2006; Scott and Ollis, 1995).

Another physical treatment process is the use of activated carbon for adsorption of organic pollutants. The major concern with such a process is the cost of activated carbon and the rapid plugging of the filter by suspended solids (Allègre et al., 2006). Adsorption is therefore a process that must be used in combination with a flocculation process as a pre-treatment stage in order to have a low colour decrease. The reactive dyes have a high water solubility and low electron affinity to these adsorbents making the adsorption process inefficient (Arslan et al., 2000).

Membrane processes such as ultrafiltration, microfiltration and nanofiltration have shown great potential amongst the physical treatment processes (Allègre et al., 2006). Ultrafiltration however has shown the most potential for separation of colour from wastewater. Membranes are exposed to pollutants and the tendency of the organic compounds to adsorb to the membrane causes a rapid decline in permeate flux (Zaghbani et al., 2007). According to Giwa and Ogunribido (2012), the nanofiltration process generates secondary sludge from the nanofiltration concentrate which requires further treatment and also has the drawback of high energy requirements due to the high feed stream pressure that is required to drive permeating components across the membranes for efficient separation.

2.7.3 Biological treatment

The use of biological treatment involves the use of microorganisms to reproduce the natural environment of aquatic self-cleaning (Allègre et al., 2006). Microorganisms such as fungi and bacteria are used under aerobic or anaerobic conditions to degrade dyes. The low biodegradability of the dyes however leads to a low efficiency in the biological treatment process (Allègre et al., 2006; Dos Santos et al., 2007) Textile dyes contain substantial amounts of organic compounds which are hard to degrade under aerobic conditions. Anaerobic conditions however are fitting to degrade such organic substances but are then reduced to carcinogenic agents. The major disadvantage in biological treatment is that the presence of toxic metals halts the efficient growth of microorganisms and the long time periods involved in the treatment process (Ghaly et al., 2014).

2.7.4 Chemical treatment

The use of chemicals to induce the decolouration of textile wastewater is known as chemical treatment. Chemical treatment methods involve reduction, oxidation, ion exchange, neutralization and complexiметric methods (Slokar and Majcen Le Marechal, 1998). The use of ozone, H_2O_2 and permanganate (MnO_4) are the most common oxidizers used in the oxidation of chemicals such as dyes (Metcalf, 2003). High cost of ozone and the low colour and COD removal by conventional chemical oxidation has brought forward the development of advanced oxidation processes (AOPs) (Hassan and Hawkyard, 2002; Anjaneyulu et al., 2005).

2.8 Advanced oxidation processes

Past research has suggested that the pollutants not destructible by biological treatment methods are characterised as highly stable and resistant to complete mineralization. Advanced oxidation processes are the result of research suggesting that a special class of oxidation methods had to be developed to treat these stable pollutants (Andreozzi et al., 1999). AOPs were first suggested for the treatment of drinking water in the 1980s and were later studied for the treatment of different wastewaters. The process of advanced oxidation involves two steps: 1) the formation or generation of a strong oxidant species and 2) the reaction of these oxidants with the organic or inorganic pollutants (Kommineni et al., 2000).

Common oxidants such as chlorine and ozone have binary functions of decontamination and disinfection whereas AOPs are utilized for the destruction of organic or inorganic contaminants in wastewater (Deng and Zhao, 2015). These processes involve the use of oxidizers such as ozone and H_2O_2 along with catalysts for example Fe, Mn and TiO_2 to produce free hydroxyl radicals (HRs) (Anjaneyulu et al., 2005; Dos Santos et al., 2007). The HRs are exceptionally reactive and have very low selectivity making them a good oxidant for the treatment of wastewater. HRs have high rate constants ranging from 10^6 to 10^9 $M^{-1}s^{-1}$ (Andreozzi et al., 1999).

The popularity of the AOPs is derived from their ability to treat effluent and leave little to no waste products behind. Radical species are generated by chemical, electrical, mechanical or radiation energy through the reduction of an electron donor (Kommineni et al., 2000). AOPs are classified under (Ghaly et al., 2014):

- chemical,
- photochemical,
- catalytic,
- photocatalytic,
- mechanical

- electrical processes

2.8.1 Fenton and photo-Fenton process

Several AOPs have been evaluated for the degradation of dye wastewater by the formation of HRs. The Fenton process is one such method whereby Fe^{2+} ions catalyse H_2O_2 in an acidic solution to produce HRs (Dos Santos et al., 2007). The Fenton reaction is very popular due to the abundance and nontoxic nature of iron as well as the use of environmentally safe H_2O_2 (Andreozzi et al., 1999).

$$Fe^{2+} + H_2O_2 \rightarrow Fe^{3+} + OH^- + OH^\bullet \quad \textbf{(2.13)}$$

The photo-Fenton process is an advancement of the Fenton process by utilization of ultraviolet light. Organic pollutant degradation is enhanced by the addition of UV light. The UV light allows for the photolysis of Fe^{3+} to regenerate Fe^{2+} ions to catalyse H_2O_2 for HR production (Andreozzi et al., 1999). In addition to the Fenton reaction, the photo-Fenton reaction (2.2) produces HRs by the following two reactions (Lucas and Peres, 2006):

$$H_2O_2 + UV \rightarrow OH^\bullet + OH^\bullet \quad \textbf{(2.14)}$$

$$Fe^{3+} + H_2O + UV \rightarrow Fe^{2+} + OH^\bullet + H^+ \quad \textbf{(2.15)}$$

In 2002, Perez et al. studied the degradation potential of the photo-Fenton reaction by treating textile bleaching effluents in the presence of UVA light. The maximum TOC reduction achieved in the study was 40% in a period of 2 hours. H_2O_2 dosage was 1000 mg/L and Fe^{2+} concentration was 100 mg/L (Pérez et al., 2002).

Lucas and Peres (2006) and Meric et al. (2004), studied the efficiency of the Fenton and photo-Fenton process by the treatment of Reactive Black 5 (RB5) (Lucas and Peres, 2006; Meriç et al., 2004). Lucas and Peres treated a 500 ml RB5 solution at a concentration of 0.1 mmol/L with 0.73 mmol/L H_2O_2 and 0.15 mmol/L Fe^{2+}. After 30 minutes, both the Fenton and photo-Fenton treatment achieved a maximum dye degradation of 97.5% and 98% respectively. The study also investigated the TOC removal and in a period of 60 minutes, the Fenton and photo-Fenton process achieved 46.6% and 21.6% respectively, Reactive Black 5 concentration of 0.1 mmol/L. It was concluded from the study that the optimum H_2O_2 concentration to Reactive Black 5 concentration was 9.6:1 at an optimum pH of 3 (Lucas and Peres, 2006). Meric et al. (2004) treated the dye in a 500 ml reactor using the Fenton's oxidation process with $FeSO_4$ as a source for Fe^{2+} ions. Dye concentrations were set at 100 mg/L and 200 mg/L. The optimum treatment achieved was 98% colour removal and 76% COD removal over a 50 minute time period with 100 mg/L $FeSO_4$, 400 mg/L H_2O_2 at a pH of 3 and temperature of 40˚C. It was also obtained that the optimum molar ratio for $FeSO_4/H_2O_2$ is 0.055 (Meriç et al., 2004).

Kang et al. (2002) investigated the Fenton's reaction for the degradation of Reactive Blue dye R94H. For the optimum treatment the dosage of Fe^{2+} and H_2O_2 were 20 mg/L and 10 mg/L respectively. A colour removal of 95% was achieved in a short time period of 1 minute when the Reactive Blue concentration was 20 mg/L (Kang et al., 2002).

Arslan et al. (2000) studied the effect on synthetic dye degradation via two different methods 1) ferrioxalate-Fenton/UV-A process and 2) TiO_2/UV-A process. In both cases synthetic dye house effluent containing a mixture of Procion H dyes was used. For the ferrioxalate-Fenton process the maximum TOC removal efficiency was about 23%, with a H_2O_2 dosage of 5 mmol, over a 60 minute period. The TiO_2/UV-A photocatalytic process achieved a mere 17% TOC removal in a 60 minute period (Arslan et al., 2000).

Feng et al. (2003) studied the photocatalytic efficiency of laponite RD clay-based Fe nanocomposite by the degradation of Reactive Red HE-3B. In a typical test, 1.8 L of HE-3B was (100 mg/L) was treated using 555 mg/L with 500 mg/L H_2O_2 as an oxidizer at a controlled pH of 3. The maximum dye breakdown achieved was 100% in 30 minutes of reaction time. The maximum TOC removal achieved was 77% in a 120 minute time period (Feng et al., 2003).

The homogeneous photo-Fenton process has a distinct disadvantage which limits its industrial application. The formation of secondary iron containing waste/sludge is costly, needs further chemical treatment and requires many staff members (Feng et al., 2003; Andreozzi et al., 1999). Another disadvantage of such a process is the very precise pH control that needs to be employed to make the process efficient (Andreozzi et al., 1999).

2.8.2 Photocatalytic processes

A second process is the UV/H_2O_2 process where the UV light forms HRs by the photolysis of H_2O_2 (Metcalf, 2003). The use of the UV-based methods catalysed by semiconductor materials such as TiO_2 and an oxidizer is another popular AOP (Grzechulska and Morawski, 2002). The UV-based methods have also been explored using solar energy for the excitation of semiconductors (Wang, 2000).

Combinations of such methods have been explored and are listed below (Galindo et al., 2000):

- Ozone/TiO_2
- Ozone/TiO_2/H_2O_2
- TiO_2/H_2O_2

Photocatalysis via TiO_2-based photocatalysts has gained massive interest in the early 1990's in the application of environmental clean-up, specifically in the destruction of organic

pollutants in air and wastewater. Photo induced chemical reactions take place at the surface of the catalyst producing HRs that lead to the destruction of organic pollutants (Linsebigler et al., 1995). Electrons in the valence band are excited into the conduction band of the semiconductor leaving a positively charged hole in the valence band. The positively charged holes react with hydroxide ions or the electrolyte to produce the powerful HRs for the oxidation of organics. TiO_2 is inexpensive, insoluble, non-toxic and has a very reactive nature under UV light irradiation which makes it a very attractive semiconductor for dye containing wastewater treatment (Tang and Huren, 1995).

Photocatalytic degradation for wastewater treatment is mostly based on slurry systems and immobilized systems in the batch form. Slurry systems have the disadvantage of low light penetration due to the reflection by catalyst particles as well as difficult catalyst separation from the treated solution. For these reasons, more research has been focussed on the immobilization of the catalyst in immobilized photoreactors (Royaee et al., 2012; Rezaei et al., 2014; Du et al., 2008; Meshram et al., 2011).

Considering the above-mentioned recommendations, Rezaei et al. (2014) designed a continuous flow photocatalytic reactor. The design of the photoreactor is based on the concept of a shell and tube heat exchanger where the baffles diverting the flow are coated with P-25 TiO_2. Four UV-C lamps are housed in the quartz tubes and aluminium housing acts as the shell. The optimized system conditions were evaluated to be a flow rate of 2.53×10^{-7} m^3/s (recycle flow 7×10^{-7} m^3/s) with an immobilized catalyst loading of 17.6 g/m^2 (BET specific surface area 47.2 m^2/g).

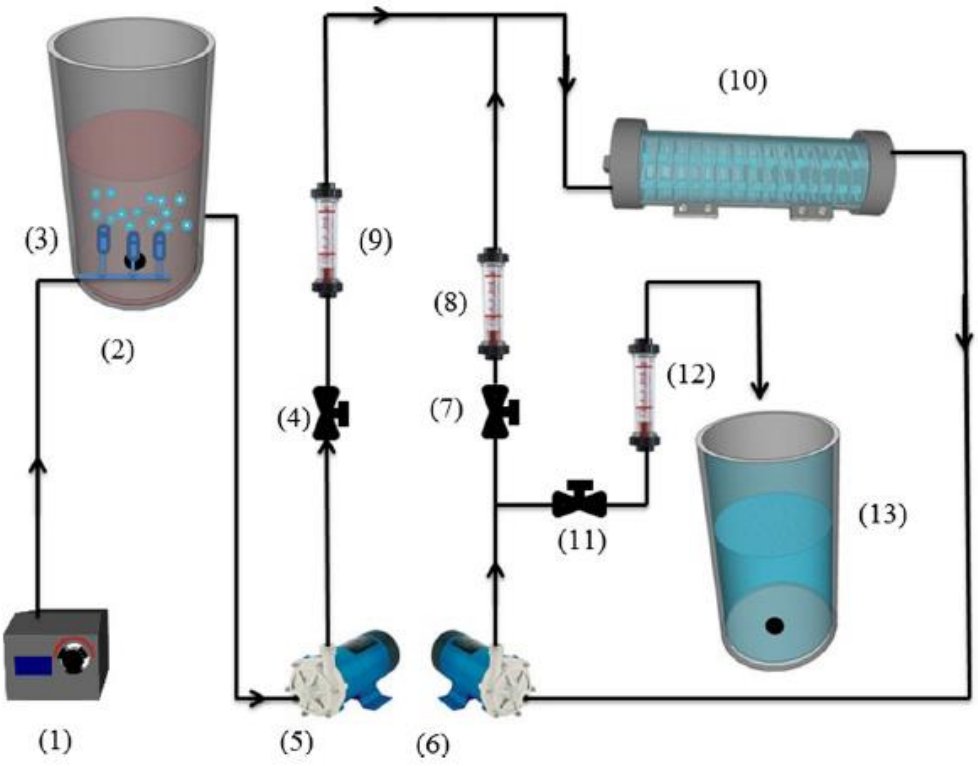

Figure 2.5: Experimental set-up of the annular baffle type photoreactor designed by (Rezaei et al., 2014)

The catalyst was immobilized using a standard coating method known as 'spray painted method'. Phenol was used as an organic pollutant at a concentration of 20 mg/L. A phenol degradation of 73.7% was achieved at a pH of 6.41 and optimized conditions. Furthermore a 47% TOC removal was achieved under the optimized conditions. Figure 2.5 is the experimental set-up of a continuous flow reactor where: (2) is the feed tank, (3) air distributor, (4) inlet valve, (5) feed pump, (6) recycle pump, (7) recycle flow valve, (10) photocatalytic reactor and (13) product container (Rezaei et al., 2014).

Referring to Table 2.2, the reactors designed by Rezaei et al., (2014), Dionysio et al., (2000), Meshram et al., (2011) and Zhang et al., (2003) show potential for the treatment of wastewater by the photocatalytic process. Although these reactors were successful in treating the wastewater, they were developed without the consideration of fundamental reactor design equations highlighting the complexity of the advanced oxidation process.

These parameters were comparable to studies done by (Dionysiou et al., 2000), (Meshram et al., 2011), and (Zhang et al., 2003) and are summarized in the Table 2.2.

Table 2.2: Comparison of continuous flow photoreactors

Reference	Rezaei et al., (2014)	Dionysiou et al., (2000)	Meshram et al., (2011)	Zhang et al., (2003)
Photoreactor	Annular baffle type photoreactor	Rotating disk photoreactor	Continuous flow stirred tank reactor	Circulating photocatalytic tube reactor (5L)
Catalyst	P-25 TiO_2 17.6 g/m^2	TiO_2 (99 % anatase) 141200 g/m^2	ZnO-bentonite 330 g/m^2	Pt-loaded TiO_2 0.114 g/m^2
Pollutant (mg/L)	Phenol at 20 mg/L	2,4,6-TCP at 25 mg/L	Phenol at 2000 mg/L	Phenol at 10 mg/L
Product flow rate (ml/min)	15.18	13.86	10.02	55.56
pH	6.41	7.0	12.0	Not stated
Irradiation	4 x 16 W UV lamps	4 x 15 W UV lamps	Spectroline UV lamp	30 W UV mercury lamp
% degradation	Phenol: 74.7% TOC: 47%	2,4,6-TCP: 83.1%	Phenol: 66%	Phenol: 100%
Reaction time (min)	3600	Not stated	10	90
Immobilization technique	Spray painted method	Permatex Blue RTV 5240 adhesive	Bar coating with an epoxy resin	Primary water-glass film, secondary Pt-TiO_2 spray gun

2.8.3 Sulfate radical formation in AOPs

AOPs have gained attention due to their high oxidation potential and the ability to treat all organic components in textile wastewater. Hydroxyl radicals are formed using oxidizers such as H_2O_2 and ozone and are the most popular radical species (Ghaly et al., 2014; Sun and Wang, 2015), but in recent years sulfate radical ($SO_4^{\bullet-}$) based AOPs have gained attention as an alternative to HRs for the oxidation process (Yang et al., 2009). Sulfate radicals (SRs) are preferred over HRs due to their high oxidation potential (SRs 2.5-3.1 V vs HRs 2.7 V) as well as their mother salts (HSO_5^-/HSO_4^- =1.82 V vs H_2O_2/H_2O = 1.76 V) and low selectivity nature making them more suitable for the mineralization of organic or inorganic pollutants than HRs (Yang et al., 2009; Deng and Zhao, 2015; Saputra et al., 2017).The high efficiency in a wide pH range makes them a very popular alternative to HRs (Sun and Wang, 2015). The

formation of SRs springs from the activation of persulfate or peroxydisulfate ($S_2O_8^{2-}$) by heat, UV or metal oxides/ions. They can however also be generated by the activation of peroxymonosulfate (PMS) that is commercially available as a triple salt in the form of $2KHSO_5$-$KHSO_4$-K_2SO_4 known as Oxone® (Sun and Wang, 2015).

According to Sun and Wang (2015) the PMS ion (HSO_5^-) is more stable in water than H_2O_2 and has a more reactive nature. It is also more easily activated than persulfate and H_2O_2 and can produce SRs as well as HRs when activated following certain methods (Sun and Wang, 2015; Deng and Zhao, 2015; Wang et al., 2015).

$$Co^{2+} + HSO_5^- \rightarrow Co^{3+} + SO_4^{2-} + OH^{\bullet} \quad \textbf{(2.16)}$$

$$SO_4^{\bullet -} + H_2O \rightarrow OH^{\bullet} + SO_4^{2-} + H^+ \quad \textbf{(2.17)}$$

$$SO_4^{\bullet -} + OH^- \rightarrow OH^{\bullet} + SO_4^{2-} \quad \textbf{(2.18)}$$

2.8.4 Homogeneous activation of PMS

Sulfate radicals are produced through the homogeneous activation of PMS via metal ions and cobalt has proved to be the most efficient activator (Anipsitakis and Dionysiou, 2004). Homogeneous activation by metal ions was found to be more efficient than UV or visible light activation and proceeds by the following reactions (Sun and Wang, 2015; Anipsitakis et al., 2005).

$$Co^{2+} + HSO_5^- \rightarrow Co^{3+} + SO_4^{\bullet -} + OH^- \quad \textbf{(2.19)}$$

$$Co^{3+} + HSO_5^- \rightarrow Co^{2+} + H^+ + SO_5^{\bullet -} \quad \textbf{(2.20)}$$

Homogeneous activation using Co^{2+}, although highly efficient, was found to be detrimental as the heavy metal ions of cobalt are extremely toxic to human health as well as other living organisms (Sun and Wang, 2015; Lison, 1996).

Homogeneous catalysis is still used in many industries and is a technological advancement of the early 20th century. With the ever-increasing public awareness of the environmental impact and economical pressure of industries, homogeneous catalysts have become intolerable in the use of catalysis. Disadvantages such as corrosion, toxicity, difficulty of handling and recovery from the reaction system, high cost and generation of solid waste have made homogeneous catalysts unpopular in the modern industries (Zhao et al., 2006).

2.8.5 Heterogeneous activation of PMS

Due to the danger of cobalt ions, heterogeneous activation of PMS gained much popularity (Sun and Wang, 2015). When a solid catalyst activates gaseous or liquid reactants it is considered as heterogeneous catalysis (Chorkendorff and Niemantsverdriet, 2003). Heterogeneous catalysts are preferred over homogeneous catalysts due to advantages like ease of separation and recovery, regeneration and usability (Zhao et al., 2006).

Heterogeneous activation of PMS was first published by Anipsitakis et al., (2005) when they used CoO and Co_3O_4 powders as the heterogeneous source for cobalt. They established that the CoO was responsible for homogeneous activation due to leached cobalt. CoO was also assumed to be responsible for the heterogeneous activation of PMS but only in the bound form of Co_3O_4 (Anipsitakis et al., 2005). The most effective activation to date has been established to occur due to Co-OH complexes being formed by the dissociation of H_2O with Co^{2+}. This step is also regarded as the rate-limiting step in the activation of PMS (Shi et al., 2014; Hu and Long, 2016; Zhang and Edwards, 1992).

$$Co^{2+} + H_2O \rightarrow CoOH^+ + H^+ \quad \textbf{(2.21)}$$

$$CoOH^+ + HSO_5^- \rightarrow CoO^+ + H_2O + SO_4^{\bullet -} \quad \textbf{(2.22)}$$

$$CoO^+ + 2H^+ \rightarrow Co^{3+} + H_2O \quad \textbf{(2.23)}$$

2.9 Nanoparticles synthesis

The synthesis of nanoparticles can be done by several different methods. The methods are classified by the phases that the processes occur in i.e. gas, liquid or solid phase processes. Some examples are gas phase flame pyrolysis or high temperature evaporation; liquid phase chemical reactions forming colloids and solid phase mechanical grinding of milling (Nagarajan and Hatton, 2008).

2.9.1 Gas phase synthesis

In the gas phase synthesis, the approach relies on the homogeneous nucleation of a supersaturated vapour which is followed by further particle growth by condensation and coagulation. Supersaturation is typically achieved by heating and evaporating a solid into a carrier gas phase followed by cooling, a chemical reaction or a combination of cooling and a chemical reaction to form a supersaturated vapour. The supersaturated vapour then forms a nucleus in the gas phase homogeneously or it can heterogeneously nucleate by contact with a solid surface. The distribution of particle sizes and morphologies are dependent on the nuclei growth by collisions and condensation (Nagarajan and Hatton, 2008).

2.9.2 Colloidal methods

The colloidal method utilizes the process of precipitation where under controlled temperature and pressure a mixture of ions forms insoluble precipitates. A wide range of nanoparticles such as metal, metal oxides and organic nanoparticles have been produced using this method. The nucleation process is controlled ultrasonic or sonochemical effects to grow nanoparticles of various sizes and morphologies (Nagarajan and Hatton, 2008). Crystal growth occurring in water under high temperature and pressure using substances that are insoluble in water under ambient conditions is known as hydrothermal synthesis (Hayashi and Hakuta, 2010).

2.9.3 Solid phase process

The solid phase methods utilize traditional methods of size reduction by milling and grinding. Nanoparticles of clay, coal and metals are produced using the processes of milling and grinding. To avoid particle aggregation in the process, a colloidal stabilizer is used (Nagarajan and Hatton, 2008)

2.10 Synthesis of Co_3O_4

Various methods for the synthesis of cobalt oxide have been studied along with the characteristics of the nanoparticles. Ding et al. (2012) produced Co_3O_4 by the reverse co-precipitation method using $Co(NO_3)_2$ and NaOH as a precipitation agent. The catalytic properties where analysed by the degradation of methylene blue through the activation of PMS. The Co_3O_4 catalyst achieved a mere 40% degradation over a period of 30 minutes at a 20 µmol/L concentration of methylene blue (Ding et al., 2012).

Chen et al. (2008) produced nano Co_3O_4 particles utilizing the precipitation method with cobalt nitrate hexahydrate as a precursor solution in the presence of CTAB (N-cetyl-N,N,N-trimethyl ammonium bromide) as suggested by Zhou et al. (2005). Cobalt nitrate and CTAB was dissolved in de-ionized water (Zhou et al., 2005). Complete degradation of Acid Orange 7 was achieved in about 50 minutes reaction time when Co_3O_4 loading was 0.5 g/L with 2 mmol PMS and an Acid Orange 7 concentration of 0.2 mmol. The reaction was done at a neutral pH as it was more efficient than at an acidic pH (Chen et al., 2008)

Liang et al. (2012) synthesized Co_3O_4 nanoparticles by solution combustion using urea at 773 K over a 30 minute period. The catalytic activity of the Co_3O_4 particles was evaluated by the degradation of phenol through a peroxymonosulfate oxidizer in the form of PMS. Catalyst loading was done at 0.5 g/L with a phenol concentration of 25 mg/L The phenol degradation achieved by the Co_3O_4 synthesized by the combustion process was a mere 50% over a 4 hour period.

Co_3O_4 was synthesised by the decomposition of cobalt nitrate by heating and crystal growth in a solvothermal system by Shi et al. in 2012 and 2014. The catalytic activity of the nanoparticles was evaluated using an PMS oxidizer and Orange II as a contaminant in water. Shi et al. (2012) obtained a maximum degradation of 83% in 60 minutes using 0.1 g/L catalyst with 2 mmol PMS concentration at 0.2 mmol Orange II concentration. In 2014 Shi et al. achieved a maximum degradation of 74% in 20 minutes with a catalyst loading of 0.05 g/L with a 6 mmol PMS dosage and 0.6 mmol Orange II concentration (Shi et al., 2014).

Saputra et al. (2013) synthesized Co_3O_4 catalyst by the hydrothermal synthesis of cobalt nitrate hexahydrate at 120 ˚C for 5 hours. The catalytic performance of the catalyst was also evaluated by phenol degradation using PMS as an oxidizer. Complete phenol degradation

was achieved in 20 minutes at ambient temperature with 0.6 g/L catalyst loading and 25 mg/L phenol concentration (Saputra et al., 2013).

Wang et al. (2015) used a modified hydrothermal synthesis method to produce Co_3O_4 nanorods at 98 ˚C from cobalt nitrate and urea. The catalytic activity of the nanorods was analyzed by the activation of PMS for the breakdown of phenol in water. Phenol concentration was kept at 20 mg/L with 0.2 g/L catalyst and 6.5 mmol PMS. The Co_3O_4 catalyst calcined at 300 ˚C in air for 3 hours showed the most catalytic activity. Complete degradation of the phenol was achieved in 45 minutes at an elevated reaction temperature of 35 ˚C (Wang et al., 2015)

Chowdhury et al. (2015) used the continuous hydrothermal flow synthesis method to produce octahedral shaped Co_3O_4 catalysts for the degradation of methyl orange. Catalyst loading was kept at 0.03 g/L at a methyl orange concentration of 40 mg/L with 0.9 mmol PMS dosages to act as an oxidizer. Complete degradation of methyl orange was achieved in just over two minutes which suggested very high catalytic properties (Chowdhury et al., 2015).

The catalytic activity of the catalysts synthesized by the above authors were tested in batch systems with reactor volumes of 200 ml (Chowdhury et al., 2015), 250 ml (Shi et al., 2012; Shi et al., 2015) and 500 ml (Ding et al., 2012; Chen et al., 2008; Liang et al., 2012b; Saputra et al., 2013; Wang et al., 2015). As suggested by Hu and Long (2016), new operating techniques to allow for continuous treatment in fixed bed reactors or membrane reactors should be investigated and developed to industrialise the application of sulfate radical AOPs (Hu and Long, 2016).

Table 2.3 shows a summary of the synthesis methods of Co_3O_4 and catalytic activities of these catalysts as tested by the authors. The hydrothermal synthesis method used by Chowdhury et al. (2015), Saputra et al. (2013) and Wang et al. (2015) has produced catalysts with the highest degradation efficiency. The work done by Chowdhury et al. (2015) showed excellent catalytic activity compared to the other authors as complete degradation of methyl orange was achieved in only 2 minutes of reaction time.

Table 2.3: Comparison of different synthesis methods as discussed above

Reference	Ding et al., (2012)	Chen et al., (2008)	Liang et al., (2012b)	Shi et al., (2012)	Saputra et al., (2013)	Wang et al., (2015)	Chowdhury et al., (2015)
Catalyst	Co_3O_4	Co_3O_4	Co_3O_4	Co_3O_4	Co_3O_4	Co_3O_4	Co_3O_4
Synthesis method	Reverse co-precipitation	Precipitation method	Solution combustion method	Solvothermal method	Hydrothermal method	Hydrothermal synthesis	Continuous hydrothermal synthesis
Precursor materials	$Co(NO_3)_2$	$Co(NO_3)_2.6H_2O$	$Co(NO_3)_2.6H_2O$	$Co(NO_3)_2.6H_2O$	$Co(NO_3)_2.6H_2O$	$Co(NO_3)_2$	$CoCl_2.6H_2O$
Particle size	Not stated	20 nm	Not stated	3 – 5 nm	0.02 – 0.25 µm	40 nm	1.3 µm
Pollutant used	Methylene Blue 20 µmol/L	Acid Orange 7 0.2 mmol	Phenol 25 mg/L	Orange II 0.2 mmol	Phenol 25 mg/L	Phenol 20 mg/L	Methyl Orange 40 mg/L
Degradation efficiency	40% (30 min)	100% (50 min)	50% (4 hours)	83 \% (60 min)	100% (20 min)	100% (45 min)	100% (2 min)
Oxidizer	PMS 0.5 mmol/L	PMS 2 mmol	PMS 2 g/L	PMS 2 mmol	PMS 2 g/L	PMS 6.5 mmol	PMS 0.9 mmol

2.11 Conclusion

Membrane processes are considered as secondary treatment processes and have shown potential in the treatment of textile effluents. There are however drawbacks to this technology such as the rapid blocking of membranes that not only reduce the efficiency but also produce secondary waste. Furthermore, membranes require high energy consumption to generate pressure for flow through the membranes. Other AOPs such as the Fenton's process and its derivatives have shown little economic advantage to be employed on an industrial scale due to the excessive cost of chemicals required for the optimum operation and production of unfavourable secondary waste and photocatalysis due to the long treatment time (Feng et al., 2003; Andreozzi et al., 1999).

Heterogeneous cobalt-based catalysts have two critical properties, stability and reusability, that makes them beneficial for the breakdown of organic contaminants and gives them a competitive edge over other AOPs by being environmentally friendly and economically feasible (Hu and Long, 2016). Research done on catalytic activity of cobalt based catalysts has been done by numerous authors such as Ding et al., (2012); Chen et al., (2014); Liang et al., (2012b); Shi et al., (2012); Shi et al., (2014); Saputra et al., (2013) and Chowdhury et al., (2015). These studies have been done in batch slurry systems only which provide much needed information on the mechanisms and conditions for optimum operation and catalytic efficiency. Due to the high efficiency and ability to treat a vast majority of all solid components in textile effluents, AOPs have shown enormous potential to be tertiary treatment methods and possibly replace secondary treatment as well. The shortfall in the SR-AOPs is in the generation of continuous treatment reactors, the scale up parameters of such reactors and catalyst immobilization techniques to give rise to economically feasible operations for continuous wastewater treatment (Hu and Long, 2016; Andreozzi et al., 1999). This study is therefore focussed on, 1) the development of an immobilization technique, 2) designing a bench scale continuous treatment reactor utilizing the self-established immobilization technique for optimum catalyst utilization and 3) develop a scale up protocol and construct an upscale system of an order of magnitude.

CHAPTER THREE: Bench scale reactor development

3.1 Introduction

In this chapter, the production and characterization of the catalyst is described and discussed, the catalyst immobilization technique is explained and evaluated followed by the development of the permeable reactive barrier along with the method of determining the pore volume of the permeable barrier. Furthermore, the steps followed to get to the final design of the reactor is provided and the final design of the reactor is discussed. Lastly, the preliminary performance of the permeable reaction barrier is provided.

3.2 Catalyst

3.2.1 Batch hydrothermally synthesized catalyst

Nano-porous cobalt oxide nanorods were produced via a batch hydrothermal synthesis method according to the technique used by Wang et al. (2009). A mixture of cobalt chloride hexahydrate ($CoCl_2.6H_2O$) and urea ($CO(NH_2)_2$) was used as the precursor solution. Cobalt chloride (18 g) and 0.9 g of urea were each dissolved in 300 ml de-ionised water where after the urea solution was added dropwise to the cobalt chloride solution while stirring. The mixture was added to a one litre Teflon-lined autoclave (Figure 3.1) and heated at 105°C for 6 hours.

Figure 3.1: One litre Teflon-lined autoclave used to synthesize the batch Co_3O_4

The cobalt hydroxide solution was centrifuged and washed using de-ionised water to remove the particles. The cobalt hydroxide $Co(OH)_2$ was then dried overnight in air at 70°C and calcined at 300°C for 3 hours to obtain the cobalt oxide (Co_3O_4) powders (see Figure 3.2).

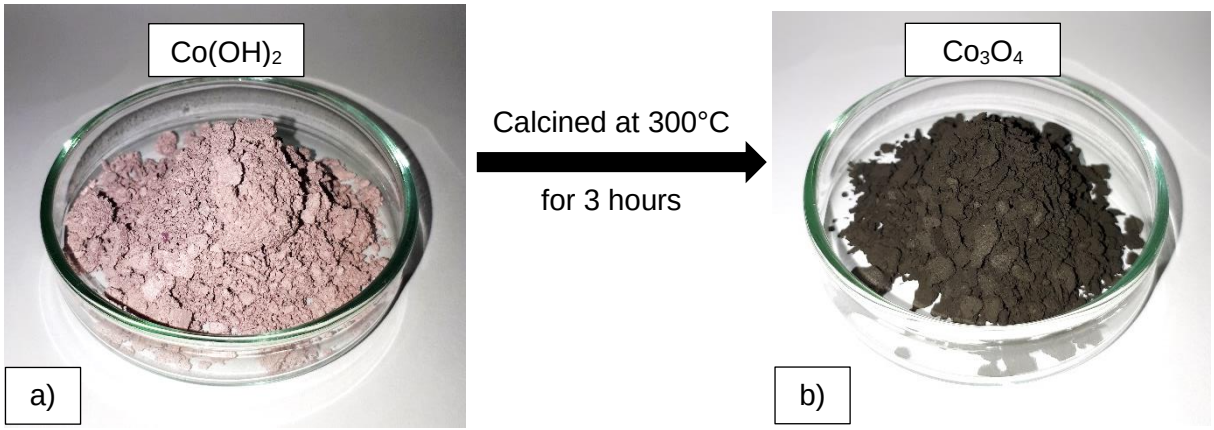

Figure 3.2: a) cobalt hydroxide powder before calcination and b) cobalt oxide powder after calcination

3.2.2 Catalyst characterisation

The nanoparticles produced were characterised by high resolution transmission electron microscopy (HRTEM). As can be observed in Figure 3.3 (a), (b) and (c), the catalyst structures were rod like. These rods of Co_3O_4 consisted of nanocrystals (see Figure 3.3 (e)) aggregated to form a nano-porous structure as seen in Figure 3.3 (d). The rods have a very large range in length, anywhere from 0.9 µm up to 2.8 µm and their width can vary anywhere from 98 nm up to 527 nm. The nanocrystals had a rhombohedral shape with an average length and width of 175 nm and 124 nm respectively. The length and width of the counted particles as well as the particle size distribution curve can be seen in Appendix D. Figure 3.3 displays the HRTEM images of the nanorods and nanocrystals produced by the batch hydrothermal synthesis. The images are arranged in order of increasing magnification with a low magnification showing the rods (Figure 3.3 (a) to (c)), and a high magnification, showing the nanocrystals that make up the nano-porous structures (Figure 3.3 (d)) and one rhombohedral shaped nano-crystal (Figure 3.3 (e)).

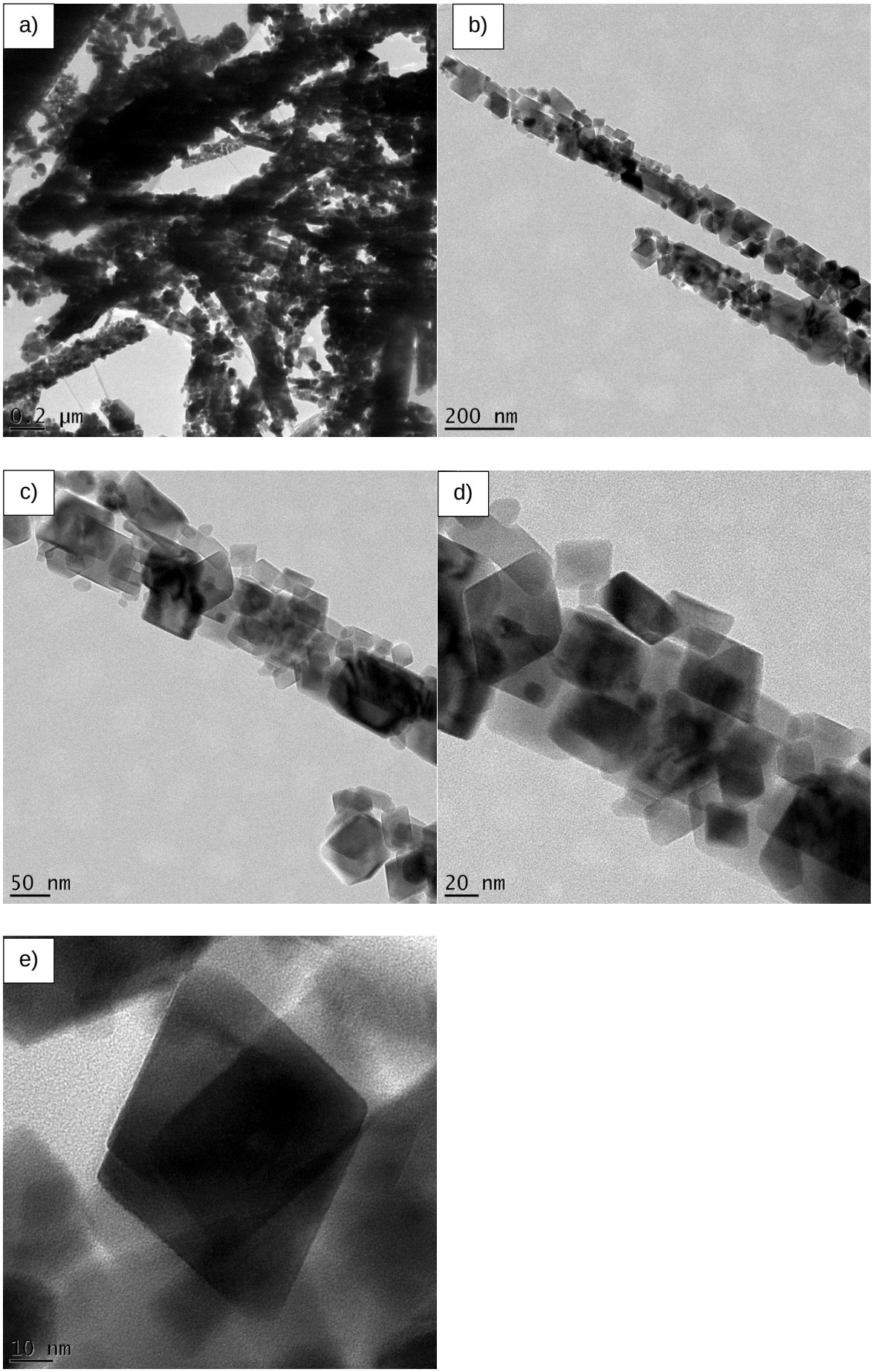

Figure 3.3: TEM of the cobalt oxide nanorods a) to c) and nanocrystals d) and e)

3.2.3 Commercially available cobalt oxide

Commercially available cobalt oxide catalysts were also tested in the application for treatment of textile dyes in the PRB. The catalysts were purchased in the sizes of ≤ 50 nm and ≤ 10 µm. The catalysts were also analysed by HRTEM and the results are presented in Figure 3.4 and Figure 3.5. It is clear in Figure 3.4 (a) and Figure 3.5 (a) and (b) that the commercially available catalysts do not form rods as the batch hydrothermally synthesized cobalt oxide. Figure 3.4 (b) clearly shows that the ≤ 50 nm particles are circular in shape as compared to that batch hydrothermally synthesized particles which tend to be more rhombohedral shaped (see Figure 3.3 (e)). It is also evident that the commercial particles tend to agglomerate forming larger particles which can be clearly seen in Figure 3.4 (a) and Figure 3.5 (a) and (b).

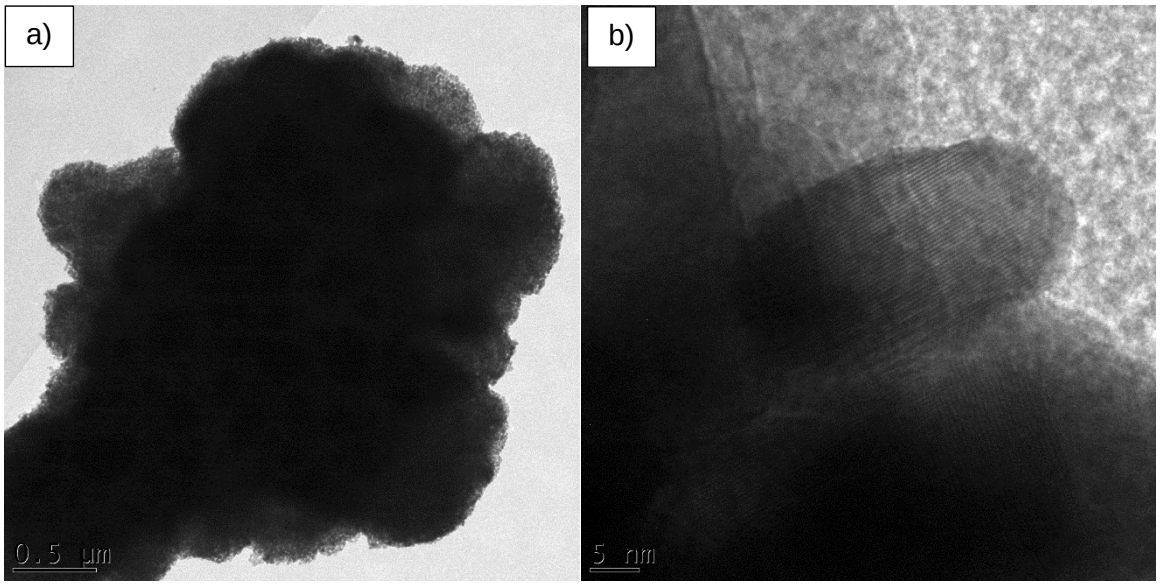

Figure 3.4: TEM of ≤ 50 nm commercially available cobalt oxide

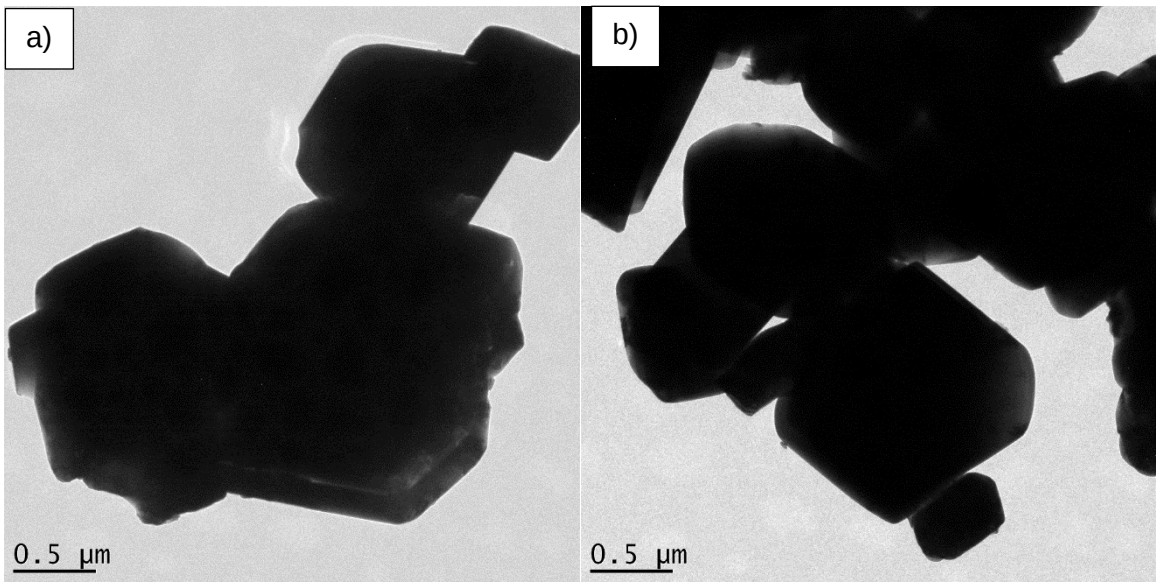

Figure 3.5: TEM of ≤ 10 µm commercially available cobalt oxide

The ≤ 10 µm commercial particles have a similar shape to the batch hydrothermally synthesized particles as they are also more rectangular shaped. They also tend to agglomerate similarly to those formed in the batch hydrothermally synthesis.

3.3 Permeable barrier

The permeable barrier used as the substrate to immobilize the catalyst on is a commercially available filter material used as a filtration bag for oil filtration. The permeable barrier is made from a polypropylene felt material that has a 1 µm nominal pore size. The BET surface area for the permeable barrier is 1.9272 m^2/g. The idea behind the use of the substrate was that the catalyst would form a filter cake inside the fibres without passing through the substrate thereby serving the purpose of a permeable reaction barrier. Figure 3.6 are SEM images of the blank permeable barrier before any catalyst has been immobilized on it.

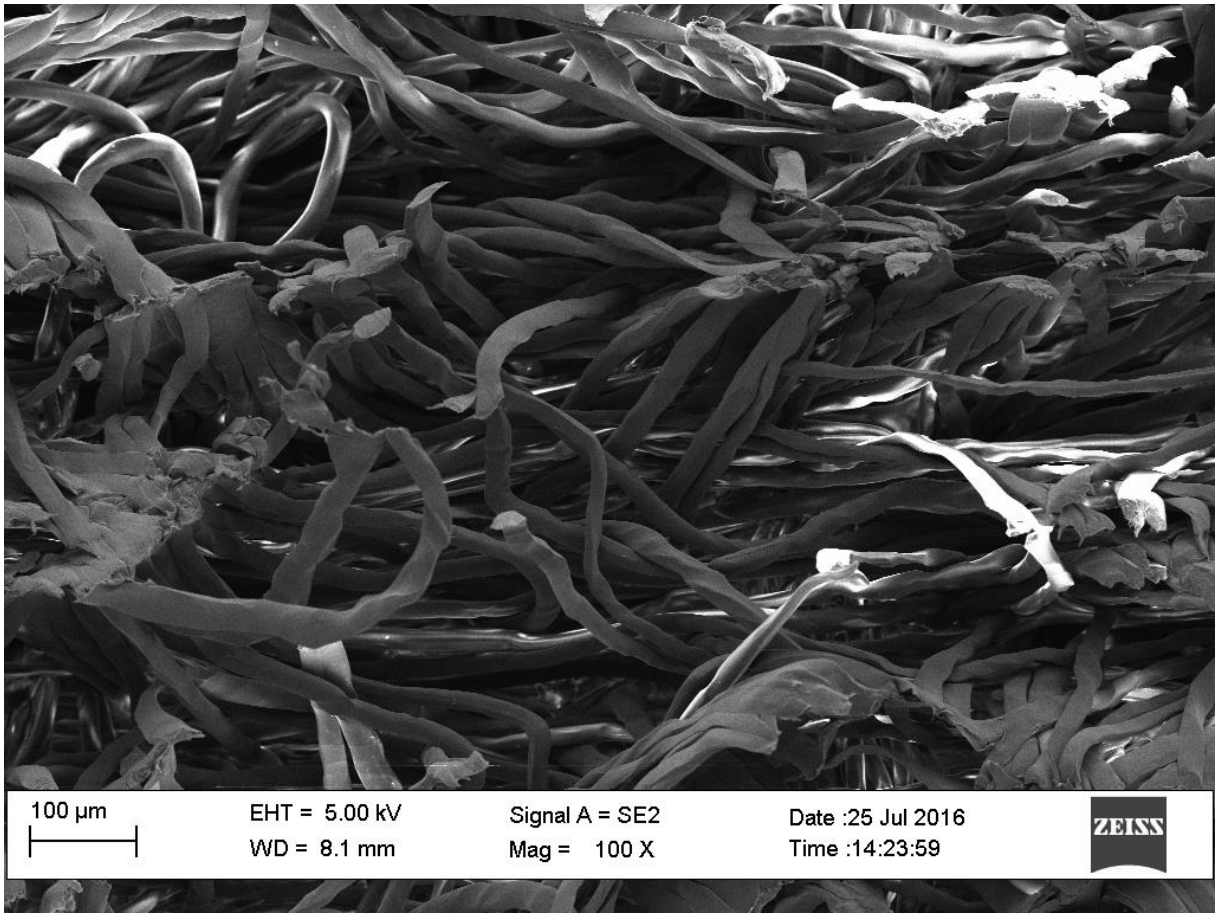

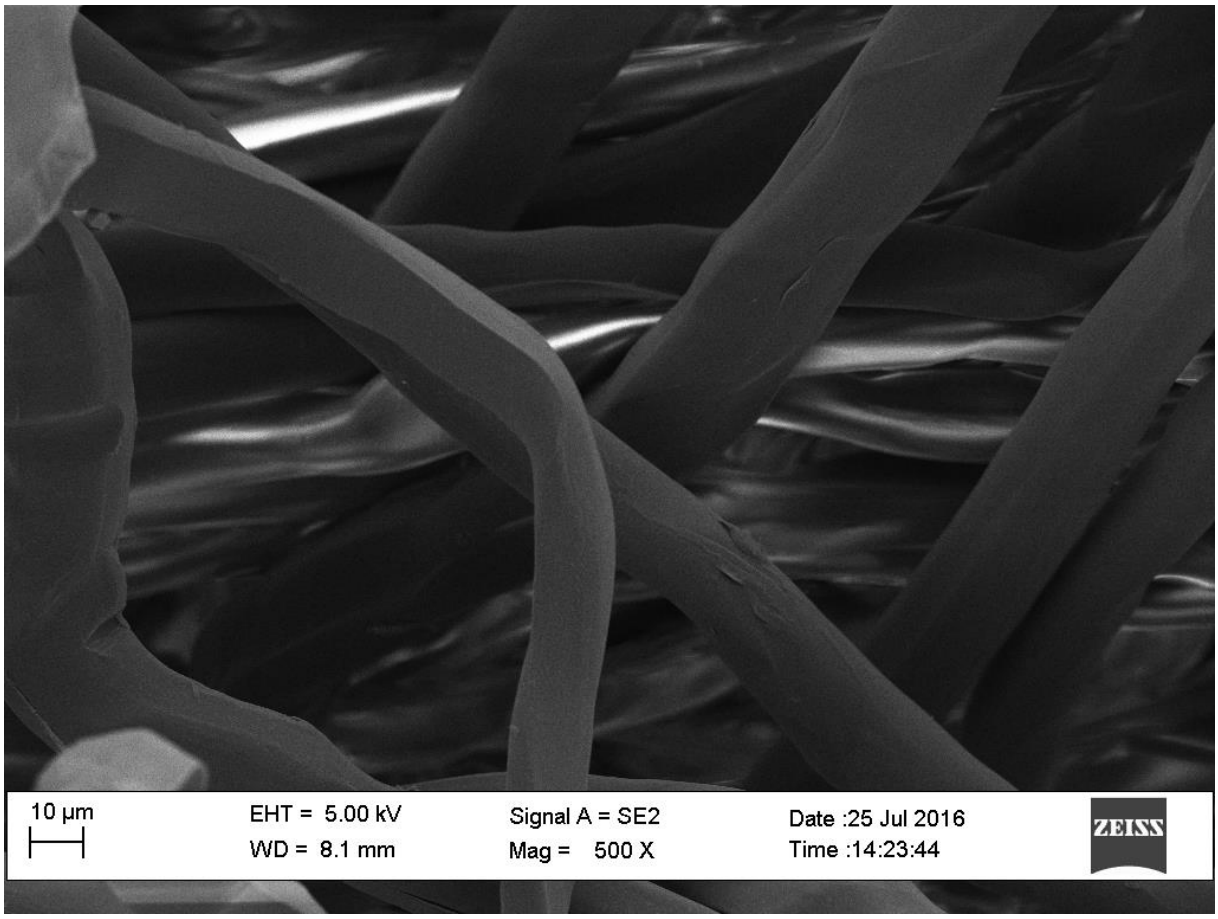

Figure 3.6: SEM of the blank permeable barrier

3.3.1 Pore volume and porosity

The pore volume is a critical parameter of the permeable barrier that needed to be determined to evaluate the residence time with the catalyst. It had to be determined experimentally by two different methods. These methods had been adapted from literature, section 2.4.3, and then modified to determine the porosity and the pore volume of the permeable barrier.

Pore volume can also be determined by the BET method as referred to in section 2.4.3. The BET pore volume is given as a volume per unit mass of solid and is determined by nitrogen adsorption. This pore volume however is the volume of the pores of the fibres of the substrate and it does not include the void spaces in between the fibres as can be seen in Figure 3.6. The BET method was therefore not relevant to determine the porosity of the substrate.

The first method used was a modified version of the water saturation method. In this method, the permeable barrier was placed in a small petri dish on a measuring scale weighing the mass of the dry permeable barrier. Water was added dropwise until the permeable barrier was fully submersed and fully saturated. The mass was then recorded and the saturated permeable barrier was removed. The mass of the remaining water was recorded. The

difference between the mass of water with the submerged permeable barrier and the mass of the leftover water is equivalent to the pore volume.

The second method used was the water evaporation method. A permeable barrier was once again submersed in water until it was fully saturated. The mass of the saturated permeable barrier was recorded and the permeable barrier was then dried overnight in an oven at 60°C. The dried permeable barrier was weighed and the difference in mass of the saturated permeable barrier and the dried barrier is equal to the mass of water in the pores which is related to the volume of the pores. Table 3.1 and Table 3.2 show the results obtained for the determination of the pore volume and porosity by the water saturation method and water evaporation method respectively.

Table 3.1: Results for the determination of porosity using the water saturation method

Circular shape permeable barrier (d = 3.9 cm, h = 0.334 cm, V = 3.990 cm^3)			
Mass of water + permeable barrier (g)	**Mass of water (without permeable barrier) (g)**	**Pore volume (cm^3)**	**Porosity**
9.702	6.569	3.133	0.79
9.700	6.548	3.152	0.79
9.697	6.556	3.141	0.79
Rectangular shape permeable barrier (l = 4 cm, b = 2 cm, h = 0.344 cm, V = 2.672 cm^3)			
10.797	8.555	2.242	0.84
10.795	8.571	2.224	0.83
10.793	8.565	2.228	0.83
Square shape permeable barrier (l = 4.5 cm, h = 0.344 cm, V = 6.764 cm^3)			
15.217	9.671	5.546	0.82
15.211	9.632	5.579	0.82
15.206	9.638	5.568	0.82
Average Porosity			0.81

To determine the porosity of the permeable barrier, the total volume of the permeable barrier had to be determined. This was done by using the dimensions and calculating the volume for each permeable barrier. The porosity was then calculated by dividing the pore volume by the total volume of the permeable barrier. To obtain a well-defined average of the pore volume, different shapes and sizes of the permeable barriers were used. The porosity is determined by Equation 3.1:

$$Porosity = \frac{Pore\ volume}{Permeable\ barrier\ volume} \quad (3.1)$$

Determining the porosity of the permeable barrier used in the bench scale reactor was important for the scale up to the larger reactor.

Table 3.2: Results for the determination of porosity via the water evaporation method

Circular shape permeable barrier (d = 3.9 cm, h = 0.334 cm, V = 3.990 cm^3)			
Saturated mass (g)	**Dried mass (g)**	**Pore volume (cm^3)**	**Porosity**
3.724	0.685	3.039	0.76
3.622	0.617	3.005	0.75
3.694	0.654	3.040	0.76
Rectangular shape permeable barrier (l = 4 cm, b = 2 cm, h = 0.344 cm, V = 2.672 cm^3)			
2.540	0.397	2.144	0.80
2.632	0.438	2.194	0.82
2.584	0.427	2.157	0.81
Square shape permeable barrier (l = 4.5 cm, h = 0.344 cm, V = 6.764 cm^3)			
6.432	1.075	5.357	0.79
6.493	1.069	5.424	0.80
6.472	1.071	5.401	0.80
Average Porosity			0.79

The porosity of the permeable barrier was determined by averaging the porosity determined by the two methods which equates to a fraction of 0.80 or 80%. Determining the pore volume of the actual circular permeable barrier used in the reactor yielded a pore volume of 3.192 cm^3. The pore volume calculation was based on the porosity determined experimentally by the two methods.

The BET pore volume determined by the nitrogen adsorption isotherm was established to be 0.001511 cm^3/g. Calculating the pore volume for the permeable barrier that has a mass of 0.68 g was 0.00103 cm^3. The pore volume determined experimentally was 3.192 cm^3 and the difference in the volumes was due to the void spaces in between the permeable barrier fibres which could not be determined by the BET method.

3.4 Catalyst immobilization process

In this section, the process and techniques used to immobilize the catalyst in the filter material to develop the PRB is presented. In addition, the results obtained by the two techniques were compared based on the degree of degradation of methylene blue.

3.4.1 Immobilization process and techniques

Due to the difficulty and excessive cost of recovering the catalyst when used in slurry systems, it is important to develop a technique which successfully immobilizes the catalyst without compromising efficiency. Hu and Long (2016) suggested that the next step in the Cobalt/PMS advanced oxidation process is to develop new catalysts and operating techniques or combine the catalysts in reactors to broaden the field of use of such a process (Hu and Long, 2016). The effective immobilization of catalysts in continuous wastewater treatment systems has been the limitation to the success of AOPs. Efficient immobilization of the catalyst will be a breakthrough in the technology.

To immobilize the cobalt oxide catalyst in the permeable barrier a filter bag with pore size of 1 micron was used, due to the porous nature of the filter bag material. The permeable barrier becomes the permeable reactive barrier (PRB) after the catalyst has been immobilized in it. Spherical sections with a diameter of 40 mm were cut from the filter bag so that they could easily be built into a piping system. To study the efficiency of the immobilization the following trials were conducted.

1. Technique 1: Dry catalyst was spread by hand over the PRB area; two other filter pieces were used to sandwich the PRB before placing it in reactor.
2. Technique 2: The catalyst was suspended in water and a Buchner funnel with the filter bag acting as the filter was used to deposit a uniform layer of the catalyst in the porous filter bag by recycling the filtered water until it is evident that the maximum amount of catalyst has been captured by the filter which now becomes a PRB. The

process for making the PRB is shown in Figure 3.7. Figure 3.7 (a) shows the placement of the permeable barrier inside the funnel, (b) shows the reconstruction of the Buchner funnel, (c) fits the suction line onto the Buchner funnel and (d) shows the suspension containing the catalyst being added to the Buchner funnel.

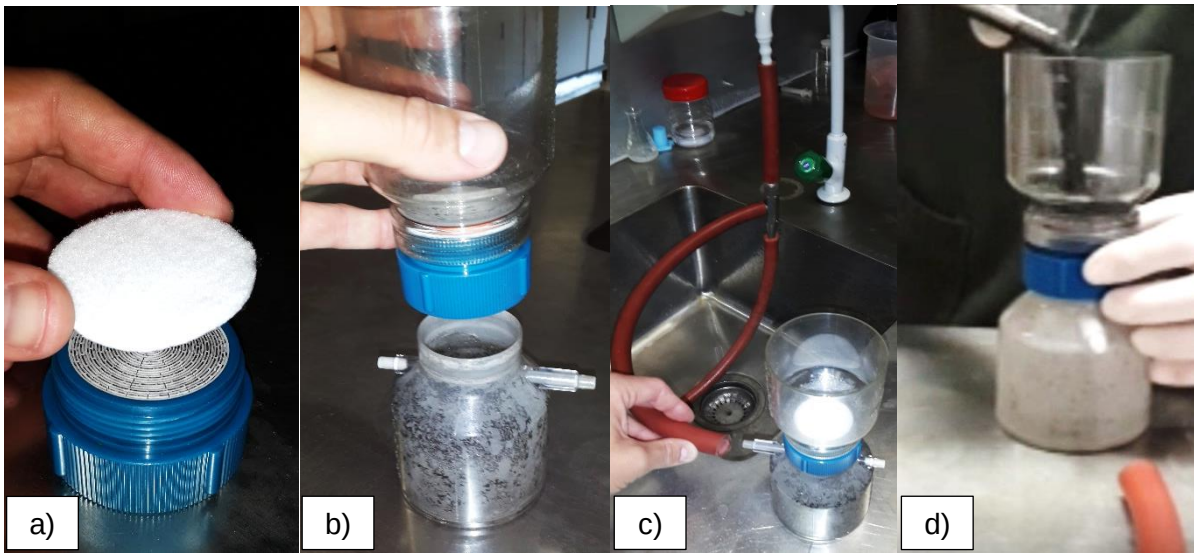

Figure 3.7: Buchner filtration setup for catalyst immobilization

3. Three (3) types of Co_3O_4 powders were used:
    - Produced in the nanotechnology laboratory using a batch hydrothermal system (BHS).
    - Commercially available Co_3O_4 > 50 nm powders
    - Commercially available Co_3O_4 > 10 µm powders

Furthermore, the PRB was studied using SEM to discover the packing of the catalyst in the fibres. The filtrate from the Buchner funnel immobilization process was dried in an oven at 70˚C. The mass of catalyst that has not been immobilized was determined to calculate the immobilization efficiency.

3.4.2 Results for catalyst immobilization

Two techniques for immobilizing the catalyst have been used in this study which was compared by treating methylene blue at a concentration of 10 mg/L (PMS dosage at 0.035 g/150 ml). The first technique involved the spreading of the catalyst using a spatula onto the permeable barrier sandwiched between two blank pieces of filter material. The second technique made use of the Buchner filtration method as discussed in section 3.4.1.

A visual comparison of the two techniques can be seen in Figure 3.8. It shows that the second technique shows a much more uniform distribution of the catalyst. The hand coated reaction barrier shows an uneven spread of catalyst over the reaction area. Such an uneven

distribution of catalyst could cause channelling through the reaction barrier resulting in an inefficient degradation process.

Figure 3.8: Reaction barriers with catalyst being immobilized by two different techniques; hand spread catalyst technique (left) and the Buchner filtration method (right)

The visual comparison of the two catalyst immobilization techniques revealed that the Buchner filtration technique is the more effective technique and future preparations of PRBs would be done using this technique. Figure 3.9 represents the results of the PRB before and after immobilization. In Figure 3.9, the extent of immobilization i.e. the efficiency of immobilization is clear as the supernatant after the immobilization is almost as clear as pure water. The dark shade visible in the supernatant is in fact mostly small cobalt oxide particles that are attached to the walls of the glass beaker by some attraction force not currently investigated.

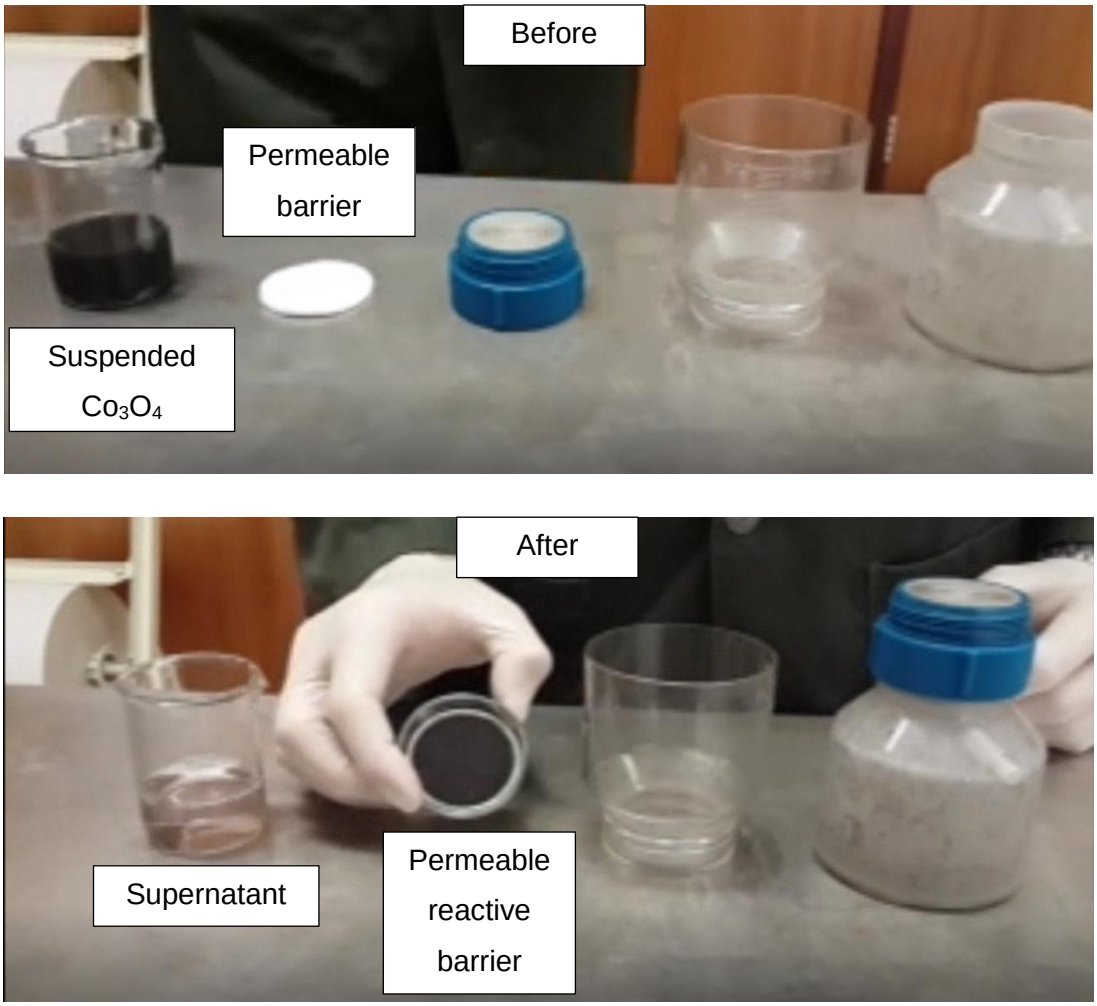

Figure 3.9: Before and after catalyst immobilization using the Buchner filtration method

The immobilization efficiency was determined to obtain the exact mass of catalyst that would participate in the reaction. By drying the supernatant in an oven at 60°C and weighing the beaker with the leftover dry catalyst, the efficiency could be determined. The difference between the clean empty glass beaker and the beaker with the leftover catalyst is the mass of catalyst not immobilized in the PRB. The efficiency is determined by taking the mass of the leftover catalyst as a fraction of the initial mass of catalyst (see Equation 3.2). The average immobilization efficiency for the Buchner filtration was 96.5%.

$$\eta = \frac{B_2 - B_1}{m_{cat}} * 100 \qquad (3.2)$$

Table 3.3 shows the calculation of the efficiency of the catalyst immobilization using Equation 3.2.

Table 3.3: Catalyst immobilization efficiency calculation

Catalyst mass m_{cat} **(g)**	**Beaker with dried catalyst** B_2 **(g)**	**Empty beaker** B_1 **(g)**	**Immobilization efficiency** η **(%)**	**Immobilised catalyst mass (g)**
0.300	47.177	47.169	97.3	0.292
0.301	48.637	48.623	95.0	0.286
0.301	49.088	49.074	95.0	0.286
0.302	48.371	48.360	96.4	0.291
0.302	48.738	48.734	98.7	0.298
0.300	50.456	50.446	96.7	0.290
Average efficiency (%)			96.5	

Figure 3.10: SEM imaging of batch hydrothermally synthesized Co_3O_4 coated PRB shows SEM images of the coated PRB with batch hydrothermally synthesized catalyst and commercially available 50 nm and 10 µm catalyst are presented in Figure 3.11 and Figure 3.12 respectively. SEM images of the reaction barrier where the catalyst was immobilized by the Buchner filtration technique show that the catalyst adheres to the permeable reaction barrier by electrostatic forces and therefore coating the surfaces of the fibres to stay lodged inside the PRB. The attraction forces that cause the catalyst to adhere to the fibres still needs further investigation and is outside the scope of this study.

It was observed that the immobilization of the batch hydrothermally synthesized catalyst resulted in a uniform and dense spread of catalyst covering the surface of the substrate fibres (see Figure 3.10 (a)). In Figure 3.11 (a) and (b) where the ≤ 50 nm commercially available catalyst was immobilized a great deal of agglomeration of catalyst on the substrate fibres was observed. The 10 micron commercially available catalyst had a very sparse distribution of catalyst particles on the substrate fibres with large areas of the fibres not being covered by the catalyst particles (see Figure 3.12 (b)).

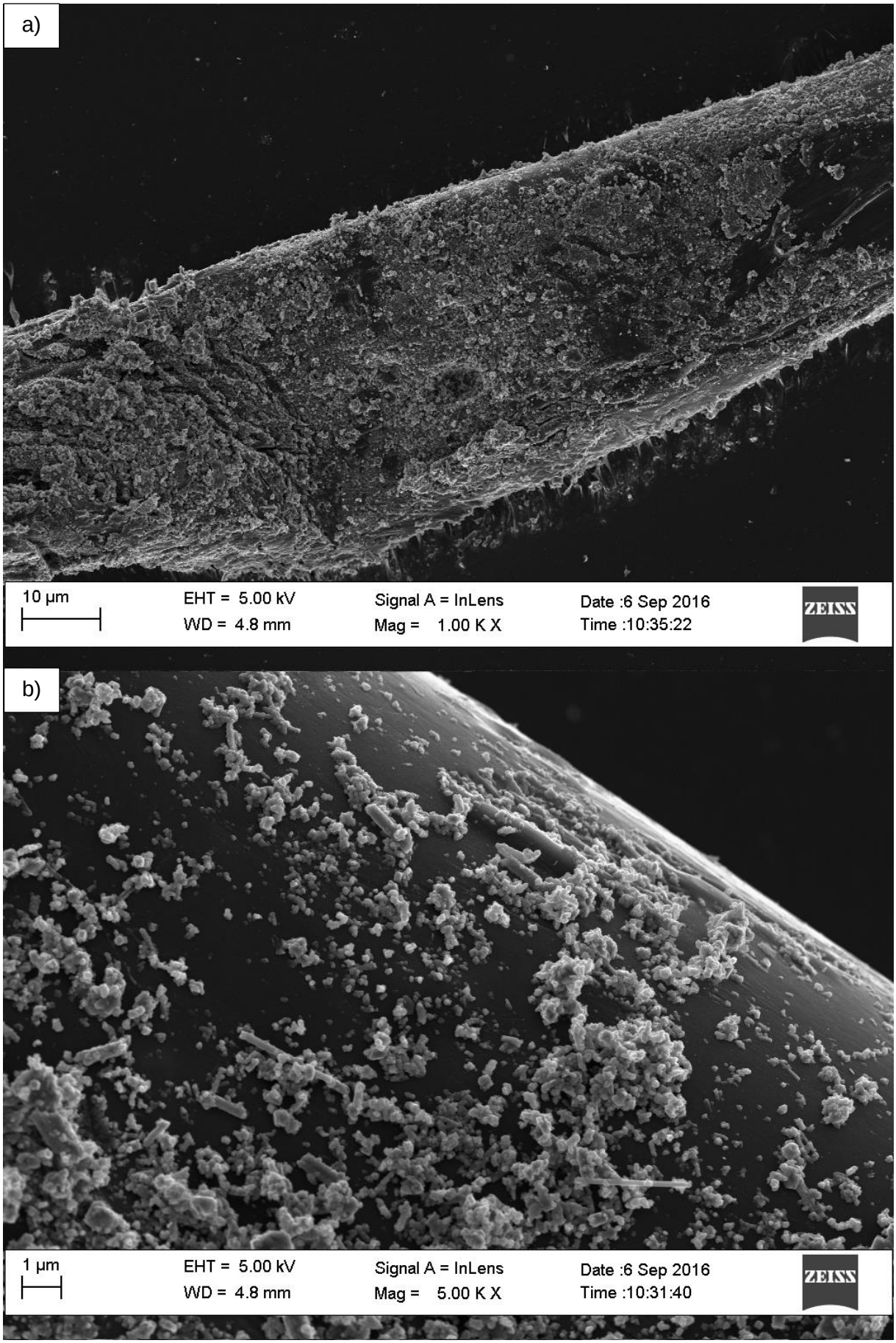

Figure 3.10: SEM imaging of batch hydrothermally synthesized Co_3O_4 coated PRB

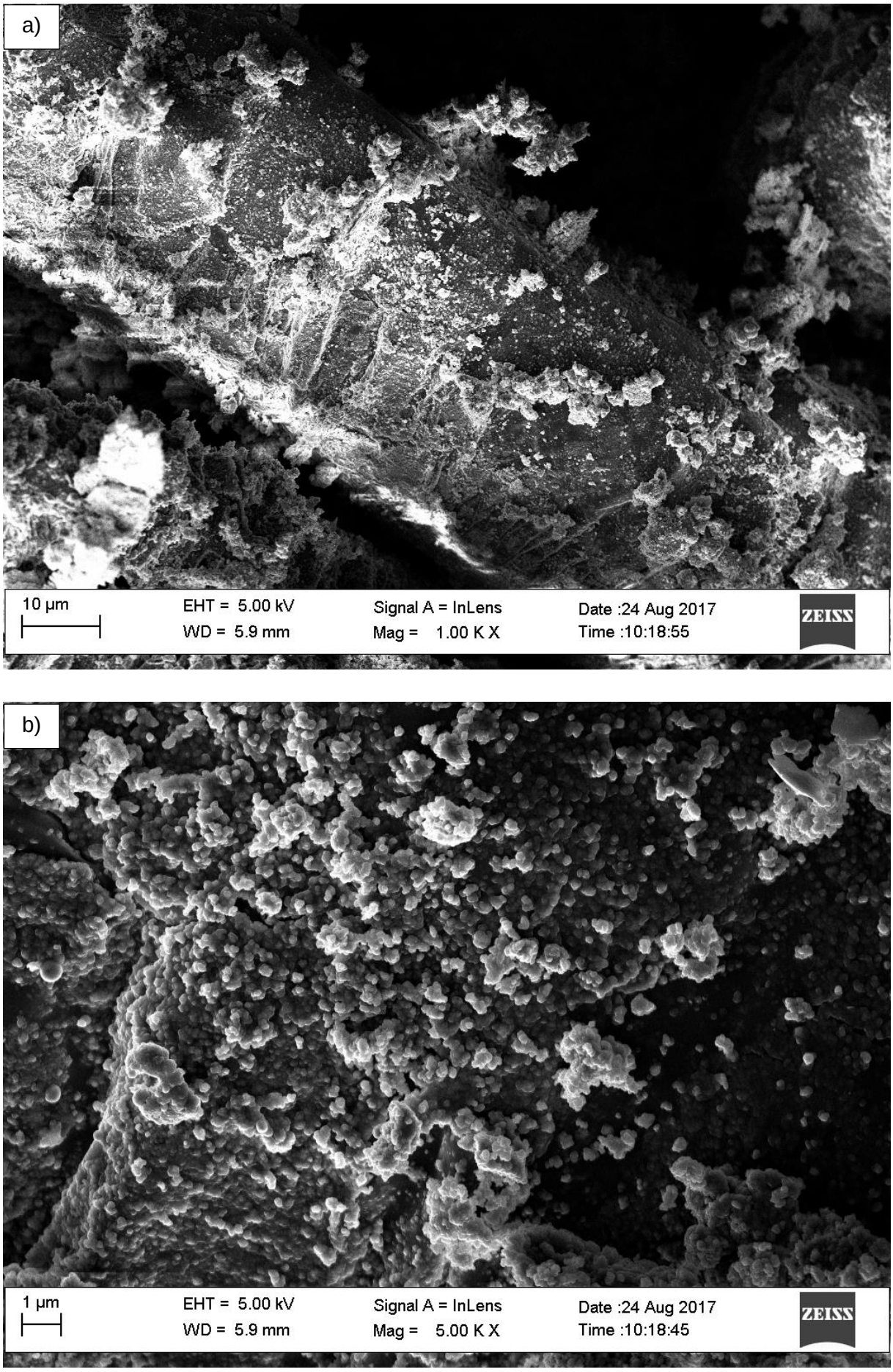

Figure 3.11: SEM images of a PRB coated with 50 nm commercially available Co_3O_4

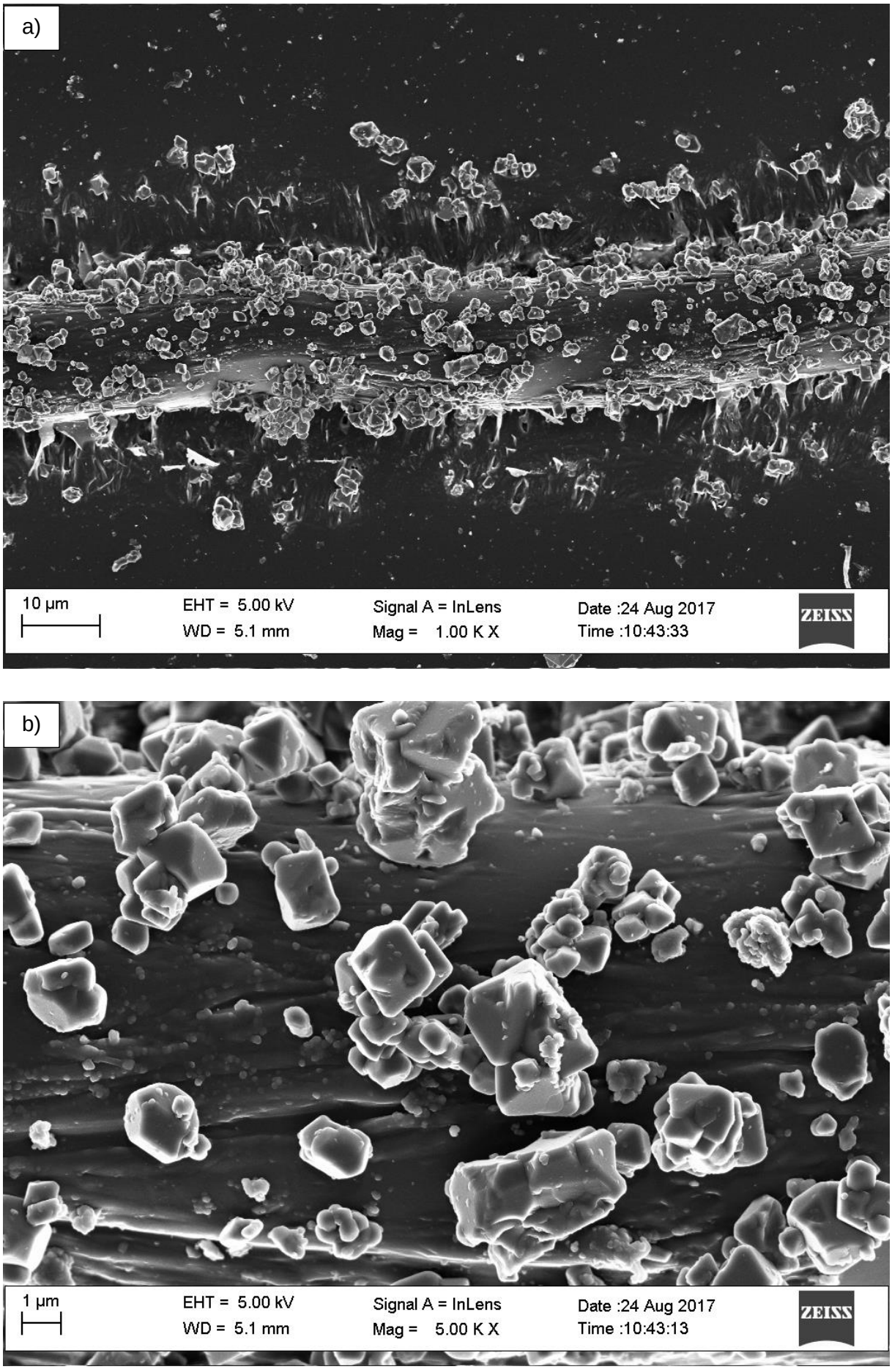

Figure 3.12: SEM images of a coated PRB with 10 µm commercially available Co_3O_4

3. Reactor design

3.5.1 PRB housing

The original idea of the PRB housing was to design a housing that could accommodate a PRB and be placed into any existing piping system. The design had to be such that the replacement of the PRB was uncomplicated and rapid as to not interfere with the treatment process. The PRB housing was specially designed so that it can easily be fitted into an existing piping system by simply making use of two flanges.

Figure 3.13 shows a technical drawing of the PRB housing along with its dimensions. It also indicates how the housing and the O-ring fit into the reactor column.

It was designed to house the permeable reactive barrier and seal off the system to prevent any leakage from occurring. A Viton O-ring is used to seal the PRB housing and to hold the PRB in place which is housed inside the acrylic housing. The Viton seal is also used to prevent channelling of the wastewater around the sides of the reactive barrier.

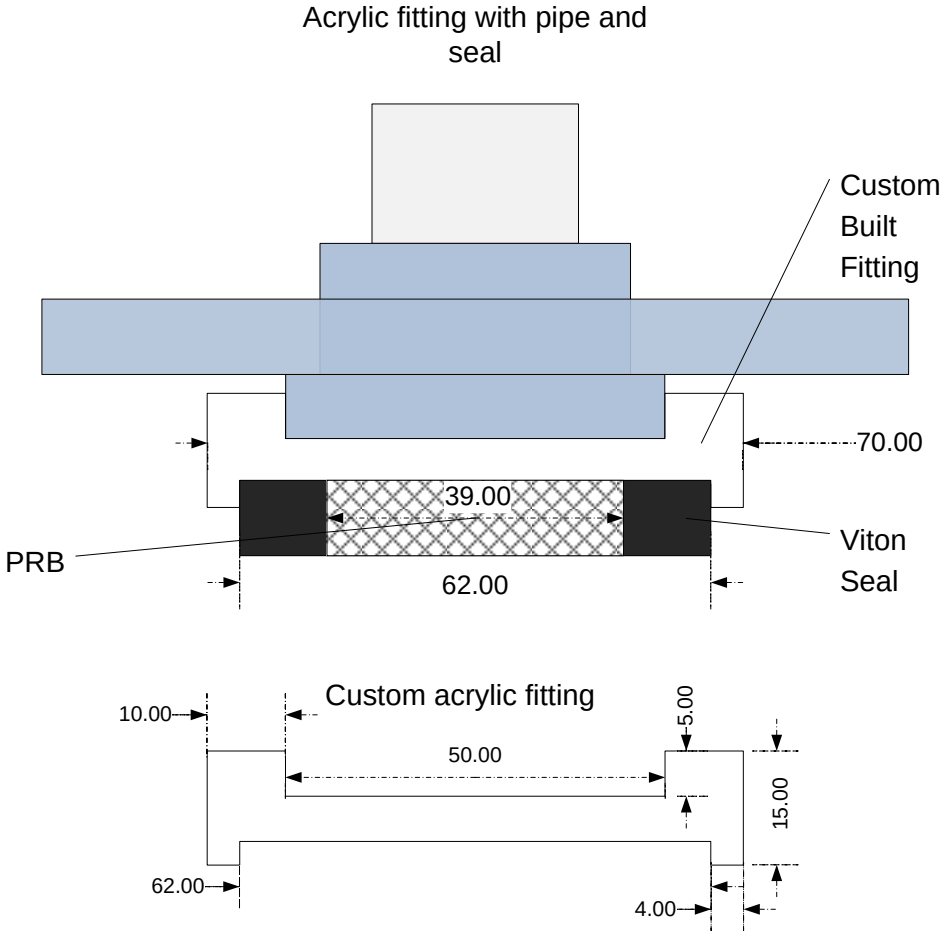

Figure 3.13: Technical drawing of the custom designed PRB housing

3.5.2 Horizontal flow reactor

As mentioned before, the original idea was to design a permeable reaction barrier (PRB) system that can easily be fitted into an existing piping system and initiate the degradation of the organic contaminants using the Co_3O_4 catalyst. A horizontal flow reactor was then constructed using a 32 mm ID PVC pipe that would sandwich the PRB using 2 flanges in the flow direction of the wastewater. Figure 3.14 (a) shows the first horizontal reactor attached to the feed pump and b) shows the sandwiched PRB.

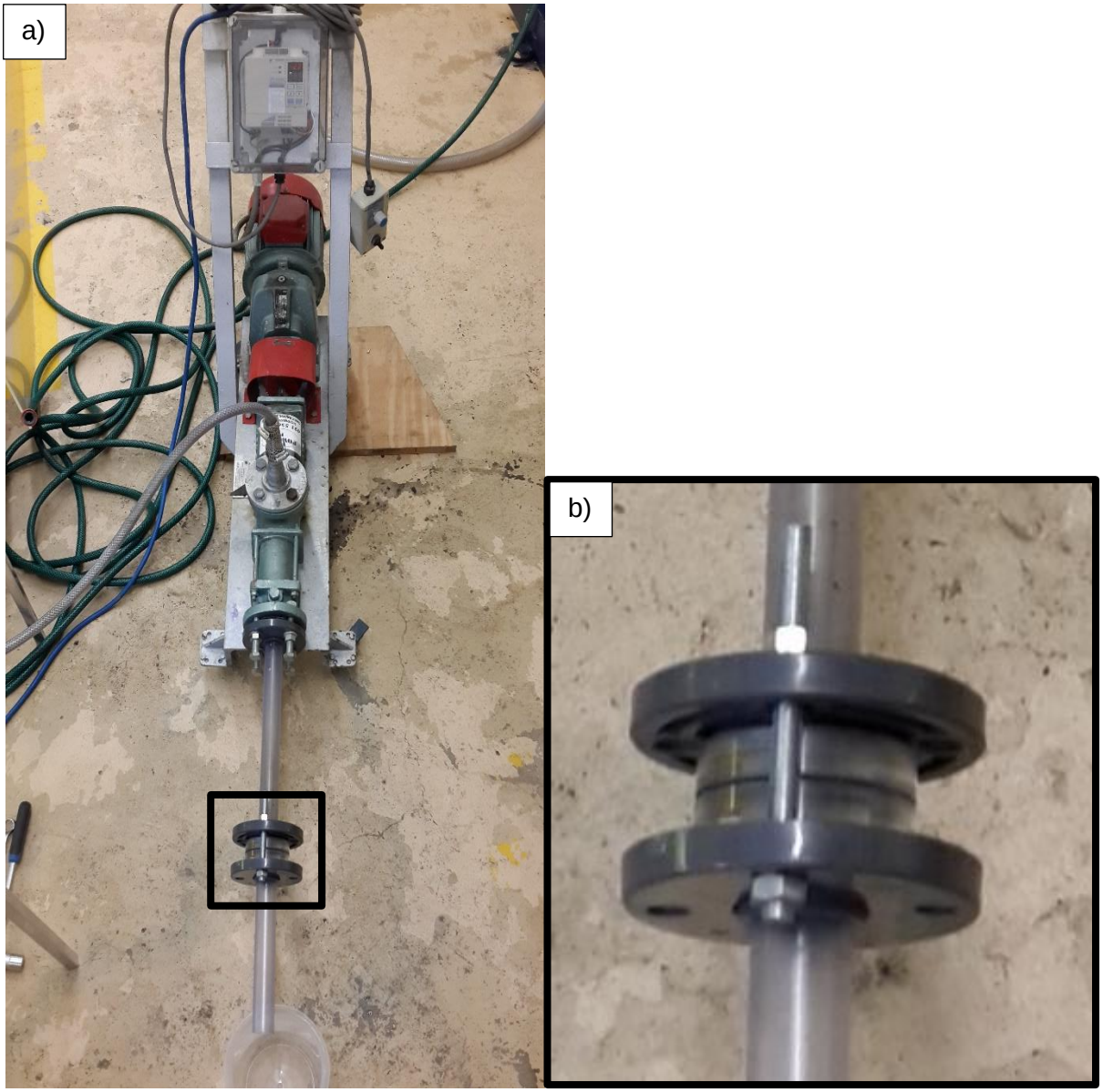

Figure 3.14: a) Horizontal flow reactor with the feed pump, b) the sandwiched PRB with two flanges

The horizontal flow reactor was used for provisional testing and design of the PRB. The permeable reaction barrier was sandwiched in between two flanges that connected a pipe to the pump. The PRB used in the horizontal flow reactor was immobilized only by the hand spread technique as the Buchner filtration technique was established after this experiment.

Three litres of methylene blue solution at a concentration of 10 mg/L were prepared and treated using the horizontal reactor. The dye solution was recycled a total of 6 times and the degradation was evaluated by UV-visible spectroscopy.

Figure 3.15 represents the degradation of methylene blue for a single PRB at a PMS dosage of 0.233 g/L. The catalyst loading in the PRB was 0.2 g and after one cycle it achieved a 96.6% degradation of methylene blue.

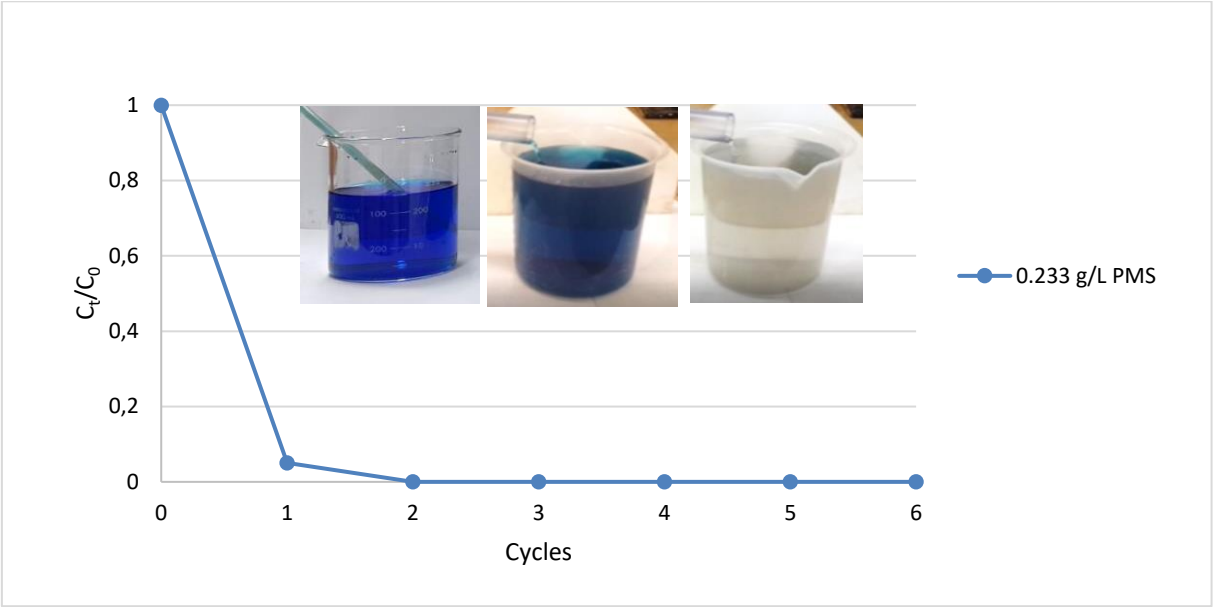

Figure 3.15: Degradation of methylene blue by cobalt oxide using a single reaction barrier with catalyst immobilized by the hand-spread technique

Although the horizontal flow arrangement showed good degradation, it did not provide enough resistance for the overall filter to be covered by the feed water. This resulted in ineffective contact with the catalyst and ineffective degradation as the solution had to be recycled and treated twice before complete degradation was observed. At this stage, it was considered to develop a vertical flow reactor to be able to have better control over the flow rate and contact area.

3.5.3 Vertical up-flow reactor

After tests have been done on the horizontal flow reactor, it was observed that the reaction barrier does not provide enough resistance to flow for the total immobilized surface area to be in contact with the wastewater. Thereafter it was considered to rearrange the flow to a vertical upward flow through the reactor to have better control over the flow rate and residence time.

The most critical parameters in the design of the reactor was the effective immobilization of the catalyst in the substrate and the optimum residence time between the catalyst and oxidizer to activate the oxidiser for sulphate radical production. The residence time can be

manipulated by increasing the thickness of the substrate or by varying the flow rate and keeping the substrate thickness constant. In this case the flow rate was varied. Due to the lack of technical information on the current research, the residence time was determined experimentally by doing the flow rate study and then determined by Equation 2.11.

$$\tau = \frac{V}{v_0} \tag{2.11}$$

The mean residence time is the average time that the sulphate radical producing molecules spend in the PRB. This is equivalent to the time that a volume of fluid, equal to the pore volume of the PRB, would spend in the PRB required to achieve a certain degradation efficiency. The mean residence time is represented by τ, the pore volume of the PRB is V and the volumetric flow rate through the reactor is v_0.

The vertical bench scale PRB system was designed and built using a 32 mm OD PVC pipe (28 mm ID), acting as a column, with custom built fittings to hold the PRB in place. The two reactor columns are held in place by flanges. A peristaltic pump fitted with a variable speed drive is used to pump the wastewater to the reactor. The wastewater is pumped vertically into the column through a 6 mm OD nozzle with a 6 mm tube (3 mm ID). The reactor specifications are:

- Total column volume of 104 cm^3
- Vertical upward flow controlled by a peristaltic pump
- Immobilized catalyst area of 11.95 cm^2
- Pore volume of the permeable reaction barrier was 3.192 cm^3. The pore volume was determined by taking the porosity (0.80) of the total volume occupied by the permeable barrier (3.990 cm^3)

Figure 3.16 represents the technical drawing of the permeable reaction barrier system that displays the details of the reactor (column) with its dimensions and fittings.

The residence time that the fluid spends in the permeable reaction barrier was determined experimentally by measuring the time taken for the fluid to pass through the permeable barriers. The time was taken from the moment that the fluid reached the first permeable barrier, Figure 3.16 point 1, to the moment the fluid exits the third (last) permeable barrier, Figure 3.16 point 2. The residence time in one permeable barrier was determined experimentally to be 5 seconds.

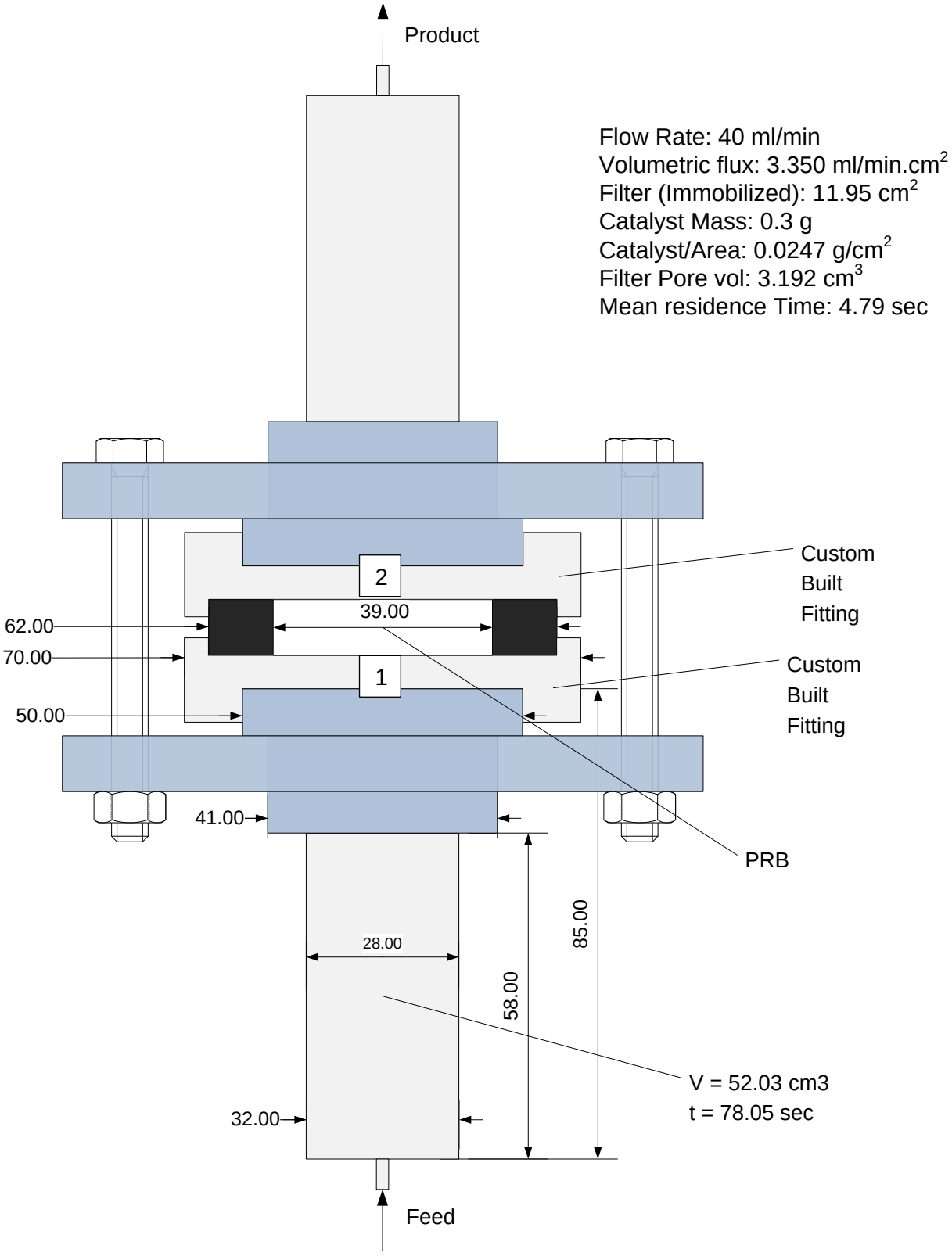

Figure 3.16: Technical drawing of the bench scale reactor (dimensions are in mm)

The bench scale permeable reaction barrier system with the peristaltic pump is presented in Figure 3.17:

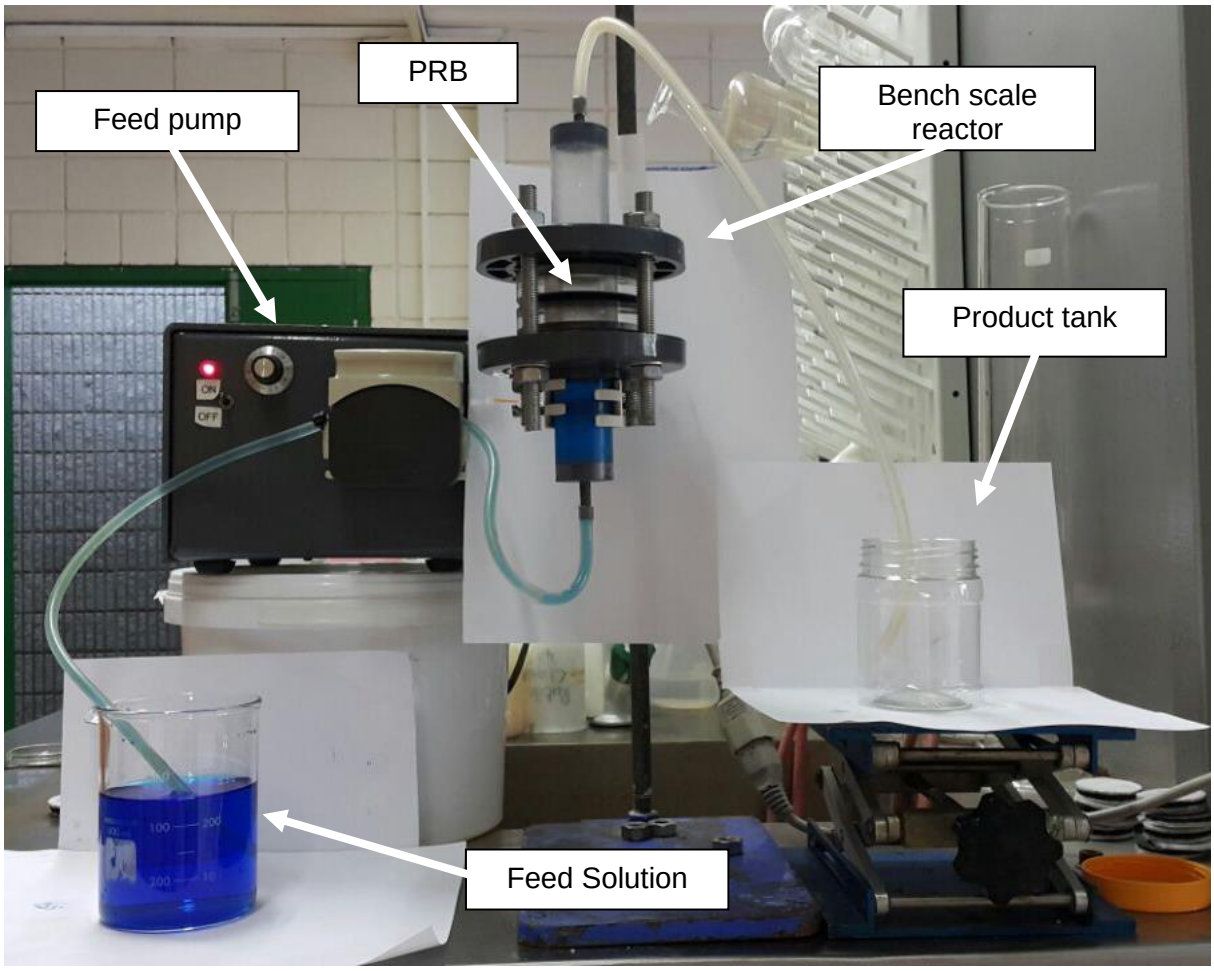

Figure 3.17: Bench scale model of the permeable reaction barrier system

3.6 Preliminary performance of the bench scale reactor

After the bench scale reactor had been designed, the operating conditions had to be optimized to achieve maximum degradation. To do so, several studies had to be done and the degradation efficiency of the reactor was evaluated.

- The two catalyst immobilization methods were compared to determine the most efficient immobilization technique by comparing degradation efficiencies.
- The reactor performance was evaluated using a model dye, methylene blue, at a concentration of 10 mg/L.
- The reactor performance was evaluated using 5 different real textile effluents; acid, base, metal complex, dispersed and reactive dye.

The efficiency of the PRB system was established by measuring the concentration change of methylene blue over the reaction period. The concentration change for methylene blue was

measured using a UV-vis spectrometer at a wavelength of 663 nm. Degradation curves were produced by plotting the concentration as a fraction of the feed concentration versus time. The percentage concentration of the dye remaining in the water over a period was established by using Equation 3.2:

$$\%\,\boldsymbol{Degradation} = \frac{C_t}{C_0} * \mathbf{100} \qquad \textbf{(3.2)}$$

Due to the complexity of real textile effluent, the concentration could not be analysed using a UV-vis spectrometer and the degree of visual colour change was used as a measure of comparison.

3.6.1 Comparison of immobilization technique

Provisional studies were done to compare the two immobilization techniques to determine the most efficient technique in the up-flow reactor. Figure 3.18 represents the concentration versus time curve for the degradation of methylene blue using two different techniques of immobilization of the catalyst in the reaction barriers.

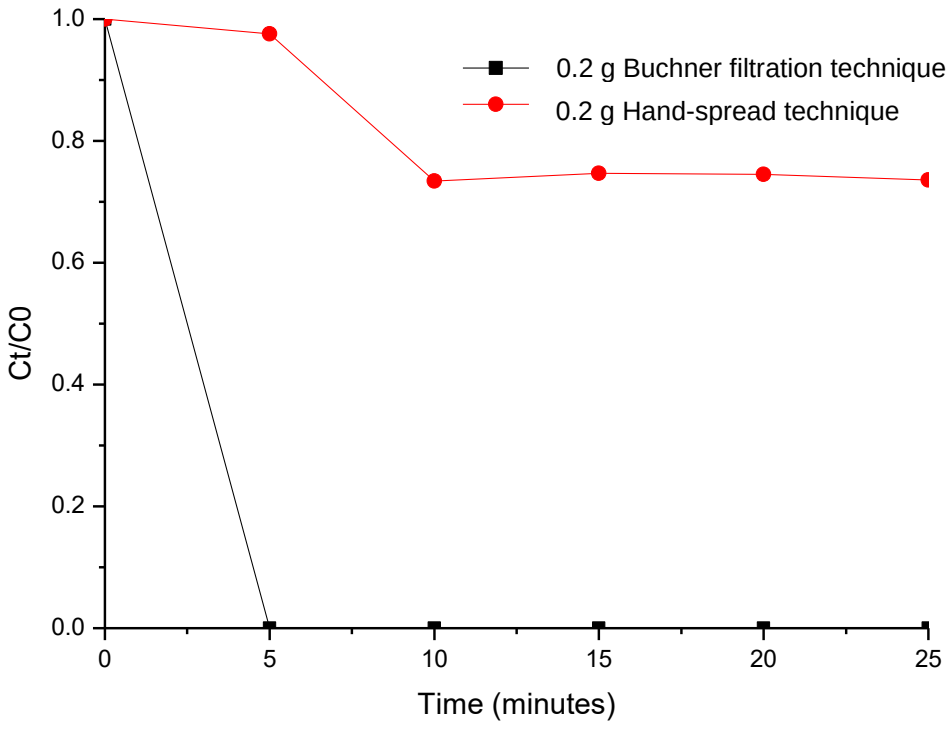

Figure 3.18: Degradation curve for reaction barriers prepared by the hand spread technique and Technique 2

Figure 3.18 shows that the degradation of methylene blue was much more efficient when Technique 2 was used to immobilize the catalyst. Complete degradation of methylene blue was achieved after just five minutes of degradation and the lowest degradation over the

25 minute period was 87.9%. The degradation using the reaction barrier prepared by the hand spread technique achieved a maximum degradation of 26.6% with its lowest degradation over the 25 minute period being 2.44%. The results obtained using immobilization of the catalyst by Technique 2 was 73.4% more efficient than the immobilization by the hand spread technique. The hand spread technique was discontinued at this stage and all further work was conducted using immobilization Technique 2.

3.6.2 Model dye results

Effect of catalyst loading

The effect of catalyst loading has been studied by doubling the catalyst mass from 0.1 g to 0.2 g. The dosage of PMS was kept constant at 0.035 g/ 150 ml and the solution concentration was kept at 10 mg/L of methylene blue. Before the run started the PMS was added to the solution and a 5 minute period for dissolving was allowed. The flow rate of the system was kept constant at 40 ml/min.

Figure 3.19 displays the degradation curve for the degradation of methylene blue for different catalyst dosages.

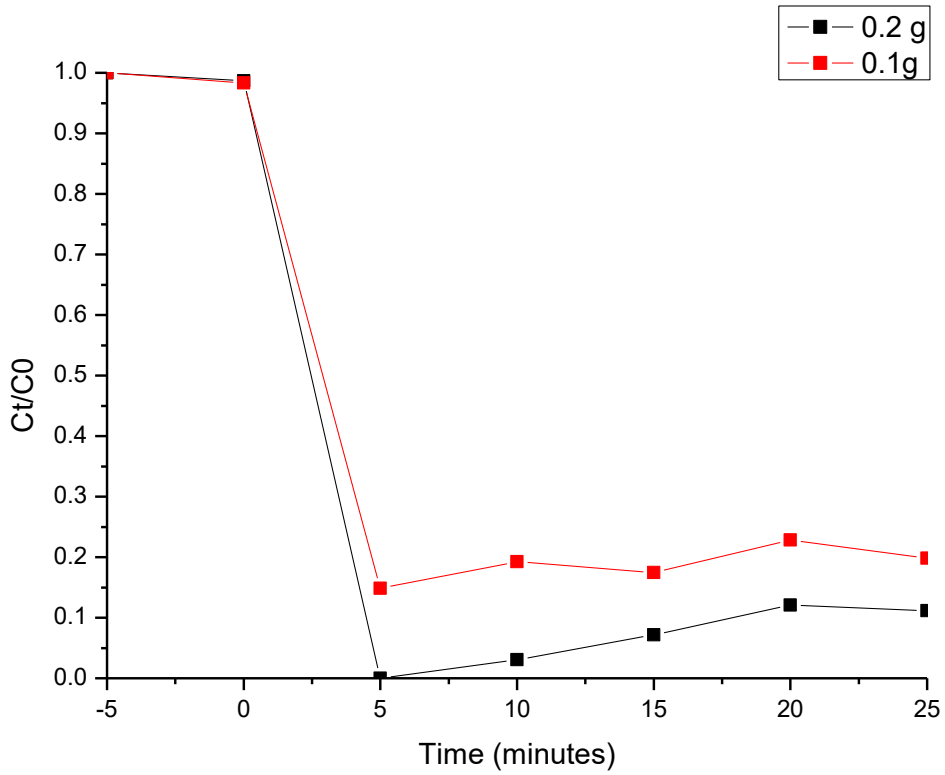

Figure 3.19: Comparison of degradation for different Co_3O_4 dosages

It is evident from Figure 3.19 that the higher catalyst dosage resulted in a more effective degradation of methylene blue. The samples were taken at the outlet stream of the reactor which allowed limited time for the homogeneous reaction to take effect.

A higher Co_3O_4 dosage resulted in a better degradation of methylene blue as the solution reached the outlet stream of the reactor. At a dosage of 0.2 g, the highest degradation reached was after 5 minutes with 100% degradation. For the mass of 0.1 g, the highest degradation was 85.2% also after 5 minutes. Higher degradation occurs by higher catalyst loading since a larger number of active sites are available to activate PMS to form $SO_4^{\bullet-}$ radicals (sulfate radicals SRs). The SRs are responsible for the breakdown of the methylene blue and hence the rate of degradation decrease with decreasing catalyst content.

Effect of tap water on the degradation of methylene blue

All tests have been done by making use of de-ionised water when preparing the methylene blue solutions. To evaluate the significance of using de-ionised water, tests were done by preparing the dye solution with tap water. The same concentration of dye was used (10 mg/L) and the same amounts of PMS were used (0.035 g/150 ml). The tests have shown no visual difference in the degradation of the dye.

Figure 3.20 shows the degradation achieved using tap water and de-ionised water for the preparation of the methylene blue. It is evident that there was no difference in the product which suggests that using tap water has no effect on the extent of the degradation.

Figure 3.20: Feed and product samples for the degradation of methylene blue prepared by using de-ionised water (left) and tap water (right)

3.6.3 Preliminary real effluent treatment

In this part of the study, real effluent was treated in the bench scale PRB reactor. Different dye types were used in the tests. Acid dye, base dye, metal complex dye, reactive dye and a

dispersed dye was used. The dyes were all obtained from the factory dye bath and all had different concentrations.

For the first set of experiments 0.07 g of PMS was used for a 300 ml sample along with 0.3 g Co_3O_4. Visual inspection of the sample showed that no degradation had occurred. The conclusion was made that the PMS dosage was too low and for the second set of experiments the PMS dosage was increased by a factor of 3.

Visual inspection of the second set of runs showed that some degradation occurred for the acid dye, base dye and metal complex dye as shown in Figure 3.21.

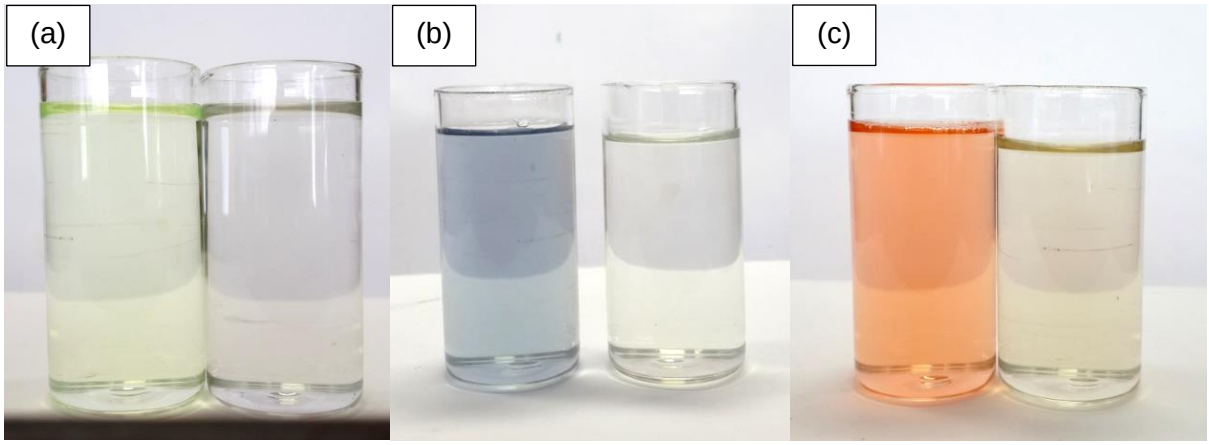

Figure 3.21: Initial and final samples of the acid dye (a), base dye (b) and metal complex dye (c)

The reactive dye and the dispersed dye did not show any visual sign of degradation after the 300 ml solution had been treated nor did they show a significant change in COD. The reactive dye had an initial pH of 10.42 and 10.50 during treatment. The SR are being scavenged by the hydroxyl radicals $OH^{\bullet}$ (HRs) which then become the dominator species at a pH above 10 (Chan and Chu, 2009). The $^{\bullet}OH$ species have a lower oxidation potential and would therefore take a longer time to degrade the dye, hence why the effect on the reactive dye was not significant. They are also more selective to which organics they degrade and therefore a very low or no degradation was observed by Sun and Wang, (2015). The precipitation of $CoOH^{+}$ complexes may occur which lowers the oxidation potential and results in a less efficient degradation of the contaminants as mentioned by Su et al., (2013).

Table 3.4 presents the results obtained after doing an analysis on the feed samples as well as the product samples of the treated dyes.

Table 3.4: Data obtained for the treatment of real textile effluent using 0.3 g Co_3O_4, 0.21 g PMS and a sample volume of 300 ml

	Acid Dye	Base Dye	Reactive Dye	Dispersed Dye	Metal Complex Dye
Concen-tration (%)	0.64	0.56	1.64	2.86	2.21
pH	4.46	4.36	10.42	4.41	4.63
pH after PMS	4.42	4.23	10.5	4.35	4.64
pH Product	4.31	4.17	10.42	4.36	4.53
COD (mg/L)	2265	2810	8395	6045	1650

The initial COD levels are presented in the form of a column chart in Figure 3.22. It is evident from Table 3.4 and Figure 3.22 that the reactive dye and the dispersed dye had COD levels significantly higher than the acid, base and metal complex dye wastewaters. As stated by Wiesmann et al., (2007), COD is an indication of the strength of organic compounds in water derived by the determination of the oxygen demand. The reactive dye and dispersed dye had COD levels of 8395 mg/L and 6045 mg/L respectively which suggested that more PMS is needed to produce more SRs to degrade the substantial amounts of organic compounds.

Standards preparation for real effluent was extremely complex as each dye drop has a different recipe and comprises of different concentrations and colours. The dye houses mix each dye drop with wash water in a sump which makes it impossible to recreate this water to form standards to calibrate the UV-visible spectrophotometer. All colours have different wavelengths and these wavelengths interfere with one another and give inaccurate analyses of concentration in the UV-visible spectrophotometer. The reduced treatment times of a maximum of 5 minutes (see Figure 3.19) forced an alternative and more rapid colour measurement technique to be obtained for future trial work. A Lovibond® spectrocolorimeter was recommended to be ideal for the purpose of rapid colour measurement and also for measuring mixed sump samples without having to prepare standards curves for calibration.

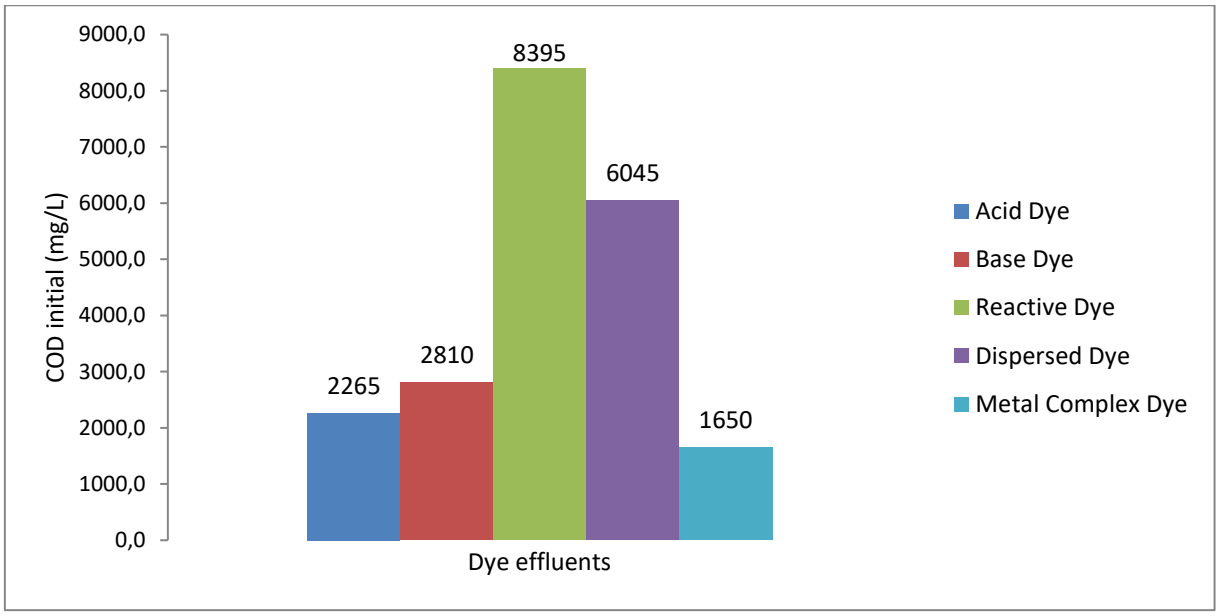

Figure 3.22: Initial COD levels for the dye wastewaters

3.7 Conclusion

The catalyst particles produced via the hydrothermal synthesis method were rod shaped particles consisting of smaller rhombohedral shaped crystals. The aggregated rods were 1.25 µm in length with an average diameter of 160 nm. These rods however were broken into rhomboids when the catalyst was immobilized in the permeable barrier. This was confirmed visually, by SEM imaging of the substrate, as no rod-shaped particles were present in the permeable barrier after the catalyst had been immobilized.

Two immobilization techniques were evaluated. The second immobilization technique, making use of the catalyst suspension and the Buchner funnel proved to be successful compared to the hand spread method. Further studies need to be done on the interaction of the catalyst with the substrate material.

Preliminary tests have shown that the horizontal flow configuration is not effective for the current substrate resistance and flow rate. The vertical flow arrangement has shown better results and has also proven that the reactor can successfully treat a model dye (methylene blue) and real textile effluent. The pH and the COD strength are key parameters to consider when treating real effluent as stated in literature.

Utilizing the UV-visible spectrophotometer was found unsuitable as the reaction was very rapid below 5 minutes for complete degradation and by the time the analysis had been done it would not reflect the true concentration of that sample at the certain time. A Lovibond® spectrocolorimeter was recommended for use due to the rapid colour measurement and simplistic calibration method that the instrument operates with.

Real dyebath effluent samples were successfully treated at a catalyst and PMS concentration of 0.3 g and 0.7 g/L respectively. Visual colour changes were observed for acid, base and metal complex effluent. Based on these results it was clear that optimization of catalyst/PMS concentrations was required for various strengths and types of effluent samples.

CHAPTER FOUR: Performance optimization of the bench scale continuous reactor

4.1 Introduction

In this chapter, the performance optimization of the bench scale reactor using methyl orange as an organic contaminant in the feed water is discussed. The efficiency of the reactor was determined by monitoring and evaluating the breakdown of the organic dye. A hand-held Lovibond colorimeter was used to analyse the product stream of the reactor. The methodology for optimizing the reactor is described as well as the results obtained are discussed. Furthermore, the treatment of actual textile effluent water is analysed and discussed.

4.2 Methodology for the optimization of the bench scale reactor

4.2.1 Experimental matrix

Since methylene blue is degraded easily by the removal of oxygen, it was decided to use methyl orange dye for the optimization of the bench scale reactor. A new instrument for the analysis of the product stream has also been obtained to get a more accurate analysis of the degradation efficiency of the catalyst and the efficiency of the reactor.

The bench scale reactor was optimized by doing the following studies and utilizing the optimum conditions in the subsequent studies:

1. PMS optimisation: The dosage of PMS was varied at the following dosages
    - 0.233 g
    - 0.300 g
    - 0.367 g
    - 0.500 g
2. Flow rate optimisation: The effect of flow rate on degradation efficiency was studied at
    - 20 ml/min
    - 40 ml/min
    - 60 ml/min
3. Catalyst optimization: Two different particle sizes of commercially available catalyst were compared to the batch hydrothermally synthesised (BHS) Co_3O_4.
    - 175 nm batch hydrothermally synthesised Co_3O_4
    - 50 nm commercially available Co_3O_4

- 10 µm Co_3O_4

4. Catalyst mass optimisation: Catalyst mass per filter was varied using the most effective catalyst of the second study.
    - 0.1 g catalyst per permeable barrier
    - 0.3 g catalyst per permeable barrier
    - 0.5 g catalyst per permeable barrier
5. Dye concentration optimisation: The effect of dye concentration was studied at the optimum concentration of PMS, catalyst mass and flow rate at
    - 10 mg/L
    - 20 mg/L
    - 30 mg/L

All the tests done were repeated three times to observe the repeatability and to obtain a good representation of the results.

4.2.2 Colour measurement and the Lovibond® spectrocolorimeter

As discussed in Chapter 3, a different technique was required to measure the almost instantaneous colour changes obtained in the PRB system. The Lovibond® spectrocolorimeter was recommended for further use. A procedure for developing degradation curves using the instrument was required. This section provides a summary of how colour is measured by this instrument as well as how the results are interpreted to obtain degradation curves.

Colour is described as a visual, perceptual property in human beings. To see colour involves three components – a source, an object and a processor. The visual light spectrum ranges from 360 to 720 nm and from blue to red. A material appears coloured depending on the wavelength of the light that it transmits or reflects (Best, 2012).

To accurately identify a certain colour, a combination of three dimensions are used: the hue, the chroma and the lightness. The hue is the colour that we see when looking at an object i.e. green, blue, red, orange etc. The chroma is a description of the dullness of the object. Chroma is also known as the saturation. It describes how close the colour is to grey or the pure hue. Colours can be classified according to their lightness, which is the luminous intensity of a colour. In other words, how light or dark a colour is. The lightness ranges from white to black (Schanda, 2007).

The CIE (international commission on illumination) colour system utilizes three coordinates to locate a colour in a colour system: 1) CIE XYZ, 2) CIE L*a*b and 3) CIE L*C*h. Colours can be quantified by instruments that gather the wavelengths of light transmitted or reflected by

an object. The different intensities formed by different wavelengths are detected by the instrument and recorded across the spectrum. The reflectance or transmittance detected is plotted corresponding to its wavelength to present a transmittance or reflectance curve (Schanda, 2007; Hunt and Pointer, 2011).

When the CIE L*a*b system is used to record colour, the L* quantifies the lightness, a* quantifies the red/green value and b* quantifies the yellow/blue value. The CIE L*a*b system uses cartesian coordinates to represent colour. The CIE L*C*h system utilizes polar coordinates to quantify colour and L* represents the lightness, C* represents the chroma of the colour and the h* represents the hue of the colour. The hue is represented as an angular measurement. Figure 4.1 describes a combination of the CIE L*a*b and the CIE L*C*h system that is used in the Lovibond® spectrocolorimeter (Nemtanu and Brasoveanu, 2010).

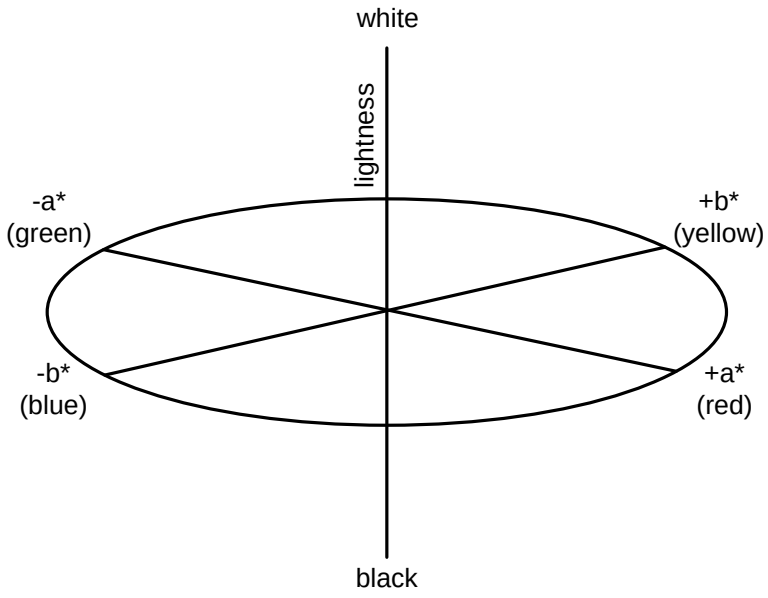

Figure 4.1: Graphical representation of the CIE L*a*b and CIE L*C*h system (Nemtanu and Brasoveanu, 2010)

The spectrocolorimeter determines a ΔE value when measuring colour. The ΔE value is calculated by a set of equations using the values of the L*, a*, b* C* and h* obtained from the measurement of a standard sample. ΔE is the colour difference between the sample and the standard in terms of the L*a*b* and the L*C*h values. The spectrocolorimeter determines a value, ΔE, for the difference in colour of the standard and the sample.

4.2.3 Data Analysis

As discussed in section 4.2.2, the Lovibond® spectrocolorimeter measures a value for colour difference, ΔE, between the measured sample and the standard sample. The standard sample was selected to be de-ionised water because the aim was to obtain complete colour removal of the effluent. During the experiments, the initial sample, which was the feed

sample after the addition of PMS, would have the largest ΔE as the sample contained the highest concentration of colour. The initial sample was labelled ΔE_0 and had been taken from the feed tank which meant it had not been treated by the PRB system. The subsequent samples were labelled ΔE_t and correspond to a sample interval of 2 minutes. The ΔE_t samples were taken directly from the product stream after undergoing treatment by the PRB system and were therefore smaller than the ΔE_0 sample. Due to the standard sample being de-ionised water, the goal was to obtain a $\Delta E_t = 0$ because this would indicate that the sample has the same colour as de-ionised water and 100% colour removal was achieved.

After treating the effluent and obtaining ΔE samples for every 2 minutes of treatment, the degradation curves were plotted. The degradation was determined by calculating $\Delta E_t/\Delta E_0$, which represents the treated sample (ΔE) as a fraction of the initial feed sample (ΔE_0). The degradation curves were plotted showing the fraction of colour remaining in the treated stream ($\Delta E_t/\Delta E_0$) on the y-axis versus the treatment time on the x-axis. To obtain the total breakdown efficiency achieved (as a percentage) by the PRB system, the colour left in the treated effluent i.e. $\Delta E_t/\Delta E_0$ was determined as a percentage by Equation 4.1.

$$\boldsymbol{Degradation\ efficiency} = \left(\mathbf{1} - \frac{\boldsymbol{\Delta E_t}}{\boldsymbol{\Delta E_0}}\right) * \mathbf{100} \qquad \textbf{(4.1)}$$

4.3 Results and discussion for the optimization of the bench scale reactor

In this section, the results of the treatment of methyl orange will be discussed as well as the determination of the optimum operating conditions for the bench scale reactor will be determined.

4.3.1 Effect of PMS

Oxone® is the commercial name for the triple salt of peroxymonosulfate (PMS) and is the oxidizer used in conjunction with cobalt oxide catalyst to produce free sulfate and hydroxyl radicals (SRs and HRs respectively) (Sun and Wang, 2015). In this process, PMS was dosed into the feed tank of the wastewater solution which was then fed to the reactor where it was activated by the catalyst to form the free radicals. The efficiency of the activation i.e. the number of free radicals formed is depended on the efficiency of the contact of the PMS with the catalyst and the initial dosage of PMS.

To optimize the PMS dosage various tests were done with different concentrations of PMS and the results are presented in Figure 4.2. It is evident that when the dosage of PMS was increased from 0.233 g/L to 0.300 g/L there was a definite increase in the degradation of methyl orange. On average at a dosage of 0.233 g/L the degradation was 74.4% and at a dosage of 0.3 g/L the degradation was 89.9%. As the concentration of PMS was further

increased, there was no further increase in the degradation efficiency. At a dosage of 0.367 g/L, 0.433 g/L and 0.5 g/L the degradation was 88.8%, 88.5% and 87.8% respectively.

It is notable that the degradation efficiency stagnates at ± 88% with an increase of PMS concentration from 0.3 g/L to 0.5 g/L. According to Chowdhury et al., (2015), it is possible that when the PMS concentration is above a critical point it can cause a radical quenching effect that can eventually lead to a decreased degradation efficiency (Chowdhury et al., 2015).

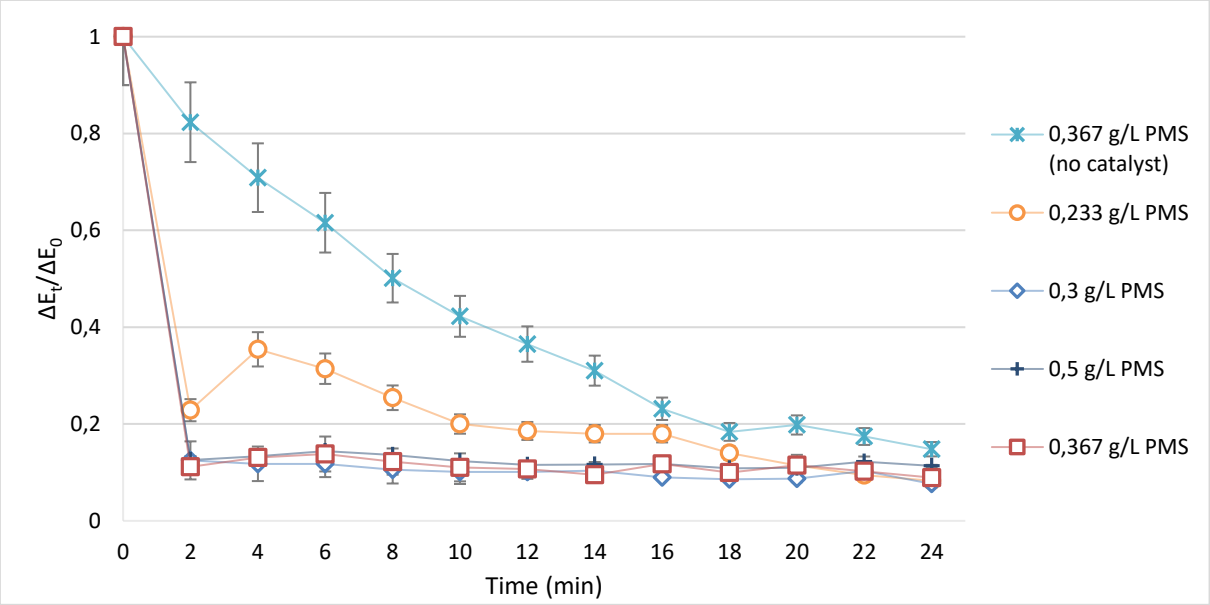

Figure 4.2: Methyl orange degradation at various PMS concentrations with 10 mg/L dye concentration and 0.3 g cobalt oxide catalyst at a flow rate of 40 ml/min

A reference test was also done to see whether the PMS itself would degrade the dye without being activated by the catalyst. It was observed that the pure PMS can degrade the methyl orange dye to a maximum of 85.2% after 24 minutes. However, after 2 minutes the degradation by PMS only was only 17.7%.

The effect of the PMS activation by the catalyst and the additional degradation caused by the increased number of radicals is displayed in Figure 4.3. The optimum PMS dosage was at a 0.367 g/L concentration which contributed to an 88.8% methyl orange degradation. At 0.300 g/L and 0.500 g/L PMS the degradation was 87.5%. The optimum concentration was chosen to be 0.367 g/L as the product was visually clear where as the product for the 0.300 g/L concentration had a slight yellow stain although the average degradation was higher by 1.1%.

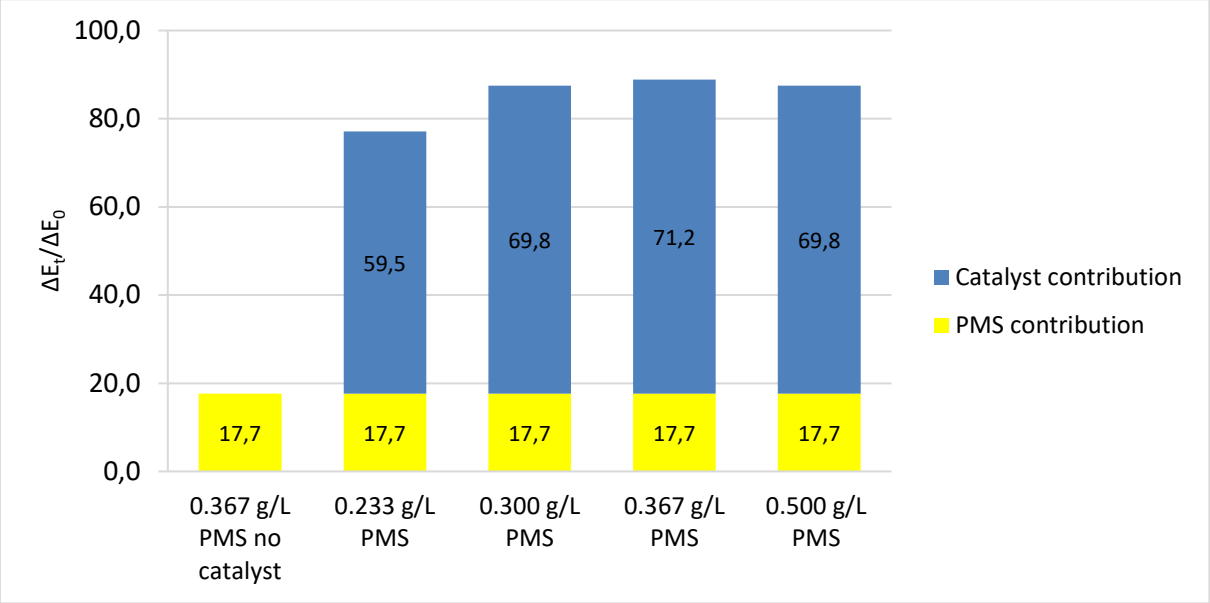

Figure 4.3: Catalyst contribution to the degradation of methyl orange at the 2 minute sample

The effect of the catalyst as described in section 2.3.3 can be observed in Figure 4.3. It is evident that the presence of a catalyst has a significant effect on the activation of PMS. The first 2 minutes of the reaction is the most relevant time as the PMS itself has only been able to degrade a maximum of 17.7% of the dye, hence this is where the catalyst will show the most effect.

In the two and four-minute time interval, the 0.3 g/L and 0.367 g/L PMS degradation curve looks very similar as the degradation achieved varies by a mere 1.8% over the 4 minute period. However, in Table 4.1 the 0.3 g/L PMS dosage had a higher percentage standard error for both the 2 - and 4 minute samples at 23.7% and 23% respectively. This was higher by 12.1% and 12.9% (2 - and 4 minute samples respectively) than the 0.367 g/L dosage. This suggests that the latter PMS dosage serves a more consistent production of free radicals which would lead to a more consistent degradation of dye.

Table 4.1: Comparison percentage degradation and percentage standard error of the mean of two different PMS dosages at the 2 and 4 minute sample

	2 minute sample		4 minute sample	
	0.3 g/L PMS	**0.367 g/L PMS**	**0.3 g/L PMS**	**0.367 g/L PMS**
% Degradation	87.4	88.8	88.1	87.0
% SE of the mean	23.7	11.6	23.0	9.1

4.3.2 Effect of flow rate

The flow rate of the feed solution passing through the reactive barrier is the most critical parameter in the design of the reactor as this governs the residence time between catalyst

and the oxidizer. A flow rate study was done to determine the optimum residence time required for the highest degradation efficiency of methyl orange.

Figure 4.4 presents the degradation curves of methyl orange at 20, 40 and 60 ml/min flow rate. It is evident that at a flow rate of 40 ml/min the degradation is most efficient. The 40 ml/min curve shows a very aggressive initial breakdown of dye and keeps that breakdown efficiency over the reaction period. The 20 and 60 ml/min however, gradually increase the degradation over the reaction period. They show a very similar degradation however the 60 ml/min reaction is very rapid in the first 3 minutes. The gradual breakdown of the dye in the 20 and 60 ml/min reaction follows a very similar shape as the reaction with PMS only.

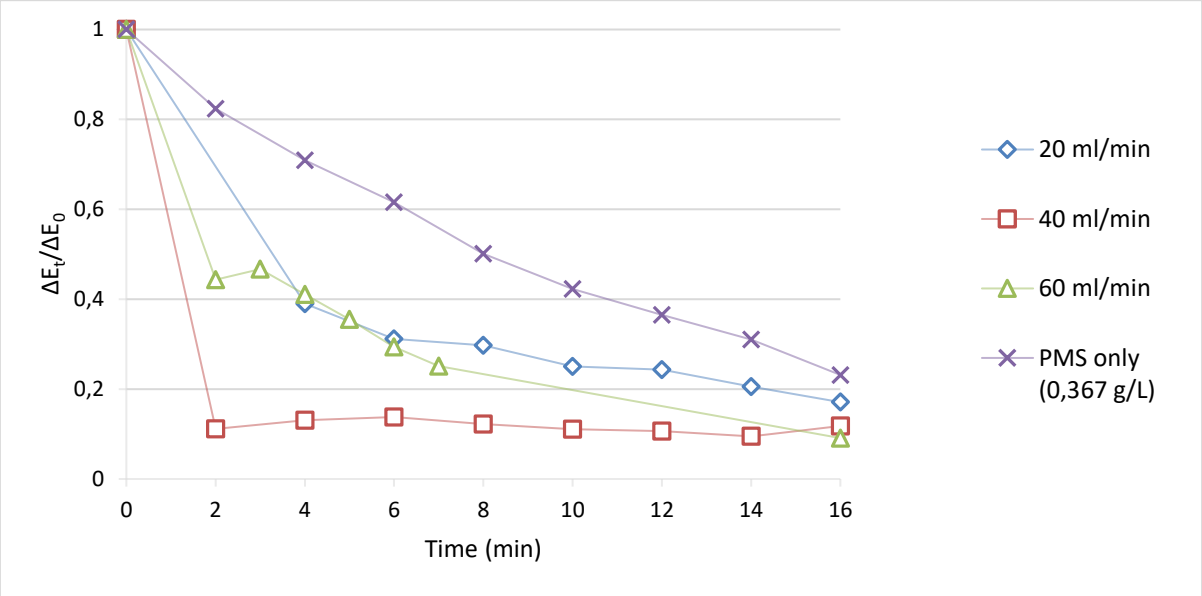

Figure 4.4: Effect of flow rate on the degradation of methyl orange at a dye concentration of 10 mg/L, 0,3 g catalyst and 0,367 g/L PMS concentration.

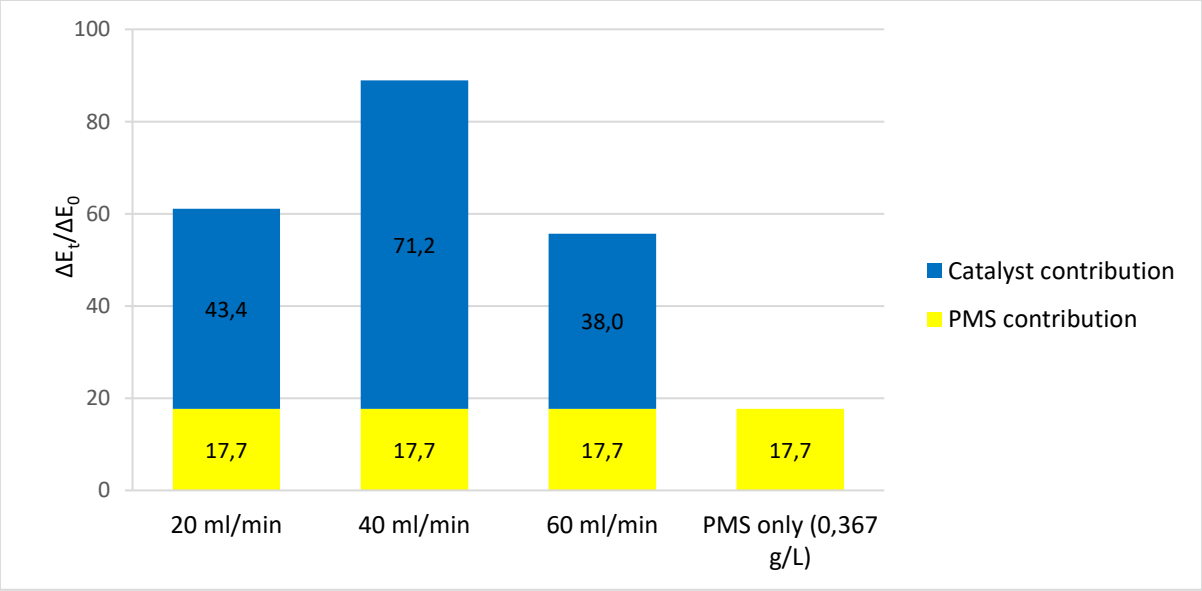

Figure 4.5: Catalyst contribution to the degradation of methyl orange at the 2 minute sample

In Figure 4.5 one can see that the contribution of the catalyst is 71.2% at a flow rate of 40 ml/min and this is 1.64 and 1.87 times greater than that of the 20 ml/min and 60 ml/min reaction. It is evident that at a flow rate of 40 ml/min the degradation is the most efficient and this suggests that the contact between catalyst and oxidizer at this flow rate is the most efficient.

4.3.3 Effect of catalyst size

Chowdhury et al., (2015) produced Co_3O_4 that had exceptional catalytic activity for the degradation of methyl orange dye. The reason for the enhanced catalytic efficiency was not evaluated in depth by Chowdhury et al., (2015). Due to this, this study evaluated the size effect of Co_3O_4 catalysts by comparing the batch produced Co_3O_4 to two different sized (50 nm and 10 µm) commercially available catalysts.

Figure 4.6 represents the degradation curves obtained for the tests done on the different catalysts. The BHS catalyst had an average degradation efficiency of 88.8% followed by the 50 nm catalyst at 81.4% and then the 10 µm catalyst which had a lower average degradation efficiency of only 64.3%.

It is evident that the BHS catalyst has a much higher catalytic efficiency than the commercially available catalysts. In the first two minutes of reaction the BHS catalyst had already achieved a degradation of 88.9% whereas the 50 nm and 10 µm catalysts have achieved only 63.8% and 24.9% degradation respectively. On average, the BHS catalyst has shown between 7% and 24% better degradation of methyl orange dye than the commercially available catalyst.

The 10 µm catalyst had the lowest degradation of the three catalysts compared. It was also the catalyst with the largest average particle size. Referring to Figure 4.6 one can observe that the degradation curve for the 10 µm was astoundingly similar to the degradation curve of pure PMS. The activation of PMS by the catalyst was very inefficient, caused by limited catalyst-oxidizer contact due to the decreased surface area.

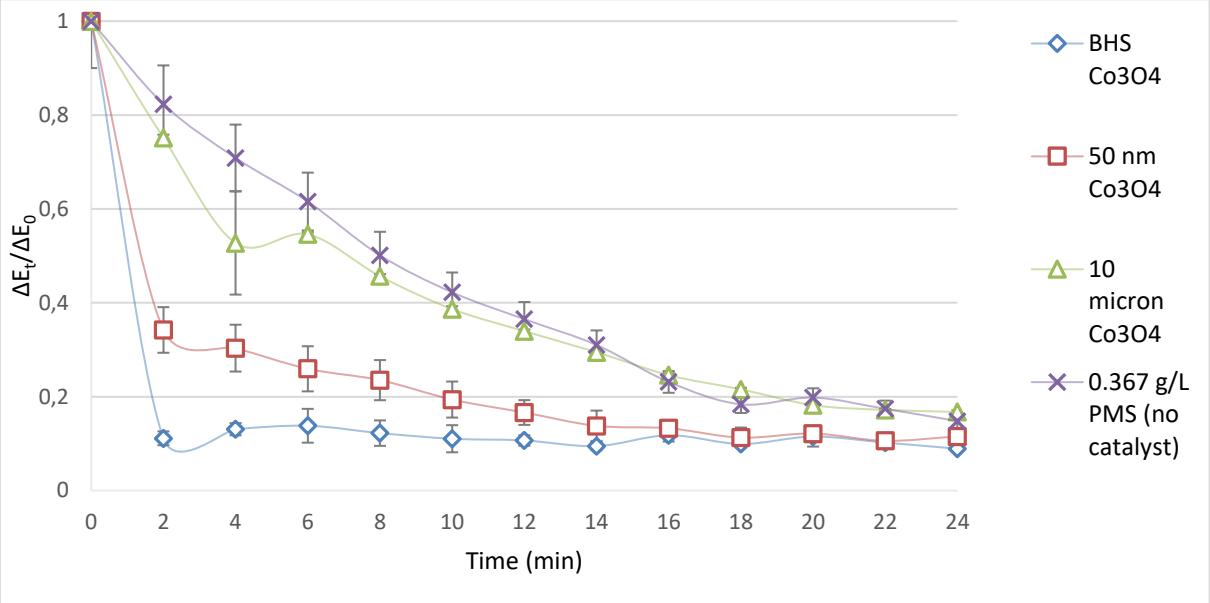

Figure 4.6: Commercially available catalyst compared to the lab produced catalyst at a dye concentration of 10 mg/L, catalyst mass of 0.3 g and PMS dosage of 0.367 g/L

The effect of the catalyst on the activation of PMS is displayed in Figure 4.7.

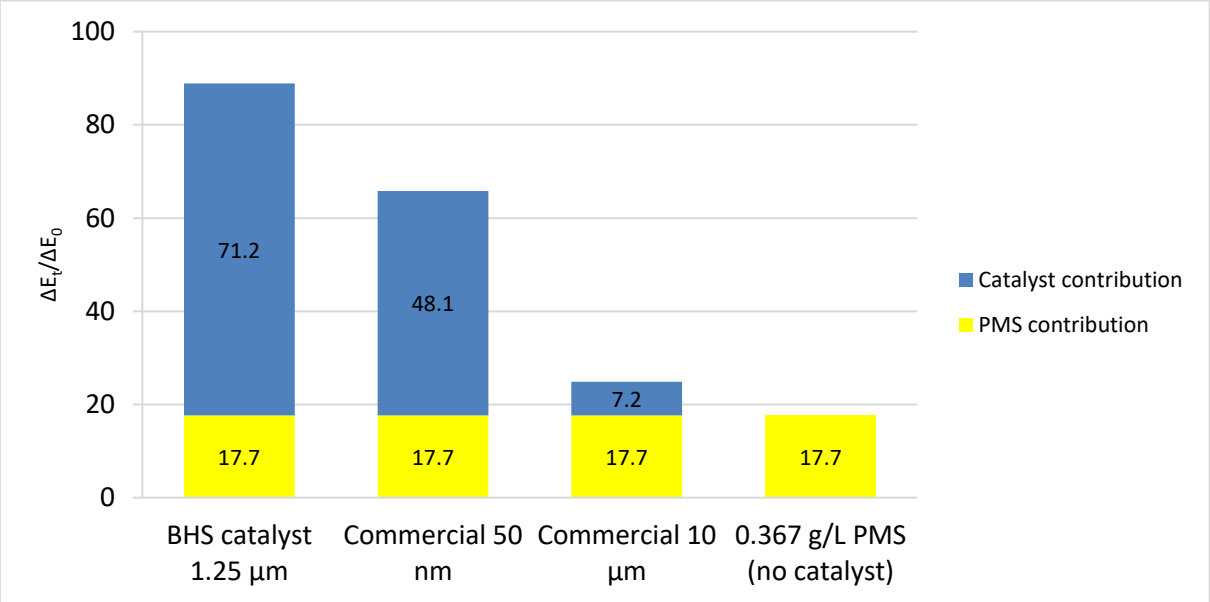

Figure 4.7: Catalyst contribution to the degradation of methyl orange at the 2-minute sample

At the two-minute data point, the degradation caused by the PMS is 17.7% whether the catalyst is present or not. In the presence of catalyst, more PMS will be activated which means radicals will be produced and the degradation will be increased. For the BHS catalyst, the supplementary degradation is 71.2%, for the 50 nm catalyst is 48.1% and the 10 µm has very limited contribution of 7.2%. This once more proves that the BHS catalyst has an exceptional ability to activate PMS.

The reason for the higher efficiency of the BHS catalyst is unknown as in the case of Chowdhury et al., (2015) and is outside the scope of this project. It is clear that the catalytic efficiency cannot simply be related to particles size. Further investigation based on BET measurements should be conducted in the future to improve understanding of Co_3O_4 catalytic efficiency.

4.3.4 Effect of catalyst mass

The mass of catalyst used in the degradation of methyl orange is related to the extent of the activation of PMS. In Figure 4.8 the degradation curves for the catalyst mass studies were plotted. For a mass of 0.1 g one can see that it has a slightly lower efficiency than for 0.3 g and 0.5 g. On average, for a mass of 0.1 g catalyst an average degradation of 78.2% was achieved. For a mass of 0.3 g and 0.5 g of catalyst a degradation of 88.8% and 87% was achieved respectively.

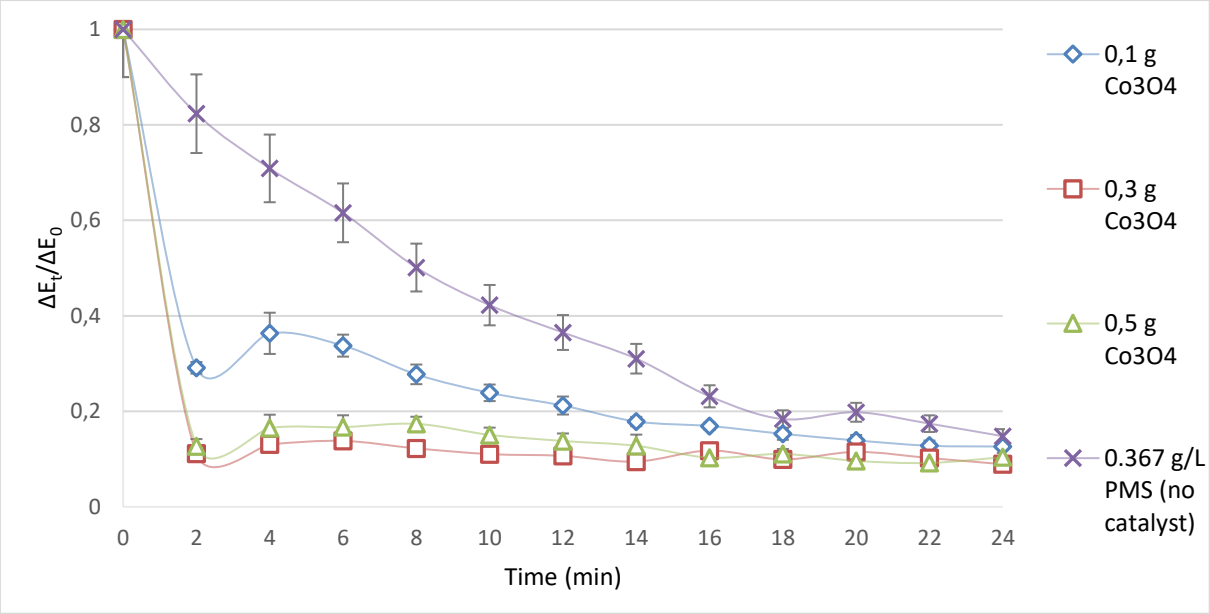

Figure 4.8: Degradation curves for various catalyst masses at 10 mg/L dye concentration and 0.367 g/L PMS dosage

Catalyst mass and PMS dosage are interrelated as they are dependent on each other. A certain mass of catalyst will be able to activate a certain dosage of PMS. The optimum catalyst mass was elected to be 0.3 g of catalyst that will efficiently activate 0.367 g PMS. The fact that 0.5 g of catalyst did not show a greater degradation could be explained due to the limited amount of PMS that was available to produce radicals. In this case, the PMS had become the limiting reactant and the catalyst was in excess.

It is observed that an increase of catalyst mass from 0.3 g to 0.5 g has an 1.8% decrease in the average degradation of the dye. This is not a significant change as the catalyst has been increased by 40% resulting in only a 1.8% change in the degradation.

4.3.5 Effect of dye concentration

In this study, the aim was to observe the effect that an increased dye concentration would have on the degradation efficiency should the catalyst loading and the PMS dosage be kept constant. Theoretically, a higher dye concentration would mean that a larger number of contaminants are present and hence a higher number of radicals would be required to obtain the same degradation percentage as shown Figure 4.9.

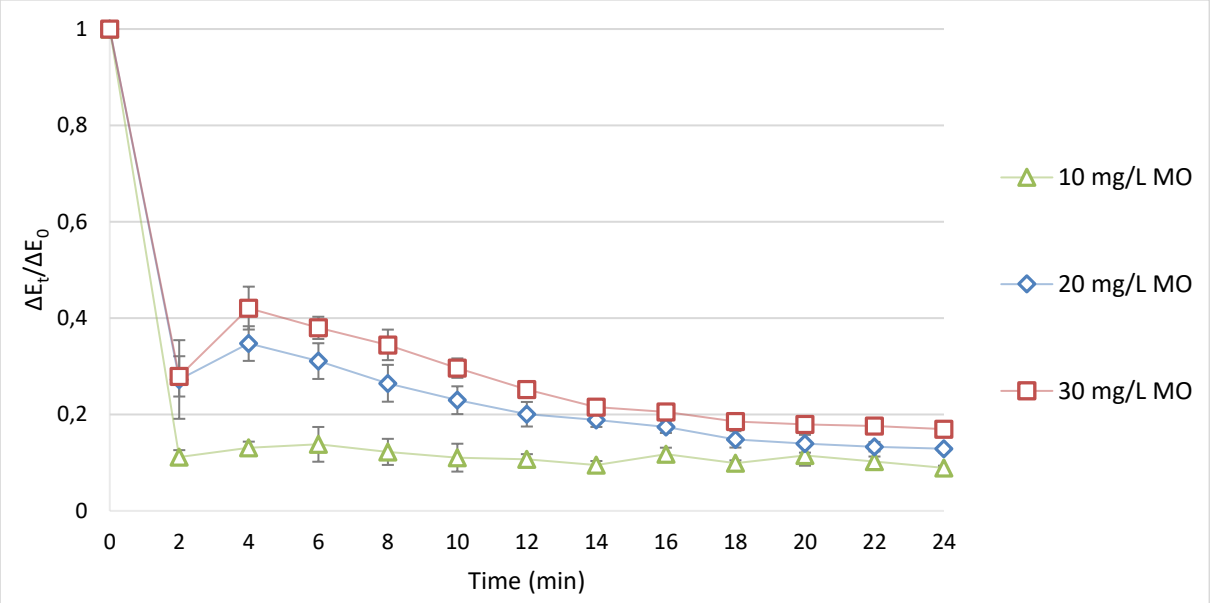

Figure 4.9: Degradation curves for different methyl orange concentrations at 0.3 g catalyst loading and 0.367 g/L PMS concentration

As the dye concentration is increased from 10 mg/L to 30 mg/L one observes a decrease in average degradation. For the concentration at 10 mg/L an average degradation of 88.8% followed by 78.8% at a 20 mg/L concentration and 74.1% at a concentration of 30 mg/L is observed. This is caused due to the increased number of organic dye pollutants at a higher dye concentration. To break down the dye at a higher concentration, a higher PMS dosage would be required to produce a larger number of free radicals for the contaminant break down.

4.3.6 Real effluent results

Real textile effluent was obtained from a local dye house in Cape Town. The sample was taken directly from the dye drop before reaching the sump. The dye drop had a total volume of 0.5 m^3 and is diluted by wash water and other sources of water in the 200 m^3 sump. The dilution factor was determined to be 1:20 which is what was used during the preparation of the real effluent feed.

Figure 4.10 summarizes the degradation of the real effluent achieved by the activation of PMS by cobalt oxide. It is observed that the addition of 0.4 g of catalyst increases the

degradation by 91.2%. The maximum degradation achieved was 96% at a catalyst mass of 0.4 g and 3 g/L PMS. At a catalyst mass of 0.4 g and 2 g/L PMS, 94.7% degradation was achieved.

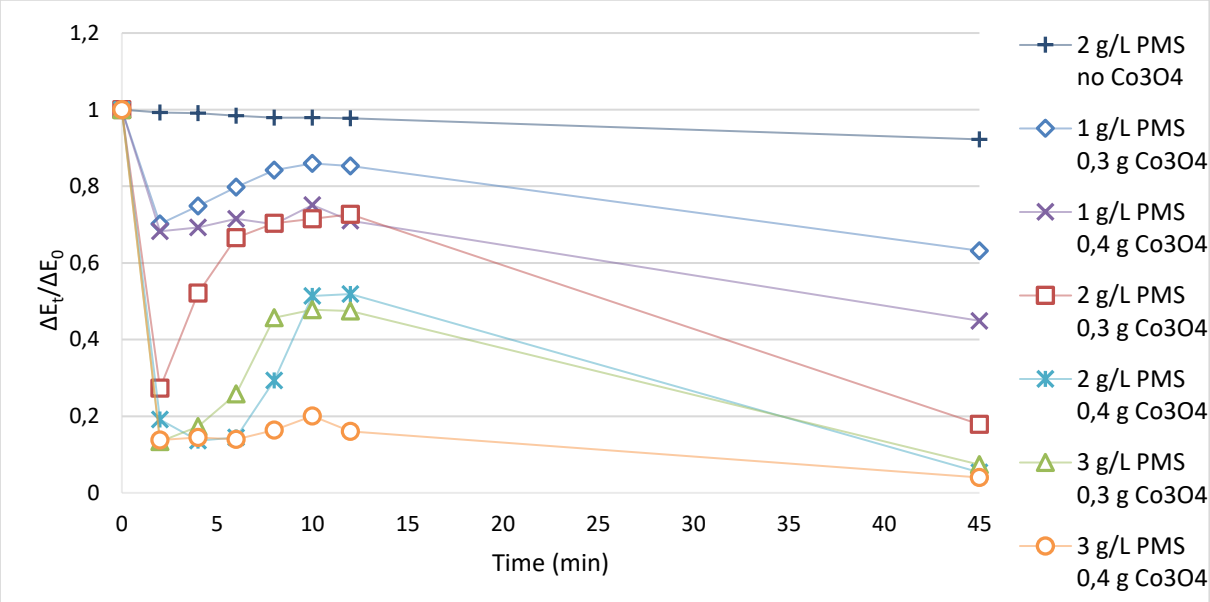

Figure 4.10: Degradation curve for real textile effluent at various catalyst and PMS concentrations

Although the degradation curves for 0.3 g catalyst with 3 g/L PMS and 0.4 g catalyst with 3 g/L PMS are quite different, the product after 45 minutes differs by only 1.3%. This value is not large enough to increase the cost of catalyst for such a small gain in degradation efficiency. Figure 4.11 shows the colour breakdown of the textile effluent achieved over the 45 minute period.

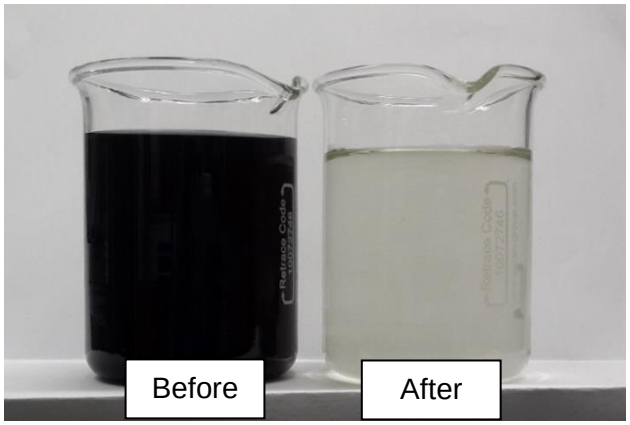

Figure 4.11: Before and after degradation at 0.4 g cobalt oxide and 2 g/L PMS dosage

It is repeatedly observed that the degradation is rapid for the first 2 minutes of the reaction where after the degradation reduces rapidly. The degradation rate seems to recover after 10 minutes of treatment depending on the operating condition. Comparing the degradation curves of the 0.4 g catalyst with 2 g/L PMS and 3 g/L PMS it is evident that the 3 g/L PMS

maintains the degradation up to the 6 minute interval where the degradation efficiency reduces but is recovered after the 10 minute interval. The 2 g/L PMS curve however, rapidly loses degradation efficiency after the 6 minute interval and keeps that trend up to 12 minutes where after it recovers the degradation rate. This drop in efficiency could be related to insufficient oxidizer available as well as catalyst amount available for the reaction.

This work, as a start, investigated only the effect of one parameter at a time in order to obtain optimum conditions for the reactor which could be used for reactor scale up. Future work will be conducted to understand the interaction between available catalyst, oxidiser and pollutant degradation using a factorial trial design.

4.4 Conclusion

The Lovibond® spectrocolorimeter was successfully utilised to measure degradation for rapid colour changes observed in the PRB system. It worked well for a single colour dye as well as real effluent. It was observed that the bench scale reactor can successfully degrade methyl orange dye in the current system arrangement utilizing the batch hydrothermally synthesized cobalt oxide that was immobilized in a permeable barrier. At a catalyst mass of 0.3 g (0.0247 g/cm^2) and a PMS dosage of 0.367 g/L the maximum degradation of 88.8% was achieved. An increased dye concentration caused a decrease in degradation efficiency and a higher PMS concentration can have a radical quenching effect where the breakdown efficiency is limited. The reactor was also successful in treating real textile effluent at 3 g/L PMS concentration and catalyst mass of 0.4 g with a flow rate of 40 ml/min to 95% after 45 minutes, but 87% degradation was already observed after only 2 minutes of treatment.

The optimum conditions were investigated to determine the scale-up parameters and to design the scale up model. The catalyst mass per PRB surface, flow rate and residence time within the PRB are the crucial parameters that need to be part of the scale up rationale to design and build an upscale system that can successfully treat textile effluent.

CHAPTER FIVE: Scale up rationale and model

5.1 Introduction

The development of new technologies includes a number of steps of which some are the optimization of the process, discussed in Chapter 4, and the scale-up from bench to pilot plant to full scale plant as stated by Wood-Black, (2014). In this chapter, the scale up rationale as well as the design of the large scale PRB system is explained. Provisional results obtained treating methylene blue and real effluent are presented and discussed. Furthermore, a hazard and operability study are provided for the PRB system.

5.2 Scale up rationale

Scale-up in chemical engineering describes the operation of a chemical reactor at different scales, operating parameters and reaction technologies by applying the quantitative rules. It does not only imply the ability to design and operate large plants but it also includes the skill to develop new technologies as well as more efficient technologies in order to produce a market competitive product that meets environmental requirements (Donati and Paludetto, 1997).

As discussed in section 2.6.2, the first step to the scale up is the determination of the general process i.e. determining the most critical operating parameters that need to be met in the scaled-up version to ensure successful operation of the pilot plant. The bench-scale reactor was used to determine the optimum operating conditions and scale up parameters as presented in Chapter 4. A linear scale up approach was selected based on these optimum parameters obtained for the design of the scaled-up reactor.

The parameters that were critical for the successful degradation of the dye were identified to be the same parameters that would be required for the scale up of the bench scale reactor. The scale up parameters were as follows:

- Catalyst mass per PRB cross-sectional area
- Residence time within the PRB
- The area of the permeable barrier required

5.3 Design equations for the scale up

The scale up parameters had to be determined to estimate the catalyst loading, the residence time in the PRB and the PRB area required to treat effluent at a specified flow rate. Three new design correlations were derived in this section and used to quantify the scale up parameters for any given size of reactor required.

5.3.1 Residence time in PRB

To determine the residence time in the permeable barrier, the optimum flow rate to achieve maximum degradation must be determined experimentally. The porosity of the permeable barrier must be known. Equation 2.11 can be modified by incorporating the porosity and pore volume to determine the residence time in the permeable barrier resulting in Equation 5.1.

$$\tau = \frac{V_{Pores}}{\dot{Q}_A}$$

$$= \frac{V_{PRB} * \emptyset}{\dot{Q}_A}$$

$$= \frac{\pi * d_A^2 * t * \emptyset}{4 * \dot{Q}_A}$$

$$\boldsymbol{\tau = 0.7854 * \frac{d_A^2 * t * \emptyset}{\dot{Q}_A}} \quad \textbf{(5.1)}$$

- $\tau \rightarrow$ residence time in the permeable barrier in units of s
- $V_{PRB}^{A} \rightarrow$ total volume of PRB A in units of cm^3
- $V_{Pore}^{A} \rightarrow$ pore volume of PRB A with in units of cm^3
- $\emptyset \rightarrow$ the porosity of the PRB
- $\dot{Q}_A \rightarrow$ volumetric flow rate through PRB A in units of cm^3/s
- $d_A \rightarrow$ diameter of the PRB of A in units of cm
- $t \rightarrow$ thickness of the PRB

The residence time is the time the molecules spend in the reactor and should therefore be the same irrespective of the size of the reactor. A residence time of 4.8 seconds was determined for this specific permeable reaction barrier system.

5.3.2 Diameter of the scaled-up PRB

To maintain the residence time, a certain PRB diameter is required for a specified flow rate. From Equation 2.11, when the residence time is known according to the optimum operating conditions to achieve maximum degradation, a new flow rate is specified and the porosity of the permeable barrier is known, the diameter of the PRB can be determined. Therefore, Equation 5.2 can be used to determine the required diameter of the scaled-up PRB.

$$\tau = \frac{V_{Pores}}{\dot{Q}_B}$$

$$= \frac{V_{PRB} * \emptyset}{\dot{Q}_B}$$

$$= \frac{\pi * d_B^2 * t * \emptyset}{4 * \dot{Q}_B}$$

$$d_B^2 = \frac{4 * \tau * \dot{Q}_B}{\pi * t * \emptyset}$$

$$\boldsymbol{d_B = \sqrt{1.2732 * \frac{\tau * \dot{Q}_B}{t * \emptyset}}} \quad \textbf{(5.2)}$$

- τ →residence time in the permeable barrier in units of s
- V_{PRB}^B→ total volume of PRB B in units of cm^3
- V_{Pore}^B→ pore volume of PRB B with in units of cm^3
- $\emptyset$ → the porosity of the PRB
- $\dot{Q}_B$ → volumetric flow rate through PRB B in units of cm^3/s
- d_B→ diameter of the PRB of B in units of cm
- t → thickness of the PRB

5.3.3 Catalyst mass and catalyst mass per PRB area ratio

To determine the catalyst mass for the scaled-up reactor, a linear scale up approach was followed, based on the diameter and the optimum catalyst mass for the bench scale reactor. To directly scale up the mass of catalyst required in the scaled-up reactor, the ratio of catalyst mass/PRB area should remain constant for the two different PRBs i.e. $M_{cat}^A = M_{cat}^B$. The ratio was utilized to determine the total catalyst mass necessary in the scaled-up reactor as given in Equation 5.3. This design correlation can be used to determine the catalyst mass required for any given PRB, given that the mass and cross-sectional area of the initial PRB is known.

$$m_{cat}^B = M_{cat}^A * A_{PRB}^B$$

$$= \left[m_{cat}^A \Big/ A_{PRB}^A \right] * A_{PRB}^B$$

$$= \left[m_{cat}^A \Big/ \frac{\pi * d_A^2}{4} \right] * \frac{\pi * d_B^2}{4}$$

$$\boldsymbol{m_{cat}^B = \frac{m_{cat}^A * d_B^2}{d_A^2}} \quad \textbf{(5.3)}$$

- m_{cat}^A → mass of catalyst in PRB A in units of g
- m_{cat}^B → mass of catalyst in PRB B in units of g
- A_{PRB}^A → cross-sectional area of PRB A in units of cm^2
- A_{PRB}^B → cross-sectional area of PRB B in units of cm^2
- d_A → diameter of PRB A in cm

- $d_B \rightarrow$ diameter of PRB B in cm
- $M_{cat}^{A} \rightarrow$ catalyst mass per cross-sectional area ratio of PRB A in units of g/cm^2
- $M_{cat}^{B} \rightarrow$ catalyst mass per cross-sectional area ratio of PRB B in units of g/cm^2

5.4 Filter area predictions

The design correlations derived in section 5.3 were applied to predict the PRB diameter and catalyst mass for a range of flow rates that commonly occur in the textile industry maintaining the optimum residence time of 4.8 seconds. The predicted values are displayed in Table 5.1 and it can be seen that for a full size industrial reactor with a flow rate of at least 25000 L/hr a PRB diameter of 397 cm would be required.

Table 5.1: Calculations for the determination of reactor diameter at increased flow rates maintaining a residence time of 4.8 seconds

Q (L/hr)	τ (s)	t (cm)	ø	$\frac{4}{\pi}$	d_B (cm) Eq. (5.2)	m_A (g)	d_A (cm)	m_B (g) Eq. (5.3)
2.40	4.8	0.334	0.8	1.27	3.90	0.3	3.9	0.3
12.75	4.8	0.334	0.8	1.27	9.00	0.3	3.9	1.6
76.50	4.8	0.334	0.8	1.27	22.05	0.3	3.9	9.6
1000.00	4.8	0.334	0.8	1.27	79.71	0.3	3.9	125.3
17000.00	4.8	0.334	0.8	1.27	328.65	0.3	3.9	2130.4
25000.00	4.8	0.334	0.8	1.27	398.54	0.3	3.9	3132.9

This is a large diameter of almost 4 meters and might not be sensible for operational or maintenance purposes. In cases like these a parallel flow assembly with multiple smaller reactors might be a better option to upscale the PRB system.

A multi-column design was therefore selected for the design of the scaled-up reactor as given in the following section.

5.5 Column layout and design

The residence time in the PRB barrier was determined using Equation 5.1 and was found to be 4.8 seconds. The residence time in the PRB is specific to this permeable barrier and should be determined experimentally should a different permeable barrier be used.

The scale up of the bench scale reactor was found to be linear by a factor of five times per column. This meant that the mass of catalyst per PRB and the flow rate through each column had to be multiplied by a factor of five to achieve the same catalyst mass/surface area ratio and PRB residence time. This calculation was applied to the scale up for one single reactor

column. The scaled-up reactor consists of six columns which means that the total catalyst mass and flow rate through the reactor was scaled-up by a factor of 30.

Table 5.2 is a comparison of the design aspects considered in the bench scale reactor and the scaled-up reactor. Quantifying the parameters follows these steps:

1. For a specified flow rate of 1275 ml/min, the residence time was calculated using Equation 5.1 which was 4.8 seconds.
2. Maintaining the residence time of 4.8 seconds at a flow rate of 1275 ml/min the diameter of the scaled-up reactor was determined to be 22.03 cm applying Equation 5.2. It was decided to use a multi-column system and therefore six columns of 9 cm diameter were selected. This resulted in a flow rate of 212.5 ml/min in each column to maintain the residence time.
3. The optimum catalyst mass was determined by the optimization of the bench scale reactor in the catalyst mass study described in Chapter 4. The mass was determined to be 0.3 g of catalyst. Based on Equation 5.3, the required catalyst mass in the scaled-up reactor was 1.6 g per PRB column. The total mass for the scaled-up PRB system was 9.6 g.

Table 5.2: Design aspects for the bench scale reactor, scaled-up reactor column and scaled-up reactor

Parameter	Bench scale reactor	Scaled-up reactor column	Scaled-up reactor total
Catalyst mass/area	0.025 g/cm^2	0.025 g/cm^2	0.025 g/cm^2
Catalyst mass	0.3 g	1.6 g	9.6 g
Flow rate	40 ml/min	212.5 ml/min	1275 ml/min
PRB residence time	4.8 seconds	4.8 seconds	4.8 seconds

The scale up model consists of a top and bottom column made from a 90 mm outside diameter PVC pipe 150 mm in length and 50 mm respectively with a custom built acrylic fitting (as in the bench scale) fitted in between the columns. A 90 mm reactive barrier is fitted in between the reactor columns into the acrylic fitting to complete the reactor. A 12 mm feed and product nozzle are fitted to both ends of the reactor for the feed and product streams. Figure 5.1 shows the layout and dimensions of the scale up reactor column.

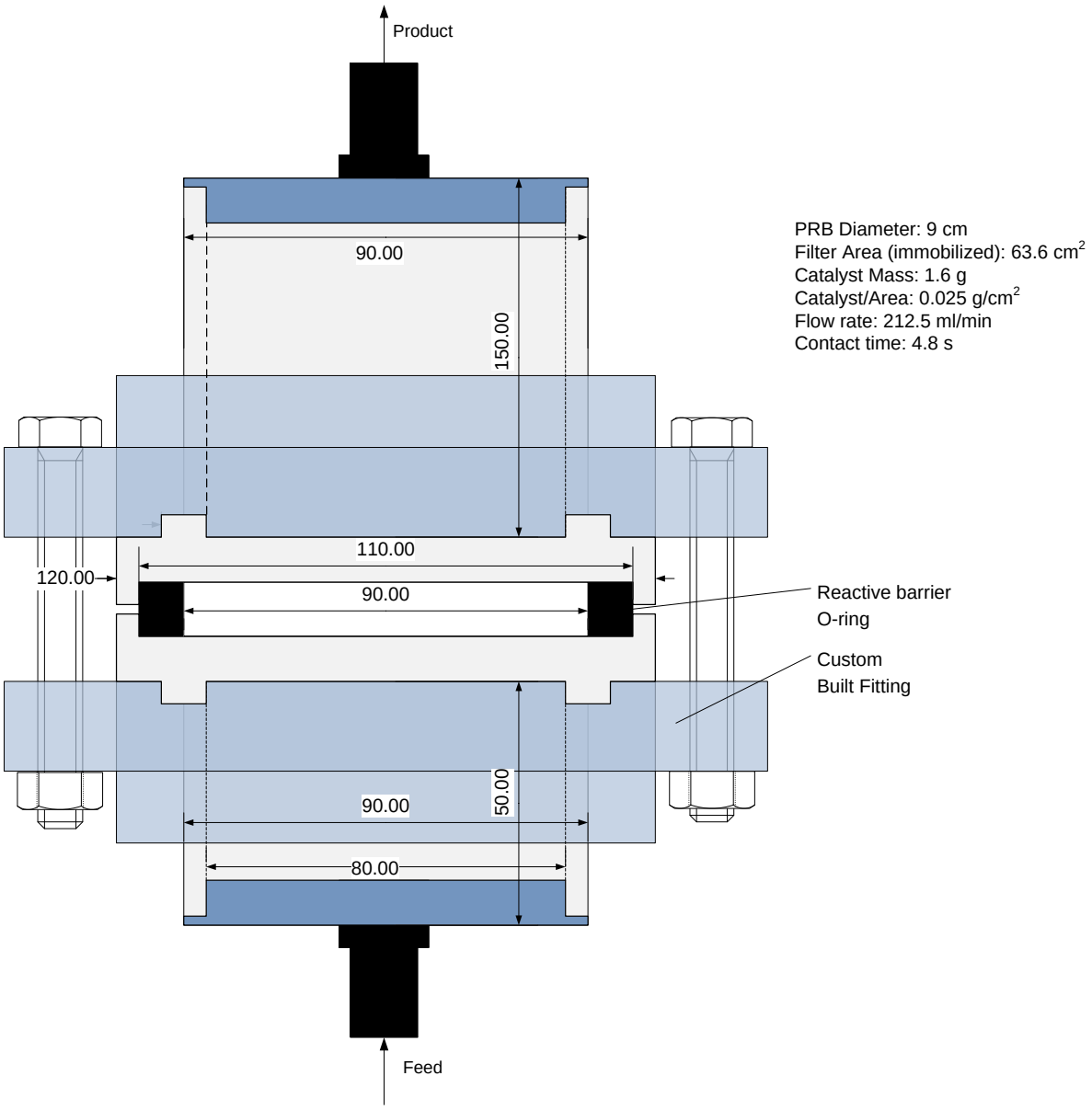

Figure 5.1: Technical drawing of a single column of the scale up reactor

5.6 Design aspects of the reactor

The reactor is designed to run in a parallel configuration feeding six reactor columns simultaneously. The feed from the pump is fed into a manifold that is designed to spread the flow into six even streams that are redirected to provide a feed stream to the six reactor columns individually. The manifold is constructed from a 90 mm OD PVC pipe with a 32 mm OD pipe feeding the manifold axially from the bottom. The outlets from the manifold (feeding the reactor columns) are distributed at 60˚ angles to allow for even flow through all pipes. The pipes feeding the reactor column from the manifold are all equal in length to allow for even flow through all reactor columns. The manifold is also fitted with a pressure gauge to monitor pressure inside the manifold. Figure 5.2 shows a top view of the layout of the

manifold and the reactor columns along with the valves and the pressure indicator situated on the manifold.

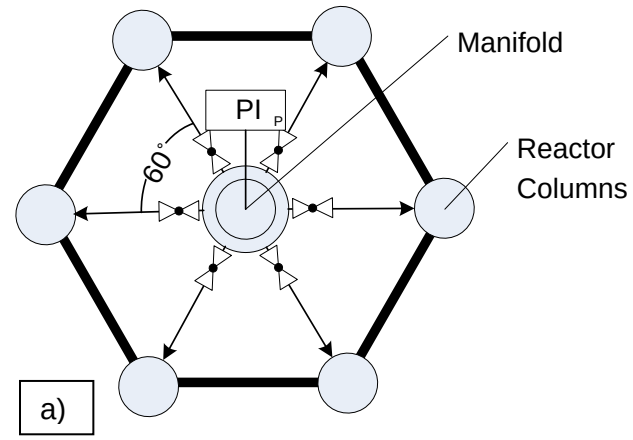

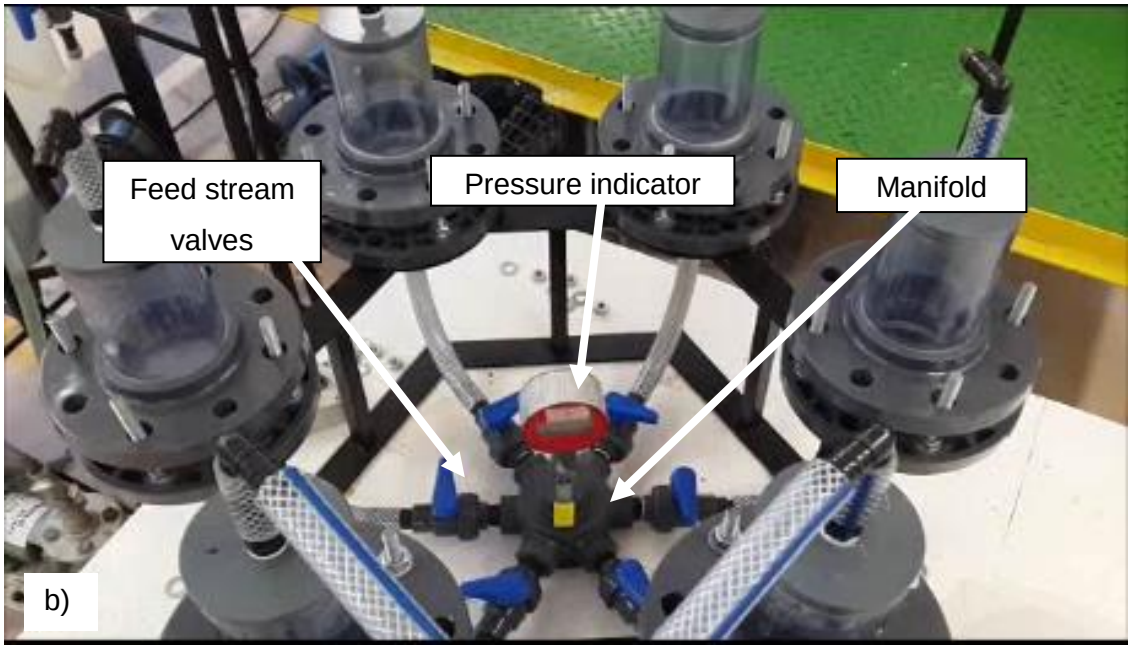

Figure 5.2: Technical drawing of the manifold in (a) and an image of the manifold feeding the reactor columns in (b)

The flow sequence through the manifold is depicted in Figure 5.3. The manifold and the reactor columns are fed from the bottom allowing for the best possible flow rate control with valves situated at the outlet streams of the manifold (V-4 to V-9). A bypass stream (P-3) flowing back to the feed tank (E-1) is fitted to the manifold feed stream (P-2) to avoid over pressure in the system and a possible pipe rupture. The feed valve (V-2) is used in conjunction with the variable speed drive on the pump to control the flow rate. Figure 5.3 is a process flow diagram (PFD) of the reactor system.

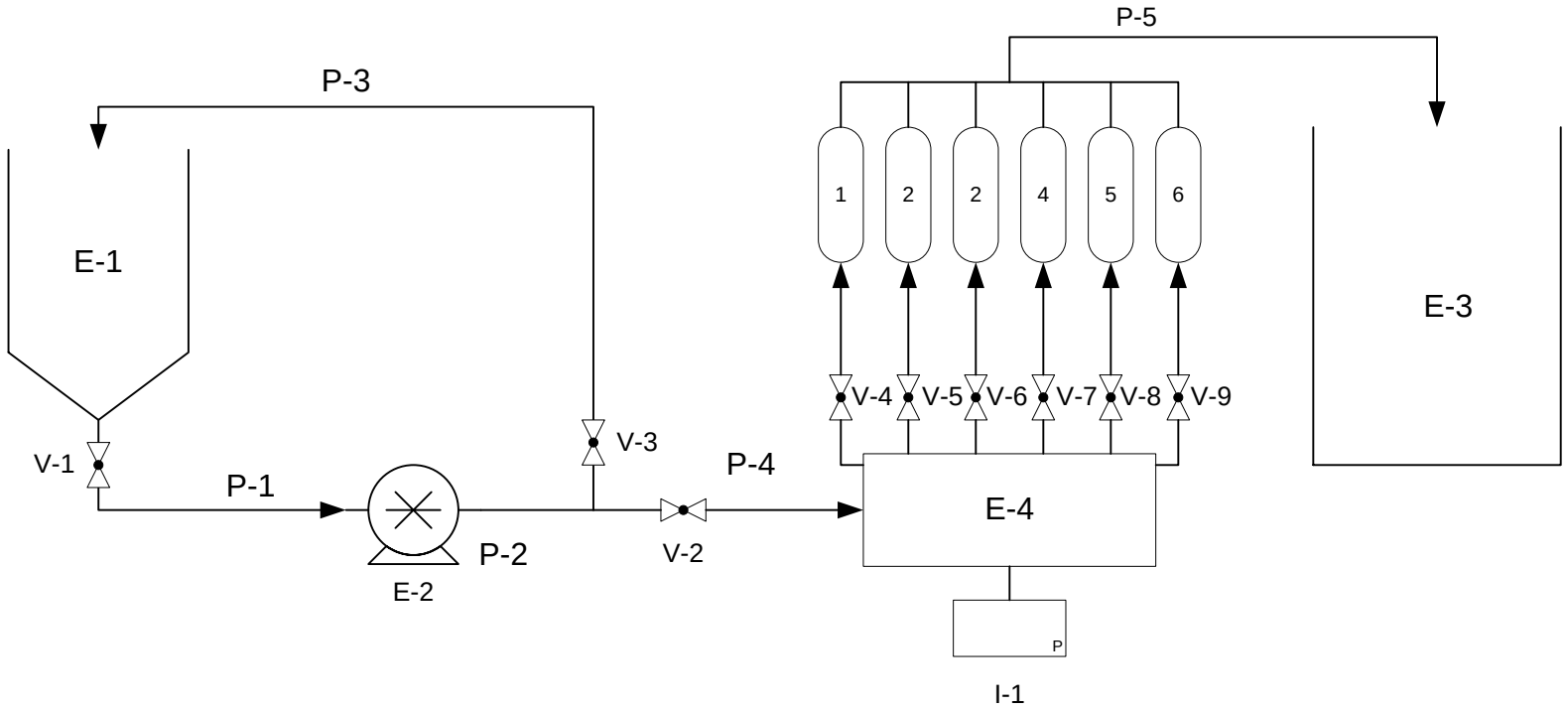

Equipment List	
Displayed Text	**Description**
E-1	Feed Tank
E-2	Feed Pump
E-3	Product Tank
E-4	Manifold

Instrument List	
Displayed Text	**Description**
I-1	Pressure indicator

Pipeline List		
Displayed Text	**Description**	**Line Size**
P-1	Pump Feed Line	12 mm
P-2	Bypass Feed Line	
P-3	Bypass Line	32 mm
P-4	Feed Pipe	32 mm
P-5	Product Pipe	12 mm

Figure 5.3: Process flow diagram for the scaled-up reactor system

5.7 Scale-up model commissioning

Methylene blue was used for commissioning the scale-up reactor to observe if flow is constant through each column and to measure the time taken for colour removal based on the estimated catalyst mass and PMS dosage. A total volume of 220 L was treated using a catalyst loading of 1.5 g per column. The PMS dosage was 0.233 g/L with Methylene blue concentration of 10 mg/L.

During start-up, there was a problem with the flow through the system as the fluid was flowing through two columns at higher flow rates. No visible degradation occurred. The higher flow rates also resulted in the release of the cobalt oxide from one of the columns which is seen in Figure 5.4 (b).

The manifold system as designed was found to be very sensitive to changes in the level for each column. After each column height was adapted by 2 to 3 mm using a spirit level, the flow was distributed evenly through each column. Samples were taken at regular intervals to inspect the product visually. The sample was not clear and still had a light blue tint immediately after leaving the reactor. The time taken for the product samples to completely breakdown the dye was measured and is displayed in Table 5.3:

Table 5.3: Degradation time for product samples taken at regular intervals

Product sample	Degradation time (min)
45 minute	0:25
90 minute	2:30
150 minute	6:00
200 minute	15:00

It was observed that over the course of treating the 220 L the homogeneous reaction became more important towards the later stages as the catalyst efficiency was decreasing. According to the literature, organic functional groups bond to the surface of the heterogeneous metal catalyst, which causes a decrease in the number of active sites and thereby inhibit the heterogeneous reaction i.e. decreasing the degradation efficiency (Poulopoulos and Inglezakis, 2006).

The reason for the continuous breakdown of the dye is due to the homogeneous reaction taking place due to the excess amount of PMS still reacting with the leached Co^{2+}. Although the leaching of the metal is undesirable, it does contribute largely to the extent of the degradation of the dye, especially when the heterogeneous catalyst becomes poisoned.

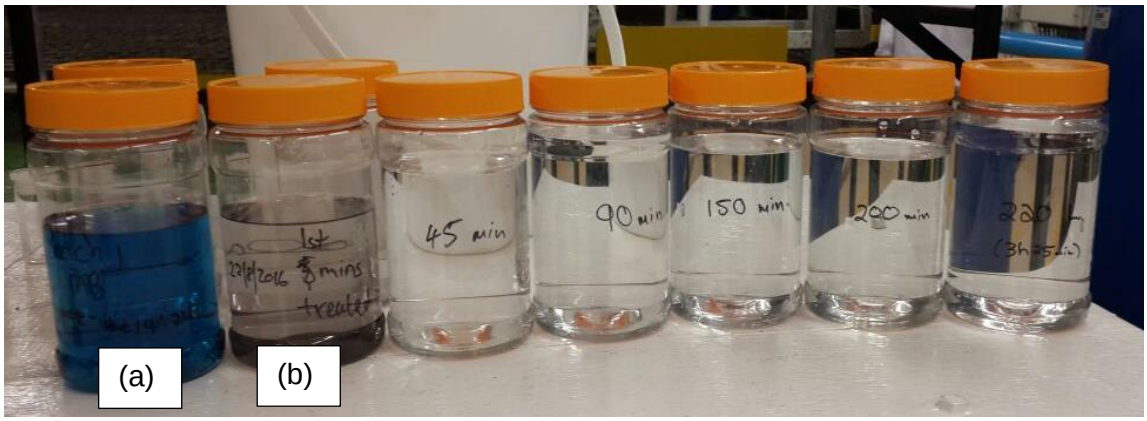

Figure 5.4: Product samples taken at regular intervals during the treatment of methylene blue in the scale-up reactor

Figure 5.4 shows the samples taken over the time of treating the 220 L. It is clear from Figure 5.4 that the scale-up reactor shows excellent treatability of methylene blue. The first sample in Figure 5.4 (a) is a sample that contains PMS only and has not been activated by Co_3O_4. The PMS only sample took 24 hours to degrade completely. This is proof that the reaction is accelerated by the activation of PMS by Co_3O_4.

5.8 Real effluent treatment

Real effluent obtained from a local dye house was treated using the scale up reactor. The concentration of PMS was 3 g/L and using a total catalyst loading of 6 g. The total volume of water treated was 100 L in a time period of 80 minutes. The flow rate was 1200 ml/min, equivalent to 200 ml/min through each individual column. Figure 5.5 displays the degradation curve of real textile effluent treated in the scaled-up reactor.

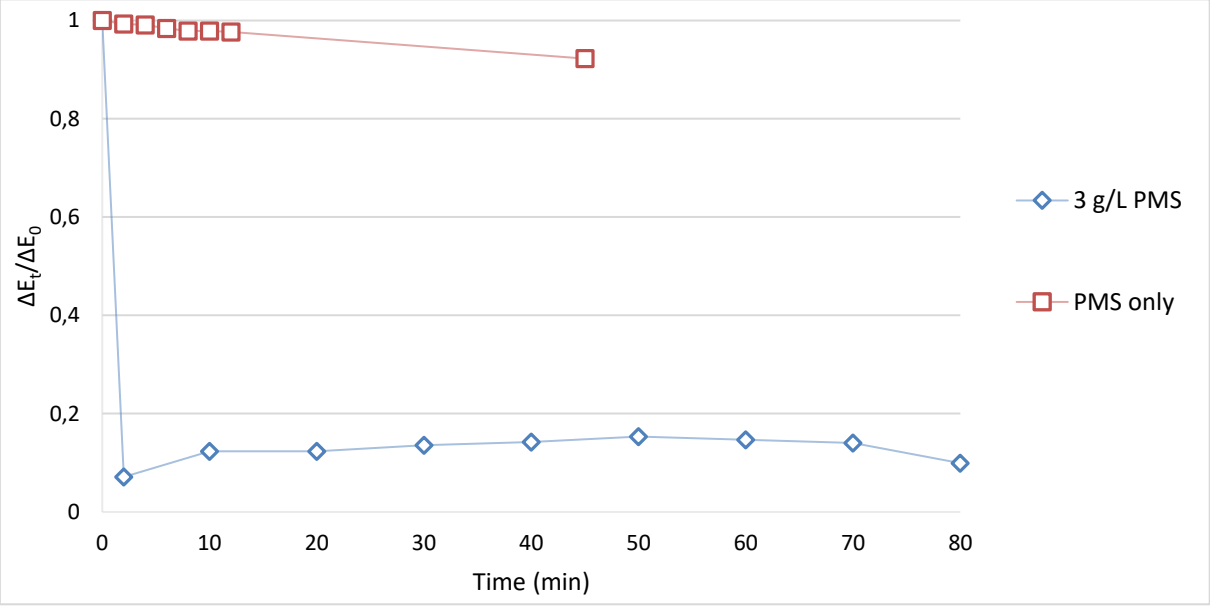

Figure 5.5: Degradation curve for real effluent treatment using 3 g/L PMS and total catalyst mass of 6 g at a flow rate of 1200 ml/min

A total volume of 100 L was treated in 80 minutes. The overall breakdown of the effluent was 87.4%. One sample with only PMS was observed to evaluate the breakdown of the dye in the absence of the catalyst. It took 25 hours for the dye to be completely broken down by the PMS only. Visually the treated water was completely clear as displayed in Figure 5.6. The results obtained in real effluent treatment in the upscale reactor were consistent with the results obtained for the bench scale reactor for the maximum degradation of 93% was observed at 2 minutes.

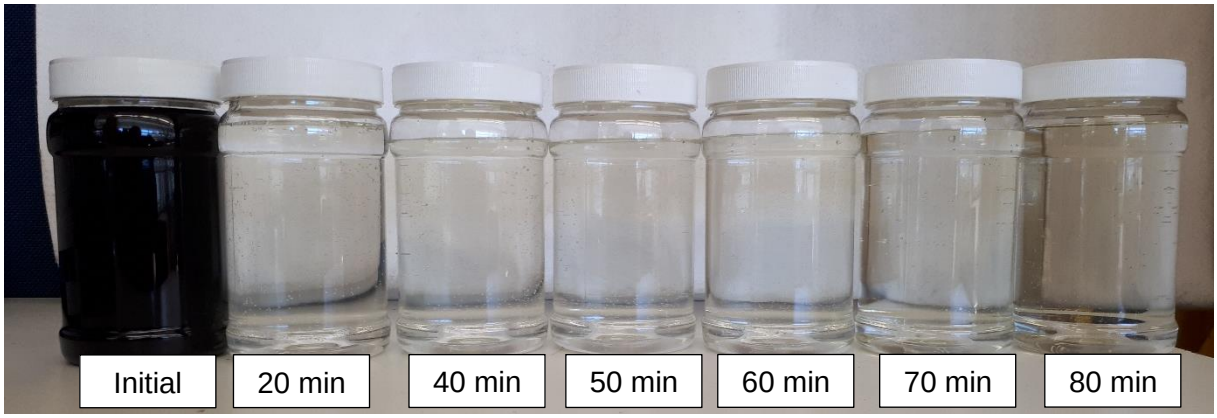

Figure 5.6: Treated samples over time compared to the initial feed effluent

The heterogeneous reaction is an instantaneous reaction as the dark effluent is completely clear as it exits the permeable reaction barrier. The homogeneous phase reaction is important to further breakdown the dye as the heterogenous catalyst becomes poisoned. This was observed due to the fact that after 60 minutes of treatment, the treated effluent leaving the reactor has a small amount of untreated dye present. The untreated dye however was rapidly broken down by the homogeneous reaction. Figure 5.7 shows that the 60 minute sample has a small amount of dye present compared to the 10 minute sample.

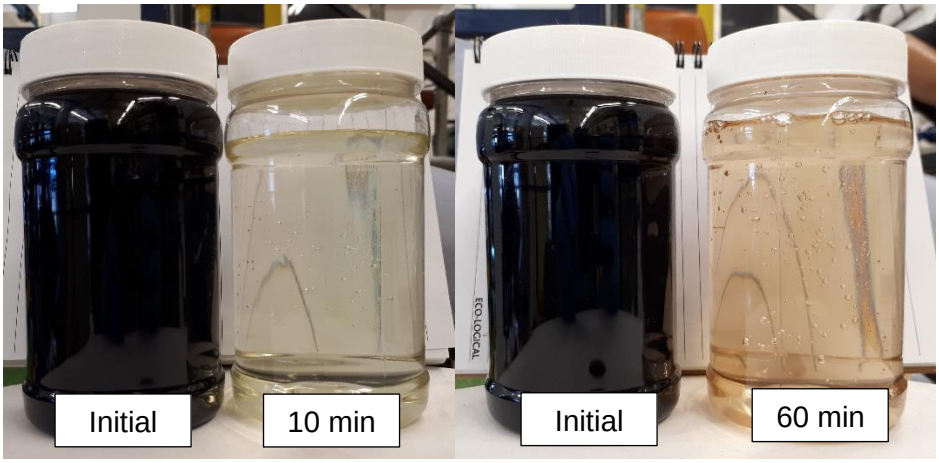

Figure 5.7: Effect of catalyst poisoning as more water is being treated by the catalyst

The poisoning of the catalyst causes a decrease in the number of active sites to produce reactive radicals which causes the slightly lower degradation. A sample taken after 2 minutes

of running resulted in a breakdown of 93% and after 60 minutes of running the degradation efficiency was 85.4%. The effect of catalyst poisoning is observed in Figure 5.7 and Figure 5.8 as the effluent leaving the PRB has a darker colour after 60 minutes compared to 10 minutes of running time. The remaining dye was then however degraded by the homogeneous reaction resulting in a water completely clear of any dye after standing for 10 minutes.

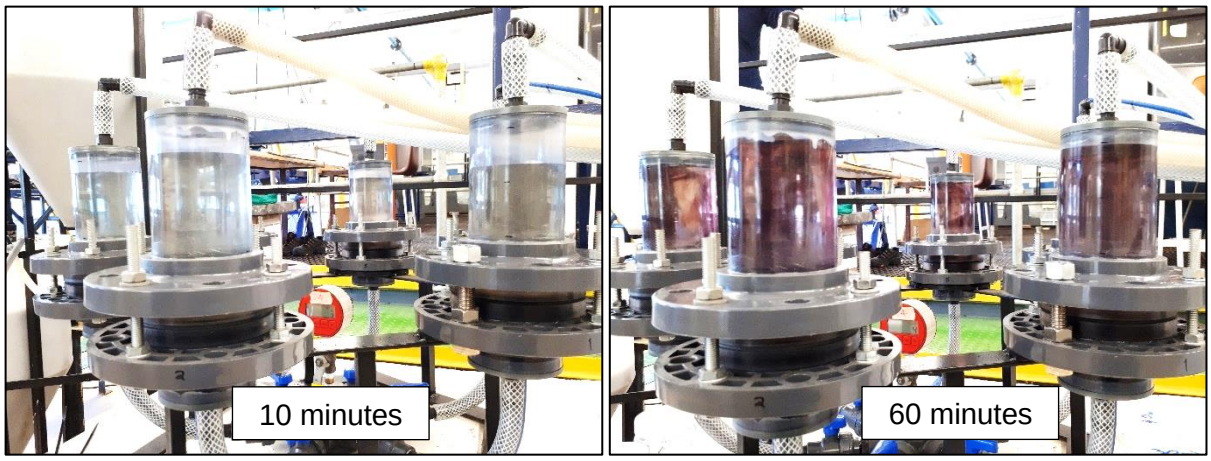

Figure 5.8: Comparison of treated effluent exiting the PRB immediately after treatment for 10 and 60 minutes of running time

5.8.1 Comparison to alternative continuous AOPs

There is no other continuous sulphate radical based AOPs discussed in open literature, therefore the PRB system compared to other continuous AOPs. The purpose of the development of the continuous reactors is to maximise the degradation of the target pollutants at a maximum flow rate and total degradation time. Although the target pollutants in the compared studies were different from this study, the flow rate and degradation time can be used as comparative parameters for the treatment technology.

As mentioned in Table 2.1, Rezaei et al., (2014), Dionysiou et al., (2000), Meshram et al., (2011) and Zhang et al., (2003) have developed continuous wastewater treatment reactors utilizing the AOP of photocatalysis. The pollutants in the water treated by these authors were phenol based and were model wastewaters and not real effluents.

Rezaei et al., (2014) and Dionysiou et al., (2000) developed an annular baffle type reactor and a rotating disk reactor respectively which both used an immobilized TiO_2 based photocatalyst. Meshram et al., (2011) developed a continuous stirred tank reactor utilizing a ZnO–bentonite photocatalyst. The catalyst loadings were 17.6 g/m^2, 141200 g/m^2 and 330 g/m^2 for Rezaei et al., (2014), Dionysiou et al., (2000) and Meshram et al., (2011) respectively. Zhang et al., (2003) developed a circulating tube reactor utilizing 0.114 g/m^2

immobilized Pt-loaded TiO_2 photocatalyst. The total reactor volume was 5 litres essentially making the reactor a semi-batch reactor and not fully continuous.

Comparing this study (the PRB system) to the above-mentioned studies it is observed that the PRB system was more efficient in terms of catalyst loading. The PRB system catalyst loading was 250 g/m^2 and was less than both that of Dionysiou et al., (2000) and Meshram et al., (2011) but still resulted in a degradation of 87.4% which was 4.3% and 21.4% more than that of Dionysiou et al., (2000) and Meshram et al., (2011) respectively. Although the catalyst loading of 250 g/m^2 was 14 times more than that used by Rezaei et al., (2014), it resulted in 87.4% degradation in 10 minutes of treatment compared to 74.7% which took 6 hours of treatment.

Rezaei et al., (2014), Dionysiou et al., (2000), Meshram et al., (2011) and Zhang et al., (2003) were able to treat at product flow rates of 15.18 ml/min, 13.86 ml/min, 10 ml/min and 55.56 ml/min respectively achieving 74.7%, 83.1%, 66% and 100% degradation. The PRB system was successful in treating 100 litres of real effluent at an 87.4% degradation with a product flow rate of 1275 ml/min.

The above-mentioned studies showed promising results but when compared to the PRB system it is concluded that the PRB system could treat the target pollutants to a higher degradation efficiency (87.4%) and at a flow rate 23 times higher. The above-mentioned studies also based their research on model pollutants whereas the PRB system was based on real effluent resulting in a more accurate representation of a real-life application.

5.9 Process safety

Process safety should be considered as part of the design and development of any new technology. Identifying key health and safety issues as part of the design will also lead to the improvement of the system. Toxicity of nanoparticles is still being debated and measured and many reports exist for particles used more regularly in industry such as nano titanium dioxide for example. Some toxicity studies were conducted and reported on cobalt and not yet for nano-cobalt oxide. In the sulphate radical AOP, even in the immobilised catalysis processes, leaching of cobalt ions occur to some extent. This phenomenon was observed in the system development in this work and therefore the leached cobalt content was measured in the product to ascertain the extent of leaching. Section 5.9.1 provides a short summary of the main toxicity points summarised by the World Health Organisation (Kim et al., 2006) with a comparison of the measured levels of cobalt in the treated product produced in this work. Section 5.9.2 presents a HAZOP study conducted on the PRB system

5.9.1 Cobalt toxicity

Cobalt is naturally found in the environment and has comparable properties to iron and nickel. Cobalt only has one stable isotope, cobalt 59. Cobalt 57 and cobalt 60 are both radioactive isotopes but they do not occur naturally and have a relatively short half-life making them not extremely dangerous. Cobalt is used in the production of superalloys (Kim et al., 2006).

Acute exposure of cobalt in humans and animals by inhalation result in respiratory effects, such as decrease in respiration function, congestion, edema and haemorrhage of the lung. Respiratory effects are also a result of chronic exposure by inhalation. The exposure level for chronic effects by inhalation has been found to be 0.005 µg/m^3 in rats and mice. This is the level at which chronic health effects are not likely to occur. Humans ingesting cobalt chloride at 150 mg/day for a period of 22 days experienced polycythaemia and an increase in haemoglobin. Cardiomyopathy was observed in humans who consumed large amounts of beer containing cobalt sulphate (Kim et al., 2006).

Cobalt can also cause asthma, wheezing, fibrosis and pneumonia. Tolerable inhalation concentration was found to be 1 x 10^{-4} mg/m^3 based on lung function decrement. Furthermore, chronic effects such as cardiac effects, congestion of the liver, kidneys and conjunctiva, and immunological effects have also been observed. Research has not yet found any conclusive evidence that cobalt is carcinogenic (Kim et al., 2006). Table 5.4 shows the cobalt concentration in real effluent treated by the bench scale reactor.

Table 5.4: Cobalt ion leaching from the Co_3O_4 catalyst for tests done with different effluents

	Acid Dye		Base Dye		Reactive Dye		Dispersed Dye		Metal Complex Dye	
	Initial	**Final**	**Initial**	**Final**	**Initial**	**Final**	**Initial**	**Final**	**Initial**	**Final**
Cobalt (µg/L)	<1	15.7	<1	10.2	<1	<1	<1	12.1	<1	19.1

Surface water and groundwater concentrations of cobalt are below 1 µg/L and in populated areas the concentrations range 1 to 10 µg/L. These concentrations are increased in mining and agricultural areas up to several hundred mg/L. The earth's crust has been reported to obtain cobalt levels of 20 to 25 mg/kg. According to Kim et al., (2006) most humans are exposed to 5 to 40 µg/day of cobalt through their food intake.

It is observed in the PRB system that some leaching of cobalt occurs due to the drop in the pH. Although the highest concentration of leached cobalt of 19.1 µg/L was higher than that

found in groundwater, it is still less than the estimated 40 µg of cobalt consumed per day by humans. Future research should be done to evaluate whether a secondary treatment process is required to remove the leached cobalt from the treated water.

5.9.2 HAZOP study

A hazard can be defined as a material or occurrence in the process that can harm people, equipment or the environment. The difference between a hazard and a risk is that the hazard does not have a component of probability. A risk analysis or risk assessment is typically done to reduce the levels of economic loss or human injury by quantifying the likelihood and the magnitude of the loss or injury that might occur (Perry and Green, 1999). One way of doing a hazard analysis is by doing a hazard and operability study (HAZOP) and this technique has become more widely used in new plants. Kletz, (1999), described a HAZOP as a technique that can identify and assess possible hazards and problems that might occur during the operation of a continuous plant that lead to inefficient operation.

A HAZOP study was done on the permeable reaction barrier system and can be seen in Table 5.5. The study was done on the two major components of the system, the feed pump and the manifold.

Table 5.5: Hazard analysis on the reactor system by a HAZOP study

Feed Pump E-2				
Guideword and deviation	**Cause**	**Consequence**	**Control Measure**	**Recommendation**
No flow	Pump failure, upstream blockage	No feed to reactor columns		Regular pump servicing
More flow	Variable speed drive failure	Excessive feed to reactor; pressure build up in manifold; possible pipe rupture	Bypass stream P-3	Inspect V-3 before starting pump
Less flow	Variable speed drive failure	Low flow rate in reactor; no effect		Inspect V-2 before starting the pump
Manifold E-3				
More flow	Blockage of V-3	Overpressure in E-3; possible pipe rupture;	Pressure gauge on Manifold	

The study was not complex due to the simplicity of the PRB system. The major hazard found in the study was the over pressure of the manifold as this is the piece of equipment that causes the highest pressure differential. Since the pump is a positive displacement pump, the risk of over pressure in the system is increased drastically. Other types of pumps should be considered to reduce the risk.

5.10 Conclusion and recommendations

The scale up correlations were established for the determination of the PRB area and the required catalyst mass for the PRB based on the pore volume of this specific permeable barrier type and the residence time obtained for optimum operating conditions in the bench scale. These correlations were derived from residence time equation and were developed based on the optimum conditions obtained from the bench scale reactor.

The scale-up of the reactor from the bench scale stage was successful as methylene blue could be degraded using a linear scale up of the operating conditions. The product was completely clear after treating 220 litres using 9 g of cobalt oxide prior to optimising the catalyst mass. Even though some trouble was experienced during the start-up of the reactor, the dye was still successfully degraded in the upscaled reactor.

The reactor was also successful treating 100 L of real textile effluent. The scale up of the system was considered to be successful as the treatment of real effluent was successful by applying the optimum operating conditions as obtained by the optimization studies in the bench scale reactor. The maximum degradation of 93% was observed at 2 minutes compared to 25 hours for PMS only. Comparison of the performance of the PRB system with other types of continuous AOP reactors in the literature showed that the PRB system could treat the target pollutant to a higher degradation efficiency and at a higher flow rate of 23 times.

The optimum residence time in the PRB was found to bet 4.8 seconds. This residence time is central to the scale up rationale. This residence time is specific to this type of permeable barrier and can be different when other materials are used as a permeable barrier. Sufficient residence time is critical to ensure optimum contact between the catalyst and PMS so that the reactive radicals could be formed to maximise the treatment of effluent by the heterogeneous catalysis. Finally, the optimisation of process parameters at the bench scale is useful to determine the optimum conditions rapidly and the total amount of catalyst used is minimised.

In terms of the toxicity of leached cobalt it was found that the leached cobalt concentrations in the treated effluent exceed the amounts found in groundwater but was lower than what was investigated to be consumed by humans on a daily basis.

CHAPTER SIX: Conclusion and Recommendations

6.1 Introduction

The study was aimed at designing a continuous process for the treatment of textile effluent utilizing a synthesized cobalt oxide catalyst and peroxymonosulfate oxidizer as the source for producing the reactive radical species. Numerous authors, such as Anipsitakis et al., (2005), Anipsitakis et al., (2006), Chen et al., (2008), Chen et al., (2014), Chowdhury et al., (2015), Liang et al., (2012a), Saputra et al., (2013) and Saputra et al., (2017) have reported on the treatment of textile wastewaters and phenol contaminated waters using a similar catalyst and the same oxidizer. These authors have however not attempted to apply this oxidation technology in a continuous process by either developing a bench scale or pilot scale model which was the objective of this work.

6.2 Conclusion

This section summarises the conclusions drawn from the design and development of a continuous treatment process for textile wastewater treatment with respect to each objective.

Objective 1: To identify a permeable barrier and immobilise a cobalt oxide catalyst in it.

A permeable reaction barrier was identified and the catalyst was successfully immobilized in the substrate. A polypropylene felt material with 1 µm nominal pore size was found suitable for the purpose of producing a permeable barrier. The nature of the material allowed for flow through the barrier with minimal feed pressure and allowed for a large surface area for catalyst immobilization with a BET surface area of 1.93 m^2/g.

A method for immobilising the catalyst on the permeable barrier was developed utilising a filtration method (described in section 3.4). Three different sizes of catalyst were used. The batch hydrothermally synthesized catalyst of 175 nm provided a dense and uniform coverage of the substrate surface compared to the commercially available catalysts that sparsely covered the surface (the 10 µm catalyst) and caused particle agglomeration with areas of high catalyst concentration leading to a non-uniform coverage for the 50 nm catalyst.

Objective 2: To design a continuous reactor utilizing a permeable reactive barrier.

A custom designed acrylic housing was built to contain the PRB to maximise flow area without compromising a low energy driven system and to maximise catalyst-oxidiser residence time for efficient radical formation. The PRB housing was firstly installed in a horizontal flow system which failed to lead to a maximised flow area utilisation due to the low

flow resistance of the permeable barrier. A vertical up flow reactor was designed as an alternative which led to maximum flow area utilisation at the desired flow rate.

Objective 3: To determine the optimum operating conditions for the removal of colour.

Utilizing the bench scale reactor, the process parameters and design parameters were established to successfully design and construct a pilot scale reactor that could treat real textile effluent.

The optimum PMS dosage was unique to each wastewater treated and it was concluded that the PMS dosage had to be optimized in the bench scale reactor before being applied in the upscale reactor. For methyl orange and synozol black real effluent a PMS dosage of 0.367 g/L and 3 g/L was required respectively for successful degradation.

The catalyst mass per PRB cross-sectional area was determined to be optimum at 0.0247 g/cm^2. An optimum flow rate of 40 ml/min was determined experimentally from which a residence time of 4.8 seconds was calculated.

The design parameters for the scale up were:

1. Residence time in the PRB which had to be kept constant at 4.8 seconds.
2. Catalyst mass per PRB cross-sectional area which was 0.0247 g/cm^2.

Objective 4: To design and build a scale-up model of an order of magnitude

The critical parameter for the success of the reactor is the efficient contact between catalyst and oxidizer species known as the residence time. The residence time was deduced to be the basis of the design of the PRB reactor. Design correlations were developed to calculate the permeable reactive barrier size (Equation 5.2) and the catalyst mass (Equation 5.3) as a function of flow rate according to the optimized conditions for treatment in the bench scale reactor.

$$d_B = \sqrt{1.2732 * \frac{\tau * \dot{Q}_B}{t * \emptyset}} \quad \textbf{(5.4)}$$

$$m_{cat}^B = \frac{m_{cat}^A * d_B^2}{d_A^2} \quad \textbf{(5.5)}$$

The scale up model was successfully done to a magnitude of 30 times, i.e. the volumetric flow rate of the bench scale reactor was 40 ml/min which was scaled up to a volumetric flow rate of 1275 ml/min. The success of the scale up model was based on the successful treatment of 220 L of model wastewater and 100 L of real textile effluent using 9 g and 6 g of catalyst at 0.367 g/L and 3 g/L PMS respectively.

6.3 Recommendations

The reactor has shown great efficiency by the degradation of methylene blue and real effluent and a few recommendations can be made on the design. Currently the reactor has a very large footprint, occupying an area of 2 m^2 with the ability to only treat 76 L/hr. If this reactor was to be scaled up to treat 25000 L/hr it would occupy an area of approximately 670 m^2 and would therefore not be economically feasible. The design of the reactor can also be optimized to not only lower the footprint but also to consider flow dynamics to design a reactor that will be able to treat 25000 L/hr. This is an important aspect due to the large volumes of effluent produced by dye houses.

A temperature study was not conducted in this study and is highly recommended for future work. The effect of temperature on the catalyst is important as the effluent discharged by dye houses can reach temperatures of up to 40°C. On the opposite side of the spectrum, it is important to know the effect of low temperature as the process could possibly be conducted in geographical areas where the minimum temperatures could be as low as 8°C during winter months.

As with any catalytic process, the catalyst loses efficiency due to various forms of catalyst deactivation such as fouling or poisoning. The deactivation is dependent on the constituents of the feed solution. It is recommended that a full study is conducted on the deactivation of the catalyst depending on the makeup of the feed solution and that a model is formulated to determine mathematically the frequency of replacing the permeable reactive barriers.

The leached cobalt in the treated effluent was observed to be greater than the amounts found in natural groundwater. Further investigation is recommended to reduce the leaching of cobalt ions by studying the effect of required PMS dosage as a function of COD and pH.

The development of the technology is still in a preliminary stage and hence an accurate technoeconomic analysis could not be done. It is recommended that in the future, once the system has been optimally designed with the appropriate materials of construction, a full technoeconomic analysis should conducted.

References

Allègre, C., Moulin, P., Maisseu, M. & Charbit, F. 2006. Treatment and reuse of reactive dyeing effluents. *Journal of Membrane Science,* 269**,** 15-34.

Andreozzi, R., Caprio, V., Insola, A. & Marotta, R. 1999. Advanced oxidation processes (AOP) for water purification and recovery. *Catalysis Today,* 53**,** 51-59.

Anipsitakis, G. P. & Dionysiou, D. D. 2004. Radical Generation by the Interaction of Transition Metals with Common Oxidants. *Environmental Science & Technology,* 38**,** 3705-3712.

Anipsitakis, G. P., Stathatos, E. & Dionysiou, D. D. 2005. Heterogeneous Activation of Oxone Using Co3O4. *The Journal of Physical Chemistry B,* 109**,** 13052-13055.

Anjaneyulu, Y., Chary, N. S. & Raj, D. S. S. 2005. Decolourization of industrial effluents–available methods and emerging technologies–a review. *Reviews in Environmental Science and Bio/Technology,* 4**,** 245-273.

Argyle, M. & Bartholomew, C. 2015. Heterogeneous Catalyst Deactivation and Regeneration: A Review. *Catalysts,* 5**,** 145.

Arslan, İ., Balcioğlu, I. A. & Bahnemann, D. W. 2000. Advanced chemical oxidation of reactive dyes in simulated dyehouse effluents by ferrioxalate-Fenton/UV-A and TiO2/UV-A processes. *Dyes and Pigments,* 47**,** 207-218.

Banat, I. M., Nigam, P., Singh, D. & Marchant, R. 1996. Microbial decolorization of textile-dyecontaining effluents: A review. *Bioresource Technology,* 58**,** 217-227.

Bejan, A., Dincer, I., Lorente, S., Miguel, A. F. & Reis, A. H. 2004. Porous Media Fundamentals. *Porous and Complex Flow Structures in Modern Technologies.* New York, NY: Springer New York.

Best, J. 2012. *Colour design: theories and applications*, Elsevier.

Buthelezi, S., Olaniran, A. & Pillay, B. 2012. Textile Dye Removal from Wastewater Effluents Using Bioflocculants Produced by Indigenous Bacterial Isolates. *Molecules,* 17**,** 14260.

Chan, K. H. & Chu, W. 2009. Degradation of atrazine by cobalt-mediated activation of peroxymonosulfate: Different cobalt counteranions in homogenous process and cobalt oxide catalysts in photolytic heterogeneous process. *Water Research,* 43**,** 2513-2521.

Chen, X., Chen, J., Qiao, X., Wang, D. & Cai, X. 2008. Performance of nano-Co3O4/peroxymonosulfate system: Kinetics and mechanism study using Acid Orange 7 as a model compound. *Applied Catalysis B: Environmental,* 80**,** 116-121.

Chen, Z., Chen, S., Li, Y., Si, X., Huang, J., Massey, S. & Chen, G. 2014. A recyclable and highly active Co3O4 nanoparticles/titanate nanowire catalyst for organic dyes degradation with peroxymonosulfate. *Materials Research Bulletin,* 57**,** 170-176.

Chollom, M., Rathilal, S., Pillay, V. & Alfa, D. 2015. The applicability of nanofiltration for the treatment and reuse of textile reactive dye effluent. *Water SA,* 41**,** 398-405.

Chorkendorff, I. & Niemantsverdriet, W. 2003. *Concepts of Modern Catalysis and Kinetics,* Weinheim, Wiley.

Chowdhury, M., Oputu, O., Kebede, M., Cummings, F., Cespedes, O., Maelsand, A. & Fester, V. 2015. Rapid and large-scale synthesis of Co3O4 octahedron particles with very high catalytic activity, good supercapacitance and unique magnetic properties. *RSC Advances,* 5**,** 104991-105002.

Christie, R. M. 2001. *Colour Chemistry,* Cambridge, United Kingdom, Royal Society of Chemistry.

Darcy, H. 1856. The public fountains of the city of Dijon. *Dalmont, Paris,* 647.

Deng, Y. & Zhao, R. 2015. Advanced Oxidation Processes (AOPs) in Wastewater Treatment. *Current Pollution Reports,* 1**,** 167-176.

Ding, Y., Zhu, L., Huang, A., Zhao, X., Zhang, X. & Tang, H. 2012. A heterogeneous Co3O4-Bi2O3 composite catalyst for oxidative degradation of organic pollutants in the presence of peroxymonosulfate. *Catalysis Science & Technology,* 2**,** 1977-1984.

Dionysiou, D. D., Khodadoust, A. P., Kern, A. M., Suidan, M. T., Baudin, I. & Laîné, J.-M. 2000. Continuous-mode photocatalytic degradation of chlorinated phenols and pesticides in water using a bench-scale TiO2 rotating disk reactor. *Applied Catalysis B: Environmental,* 24**,** 139-155.

Donati, G. & Paludetto, R. 1997. Scale up of chemical reactors. *Catalysis Today,* 34**,** 483-533.

Dos Santos, A. B., Cervantes, F. J. & Van Lier, J. B. 2007. Review paper on current technologies for decolourisation of textile wastewaters: Perspectives for anaerobic biotechnology. *Bioresource Technology,* 98**,** 2369-2385.

Du, P., Carneiro, J. T., Moulijn, J. A. & Mul, G. 2008. A novel photocatalytic monolith reactor for multiphase heterogeneous photocatalysis. *Applied Catalysis A: General,* 334**,** 119-128.

Feng, J., Hu, X., Yue, P. L., Zhu, H. Y. & Lu, G. Q. 2003. Discoloration and mineralization of Reactive Red HE-3B by heterogeneous photo-Fenton reaction. *Water Research,* 37**,** 3776-3784.

Fogler, H. S. 1999. *Elements of chemical reaction engineering,* Essex, Pearson Education Limited.

Galindo, C., Jacques, P. & Kalt, A. 2000. Photodegradation of the aminoazobenzene acid orange 52 by three advanced oxidation processes: UV/H 2 O 2, UV/TiO 2 and

VIS/TiO 2: comparative mechanistic and kinetic investigations. *Journal of Photochemistry and Photobiology A: Chemistry,* 130**,** 35-47.

Ghaly, A., Ananthashankar, R., Alhattab, M. & Ramakrishnan, V. 2014. Production, characterization and treatment of textile effluents: a critical review. *Journal of Chemical Engineering & Process Technology,* 2014.

Greenkorn, R. A. 1981. Steady flow through porous media. *AIChE Journal,* 27**,** 529-545.

Grzechulska, J. & Morawski, A. W. 2002. Photocatalytic decomposition of azo-dye acid black 1 in water over modified titanium dioxide. *Applied Catalysis B: Environmental,* 36**,** 45-51.

Harriott, P. 2002. *Chemical reactor design*, CRC Press.

Hassan, M. & Hawkyard, C. J. 2002. Decolourisation of aqueous dyes by sequential oxidation treatment with ozone and Fenton's reagent. *Journal of Chemical Technology and Biotechnology,* 77**,** 834-841.

Hayashi, H. & Hakuta, Y. 2010. Hydrothermal synthesis of metal oxide nanoparticles in supercritical water. *Materials,* 3**,** 3794-3817.

Holdich, R. & Todd, A. 2002. *Fundamentals of Particle Technology,* Louborough, UK, Midland Information Technology and Publishing.

Hu, P. & Long, M. 2016. Cobalt-catalyzed sulfate radical-based advanced oxidation: A review on heterogeneous catalysts and applications. *Applied Catalysis B: Environmental,* 181**,** 103-117.

Huang, P. M., Li, Y. & Sumner, M. E. 2011. *Handbook of soil sciences: resource management and environmental impacts*, CRC Press.

Hunt, R. W. G. & Pointer, M. R. 2011. *Measuring colour*, John Wiley & Sons.

Kang, S.-F., Liao, C.-H. & Chen, M.-C. 2002. Pre-oxidation and coagulation of textile wastewater by the Fenton process. *Chemosphere,* 46**,** 923-928.

Kim, J. H., Gibb, H. J., Howe, P. D. & Organization, W. H. 2006. Cobalt and inorganic cobalt compounds.

Kletz, T. A. 1999. *HAZOP and HAZAN: identifying and assessing process industry hazards*, IChemE.

Kommineni, S., Zoeckler, J., Stocking, A., Liang, S., Flores, A., Kavanaugh, M., Rodriguez, R., Browne, T. & Roberts, R. 2000. Advanced Oxidation Process. *In:* MELIN, G. (ed.) 2nd ed. California: National Water Research Institute.

Levenspiel, O. 1999. Chemical reaction engineering. *Industrial & engineering chemistry research,* 38**,** 4140-4143.

Liang, H., Sun, H., Patel, A., Shukla, P., Zhu, Z. H. & Wang, S. 2012a. Excellent performance of mesoporous Co3O4/MnO2 nanoparticles in heterogeneous activation of peroxymonosulfate for phenol degradation in aqueous solutions. *Applied Catalysis B: Environmental,* 127**,** 330-335.

Liang, H., Ting, Y. Y., Sun, H., Ang, H. M., Tadé, M. O. & Wang, S. 2012b. Solution combustion synthesis of Co oxide-based catalysts for phenol degradation in aqueous solution. *Journal of Colloid and Interface Science,* 372**,** 58-62.

Lin, S. H. & Chen, M. L. 1997. Treatment of textile wastewater by chemical methods for reuse. *Water Research,* 31**,** 868-876.

Linsebigler, A. L., Lu, G. & Yates Jr, J. T. 1995. Photocatalysis on TiO2 surfaces: principles, mechanisms, and selected results. *Chemical reviews,* 95**,** 735-758.

Lison, D. 1996. Human toxicity of cobalt-containing dust and experimental studies on the mechanism of interstitial lung disease (hard metal disease). *Critical reviews in toxicology,* 26**,** 585-616.

Lucas, M. S. & Peres, J. A. 2006. Decolorization of the azo dye Reactive Black 5 by Fenton and photo-Fenton oxidation. *Dyes and Pigments,* 71**,** 236-244.

Masterton, W. L., Hurley, C. N. & Neth, E. J. 2012. *Chemistry: Principles and Reactions,* Belmont, USA, Brooks/Cole.

Meriç, S., Kaptan, D. & Ölmez, T. 2004. Color and COD removal from wastewater containing Reactive Black 5 using Fenton's oxidation process. *Chemosphere,* 54**,** 435-441.

Meshram, S., Limaye, R., Ghodke, S., Nigam, S., Sonawane, S. & Chikate, R. 2011. Continuous flow photocatalytic reactor using ZnO–bentonite nanocomposite for degradation of phenol. *Chemical Engineering Journal,* 172**,** 1008-1015.

Metcalf, I. 2003. Eddy, Wastewater Engineering Treatment and Reuse. New York: McGraw Hill.

Mittal, A. 2011. Biological wastewater treatment. *Water Today,* 1**,** 32-44.

Moustafa, S. 2008. Environmental impacts of textile industries. Process analysis of textile manufacturing. UNESCO-IHE, Delft.

Nagarajan, R. & Hatton, T. A. 2008. *Nanoparticles: Synthesis, Stabilization, Passivation and Functionalization,* Washington DC, United States of America, American Chemical Society.

Nemtanu, M. & Brasoveanu, M. 2010. Functional properties of some non-conventional treated starches. *Biopolymers.* InTech.

Pérez, M., Torrades, F., Domènech, X. & Peral, J. 2002. Fenton and photo-Fenton oxidation of textile effluents. *Water Research,* 36**,** 2703-2710.

Perry, R. H. & Green, D. W. 1999. *Perry's chemical engineers' handbook,* New York, McGraw-Hill Professional.

Poulopoulos, S. G. & Inglezakis, V. J. 2006. *Adsorption, ion exchange and catalysis: design of operations and environmental applications,* Oxford, UK, Elsevier.

Rezaei, M., Rashidi, F., Royaee, S. J. & Jafarikojour, M. 2014. Performance evaluation of a continuous flow photocatalytic reactor for wastewater treatment. *Environmental Science and Pollution Research,* 21**,** 12505-12517.

Rollin, A. L., Denis, R., Estaque, L. & Masounave, J. 1982. Hydraulic behavior of synthetic non-woven filter fabrics. *The Canadian Journal of Chemical Engineering,* 60**,** 226-234.

Royaee, S. J., Sohrabi, M. & Barjesteh, P. J. 2012. Performance evaluation of a continuous flow Photo-Impinging Streams Cyclone Reactor for phenol degradation. *Chemical Engineering Research and Design,* 90**,** 1923-1929.

Saputra, E., Duan, X., Armedi Pinem, J., Bahri, S. & Wang, S. 2017. Shape-controlled Co3O4 catalysts for advanced oxidation of phenolic contaminants in aqueous solutions. *Separation and Purification Technology*.

Saputra, E., Muhammad, S., Sun, H., Ang, H.-M., Tadé, M. O. & Wang, S. 2013. A comparative study of spinel structured Mn3O4, Co3O4 and Fe3O4 nanoparticles in catalytic oxidation of phenolic contaminants in aqueous solutions. *Journal of Colloid and Interface Science,* 407**,** 467-473.

Schanda, J. 2007. *Colorimetry: understanding the CIE system*, John Wiley & Sons.

Scott, J. P. & Ollis, D. F. 1995. Integration of chemical and biological oxidation processes for water treatment: Review and recommendations. *Environmental Progress,* 14**,** 88-103.

Shi, P., Dai, X., Zheng, H., Li, D., Yao, W. & Hu, C. 2014. Synergistic catalysis of Co3O4 and graphene oxide on Co3O4/GO catalysts for degradation of Orange II in water by advanced oxidation technology based on sulfate radicals. *Chemical Engineering Journal,* 240**,** 264-270.

Shi, P., Su, R., Wan, F., Zhu, M., Li, D. & Xu, S. 2012. Co3O4 nanocrystals on graphene oxide as a synergistic catalyst for degradation of Orange II in water by advanced oxidation technology based on sulfate radicals. *Applied Catalysis B: Environmental,* 123–124**,** 265-272.

Shi, P., Wang, X., Zhou, X., Min, Y., Fan, J. & Yao, W. 2015. Influence of calcination temperature on the catalytic performance of Co3O4/GO nanocomposites for Orange II degradation. *RSC Advances,* 5**,** 34125-34133.

Slokar, Y. M. & Majcen Le Marechal, A. 1998. Methods of decoloration of textile wastewaters. *Dyes and Pigments,* 37**,** 335-356.

Su, S., Guo, W., Leng, Y., Yi, C. & Ma, Z. 2013. Heterogeneous activation of Oxone by Co x Fe 3− x O 4 nanocatalysts for degradation of rhodamine B. *Journal of hazardous materials,* 244**,** 736-742.

Sun, H. & Wang, S. 2015. Catalytic oxidation of organic pollutants in aqueous solution using sulfate radicals. *Catalysis: Volume 27.* The Royal Society of Chemistry.

Tang, W. Z. & Huren, A. 1995. UV/TiO2 photocatalytic oxidation of commercial dyes in aqueous solutions. *Chemosphere,* 31**,** 4157-4170.

Wang, Y. 2000. Solar photocatalytic degradation of eight commercial dyes in TiO 2 suspension. *Water Research,* 34**,** 990-994.

Wang, Y., Zhou, L., Duan, X., Sun, H., Tin, E. L., Jin, W. & Wang, S. 2015. Photochemical degradation of phenol solutions on Co3O4 nanorods with sulfate radicals. *Catalysis Today,* 258, Part 2**,** 576-584.

Welham, A. 2000. The theory of dyeing(and the secret of life). *Journal of the Society of Dyers and Colourists,* 116**,** 140-3.

Wiesmann, U., Choi, I. S. & Dombrowski, E.-M. 2007. *Fundamentals of biological wastewater treatment*, John Wiley & Sons.

Wood-Black, F. 2014. Considerations for Scale-Up ? Moving from the Bench to the Pilot Plant to Full Production. *Academia and Industrial Pilot Plant Operations and Safety.* American Chemical Society.

Yang, Q., Choi, H., Al-Abed, S. R. & Dionysiou, D. D. 2009. Iron–cobalt mixed oxide nanocatalysts: Heterogeneous peroxymonosulfate activation, cobalt leaching, and ferromagnetic properties for environmental applications. *Applied Catalysis B: Environmental,* 88**,** 462-469.

Yao, Y., Yang, Z., Sun, H. & Wang, S. 2012. Hydrothermal Synthesis of Co3O4–Graphene for Heterogeneous Activation of Peroxymonosulfate for Decomposition of Phenol. *Industrial & Engineering Chemistry Research,* 51**,** 14958-14965.

Zaghbani, N., Hafiane, A. & Dhahbi, M. 2007. Separation of methylene blue from aqueous solution by micellar enhanced ultrafiltration. *Separation and Purification Technology,* 55**,** 117-124.

Zhang, L., Kanki, T., Sano, N. & Toyoda, A. 2003. Development of TiO2 photocatalyst reaction for water purification. *Separation and Purification Technology,* 31**,** 105-110.

Zhang, Z. & Edwards, J. O. 1992. Chain lengths in the decomposition of peroxomonosulfate catalyzed by cobalt and vanadium. Rate law for catalysis by vanadium. *Inorganic Chemistry,* 31**,** 3514-3517.

Zhao, X. S., Bao, X. Y., Guo, W. & Lee, F. Y. 2006. Immobilizing catalysts on porous materials. *Materials Today,* 9**,** 32-39.

Zhou, L., Xu, J., Miao, H., Wang, F. & Li, X. 2005. Catalytic oxidation of cyclohexane to cyclohexanol and cyclohexanone over Co3O4 nanocrystals with molecular oxygen. *Applied Catalysis A: General,* 292**,** 223-228.

Zollinger, H. 1987. *Color Chemistry - Syntheses, Properties and Applications of Organic Dyes Pigments,* New York, NY, VCH.

Appendices

Appendix A: Additional TEM images of the catalyst

Appendix A provides additional TEM images of the batch hydrothermally synthesized cobalt oxide catalyst.

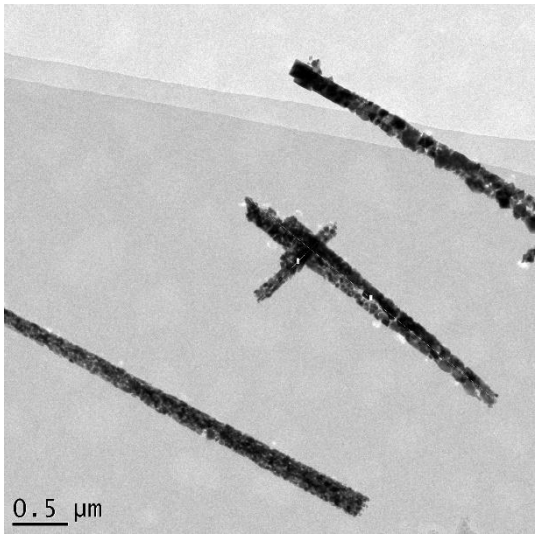

Figure A.1: TEM imaging of the batch hydrothermally synthesised cobalt oxide

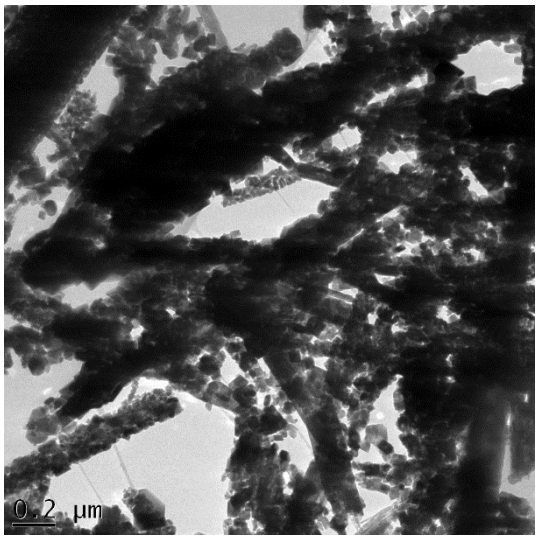

Figure A.2: TEM imaging of the batch hydrothermally synthesised cobalt oxide

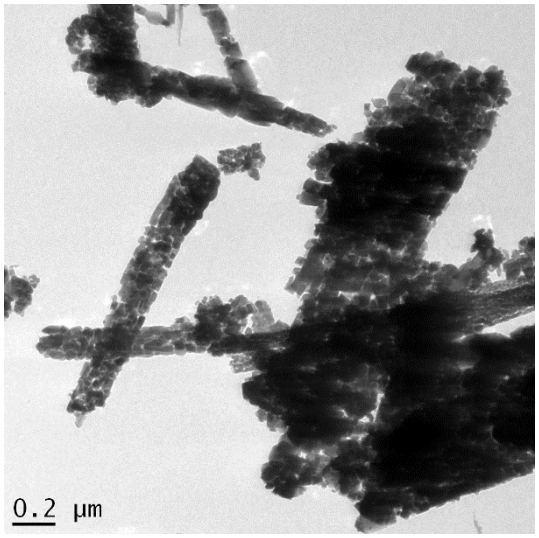

Figure A.3: TEM imaging of the batch hydrothermally synthesised cobalt oxide

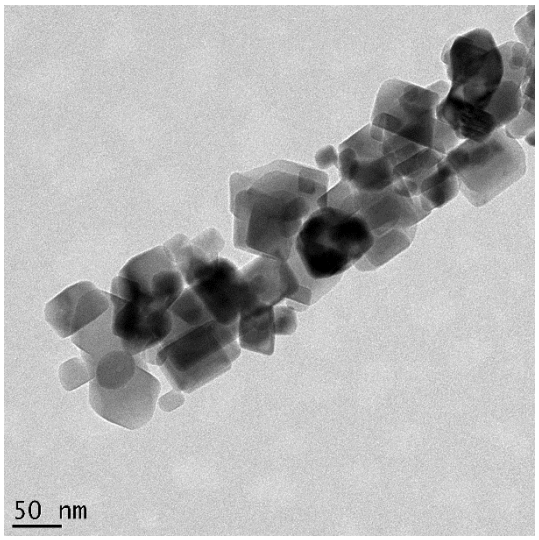

Figure A.4: TEM imaging of the batch hydrothermally synthesised cobalt oxide

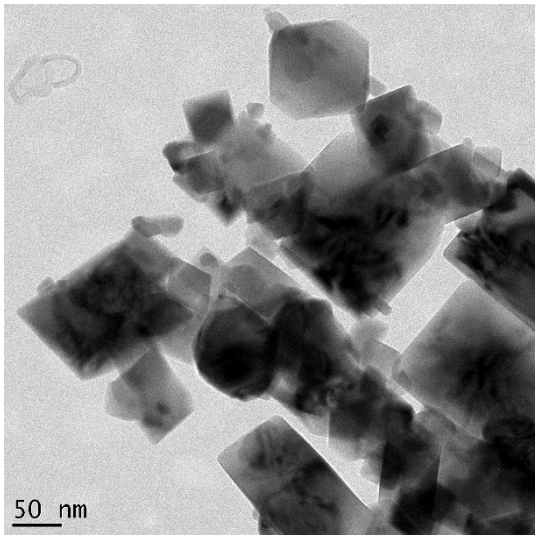

Figure A.5: TEM imaging of the batch hydrothermally synthesised cobalt oxide

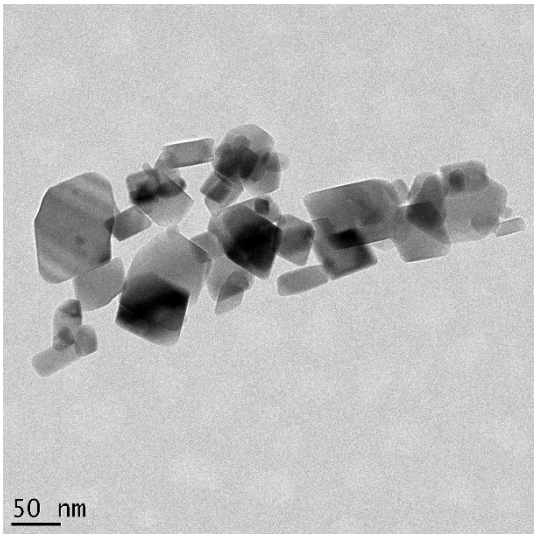

Figure A.6: TEM imaging of the batch hydrothermally synthesised cobalt oxide

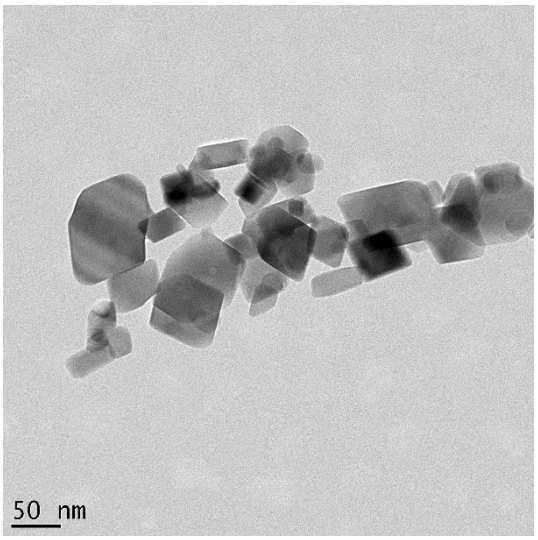

Figure A.7: TEM imaging of the batch hydrothermally synthesised cobalt oxide

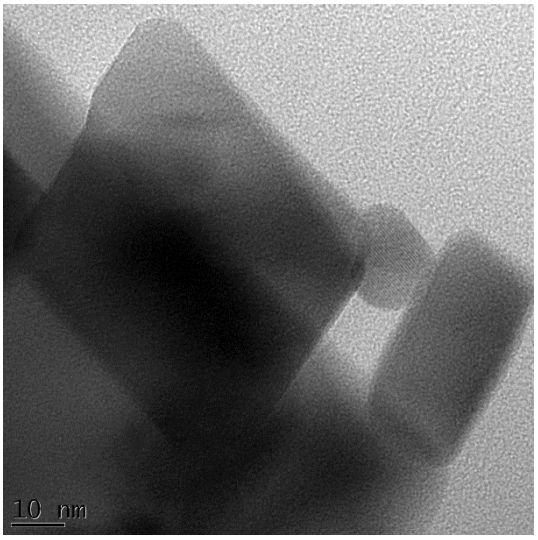

Figure A.8: TEM imaging of the batch hydrothermally synthesised cobalt oxide

Appendix B: Additional SEM images of cobalt oxide nanoparticles

Additional TEM images of the immobilized cobalt oxide catalysts (the batch hydrothermally synthesized, 50 nm and the 10 µm commercially available) used in the study are provided in Appendix B.

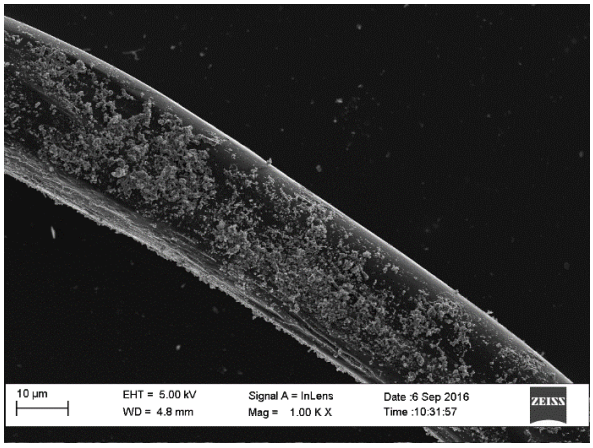

Figure B.1: SEM of the batch hydrothermally synthesised cobalt oxide catalyst immobilized in the PRB

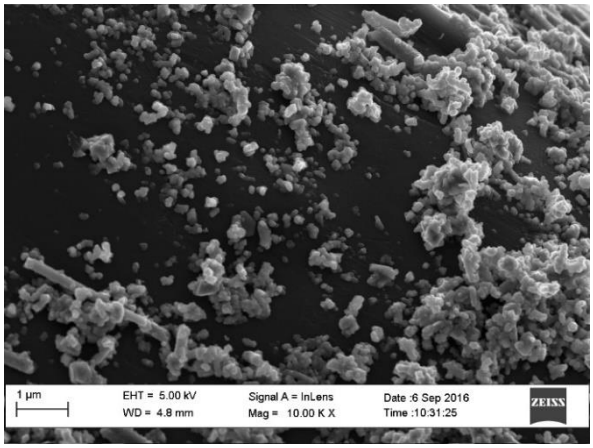

Figure B.2: SEM of the batch hydrothermally synthesised cobalt oxide catalyst immobilized in the PRB

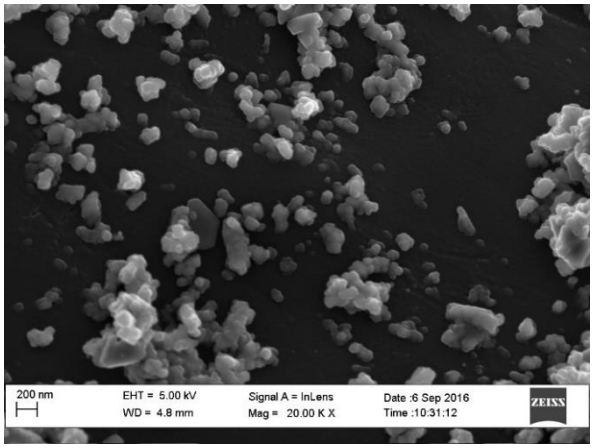

Figure B.3: SEM of the batch hydrothermally synthesised cobalt oxide catalyst immobilized in the PRB

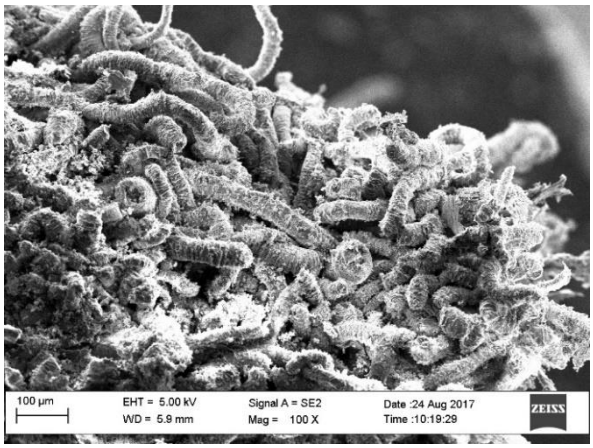

Figure B.4: SEM of the 50 nm commercially available cobalt oxide catalyst immobilized in the PRB

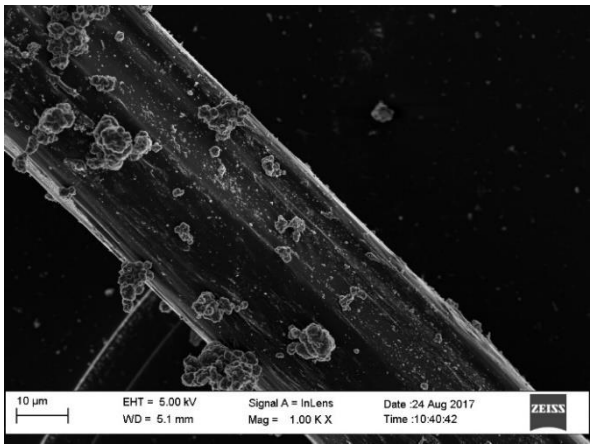

Figure B.5: SEM of the 50 nm commercially available cobalt oxide catalyst immobilized in the PRB

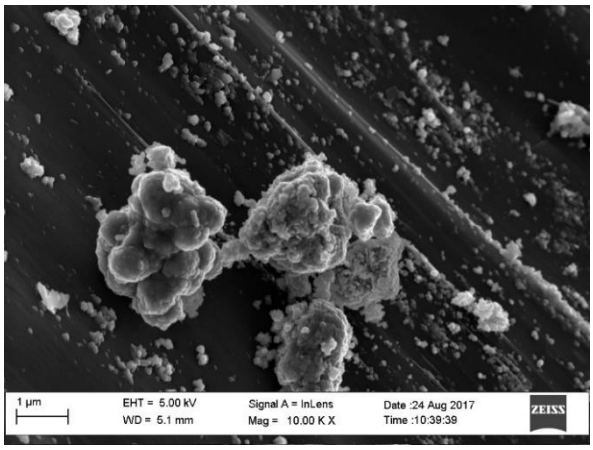

Figure B.6: SEM of the 50 nm commercially available cobalt oxide catalyst immobilized in the PRB

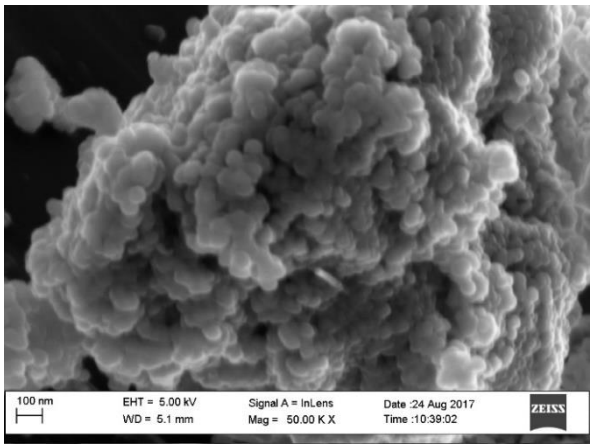

Figure B.7 SEM of the 50 nm commercially available cobalt oxide catalyst immobilized in the PRB

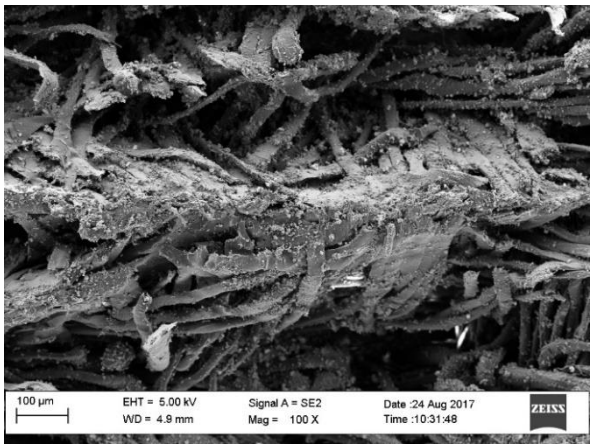

Figure B.8: SEM of the 10 µm commercially available cobalt oxide catalyst immobilized in the PRB

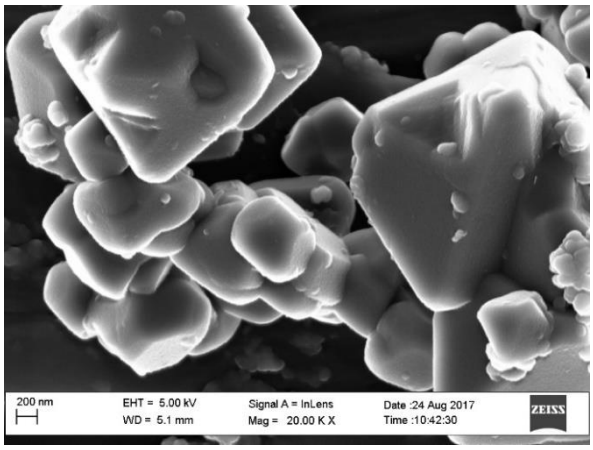

Figure B.9: SEM of the 10 µm commercially available cobalt oxide catalyst immobilized in the PRB

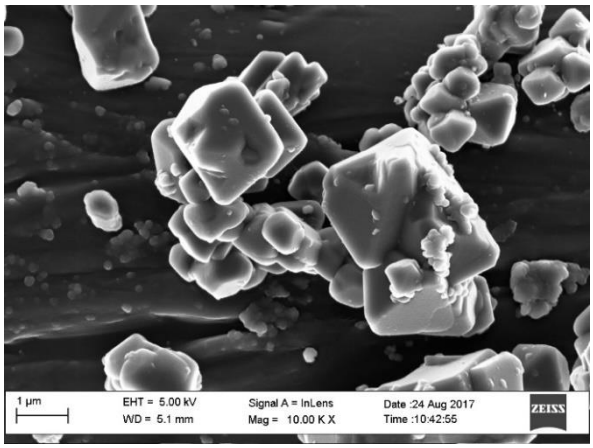

Figure B.10: SEM of the 10 µm commercially available cobalt oxide catalyst immobilized in the PRB

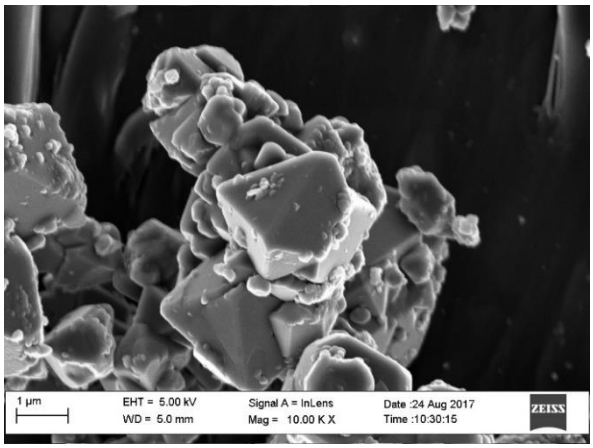

Figure B.11: SEM of the 10 µm commercially available cobalt oxide catalyst immobilized in the PRB

Appendix C: Real textile effluent treatment on the scale up model

In Appendix C images of the reactor columns of the scale up reactor are compared over the 80 minute running time

Figure C.1: Reactor columns with degraded real effluent at 2 minutes of running time

Figure C.2: Reactor columns with degraded real effluent at 20 minutes of running time

Figure C.3: Reactor columns with degraded real effluent at 30 minutes of running time

Figure C.4 Reactor columns with degraded real effluent at 40 minutes of running time

Figure C.5: Reactor columns with degraded real effluent at 60 minutes of running time

Figure C.6: Reactor columns with degraded real effluent at 70 minutes of running time

Appendix D: Particle size distribution

Table D.1: Length and width of batch hydrothermally synthesized cobalt oxide particles used for particle size analysis

Length	Width		Length	Width		Length	Width
254	232		44	44		300	206
194	182		49	25		750	88
223	117		47	36		519	207
149	147		77	46		474	491
152	110		49	45		693	474
141	100		31	66		135	443
74	49		71	30		349	454
262	226		36	31		127	110
174	160		27	53		365	292
106	86		83	36		369	117
111	102		23	23		300	225
184	136		60	70		204	384
113	97		61	15		483	268
206	132		44	48		290	190
189	169		45	46		168	410
210	142		21	38		260	236
187	124		34	43		113	142
99	97		212	19		589	186
220	188		630	22		122	112
148	119		252	131		174	509
178	122		251	416		250	110
97	67		125	248		119	150
335	193		158	156		295	153
163	147		382	122		133	78
91	48		208	157		313	244
267	212		194	316		117	113
286	247		255	152		258	148
211	250		345	95		268	91
177	177		213	247		312	152
169	211		210	291		193	79
119	176		349	88		217	148
225	129		163	165		202	160
218	102		145	243		181	147
184	158		200	152		141	157
105	177		221	99		178	106
218	171		157	94		300	140
301	98		206	202		234	82
88	215		124	95		277	192
43	165		174	157		256	155
25	59		246	56		308	175
91	37		349	139		100	165
49	20		207	174		376	44
26	66		133	432		385	83

Length	Width		Length	Width
360	119		360	119
382	221		382	221
227	208		227	208
144	256		144	256
266	132		266	132
178	126		178	126
421	132		421	132
291	384		291	384
255	242		255	242
168	180		168	180
253	186		253	186
165	159		165	159
233	146		233	146
193	124		193	124
237	131		237	131
213	71		213	71
264	91		264	91
246	128		246	128
300	112		300	112
268	190		268	190
264	213		264	213
229	184		229	184
595	263		595	263
494	152		494	152
89	78		89	78
157	87		157	87
213	77		213	77
637	115		637	115
331	131		331	131
87	198		87	198
77	58		77	58
64	41		64	41
75	46		75	46
72	55		72	55
67	32		67	32
67	53		67	53
48	57		48	57
66	24		66	24
46	23		46	23
56	42		56	42
54	32		54	32
54	28		54	28
101	45		101	45
56	38		56	38
		Average	175	124
		Standard deviation	134	98

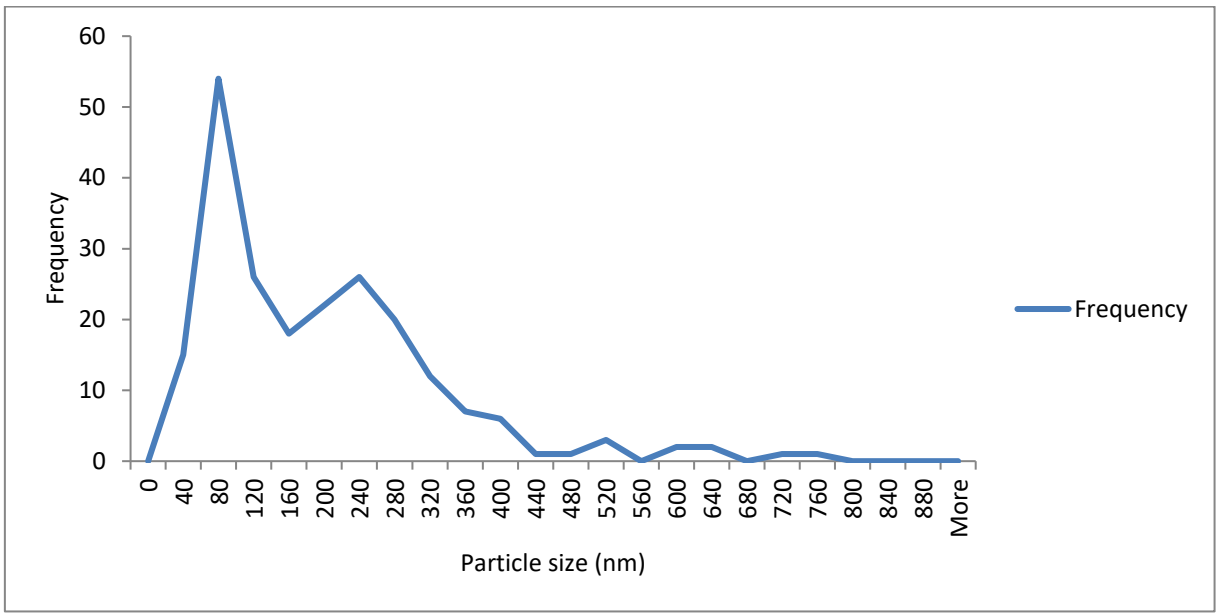

Figure D.1: Particle size distribution for batch hydrothermally synthesized cobalt oxide particles